UNIVERSITY OF CALGARY

Residual statics analysis using prestack equivalent offset migration

By

Xinxiang Li

A THESIS

SUBMITTED TO THE FACULTY OF GRADUATE STUDIES

IN PARTIAL FULFILMENT OF THE REQUIREMENTS FOR THE

DEGREE OF MASTER OF SCIENCE

DEPARTMENT OF GEOLOGY AND GEOPHYSICS

CALGARY, ALBERTA

JUNE, 1999

ABSTRACT

The equivalent offset mapping (EOMAP) method of residual statics analysis uses the concepts of equivalent offset and common scatterpoint gathering, which were introduced for prestack time migration. Static reference traces are formed at each input trace location by the forward and inverse EOMAP's. Conventional cross-correlation and decomposition combine to produce the surface consistent source and receiver statics. The prestack migration and de-migration processes involved allow the statics analysis to be performed before NMO correction without either offset or structure dependence. The offset and structure independence allows the cross-correlation between the summation traces of each source or receiver gather to directly estimate the statics with more stability.

The EOMAP processes do not involve any time shift. By using the asymptotic equivalent offset concepts, they can be totally velocity independent.

Acknowledgements

I am very grateful to the patient guidance of Dr. John C. Bancroft, my supervisor, through out the almost four years of study in CREWES. More than an advisor, John, with his family, has constantly helped during my "tough" time as a new foreign student. John and his family made me feel like back to my own warm home in those freezing 1996 and 1997 Calgary winters, when I just came to Calgary from China, could not even speak one full English sentence, and sometimes could not find a proper place to sleep. Thank you very much John, Fay, and your six wonderful children.

The sponsors of the CREWES Project has provided financial support to my graduate study, and without this generous help, I could not even come to Canada and pursue my new career as a geophysicist. The GRS program of Department of Geology and Geophysics supported me during the summer time in 1996, and special thanks belong to Dr. Don Lawton for the GRS support.

I have benefited from the best and updated CREWES computer facilities, and I would like to thank Henry Bland and Darren Foltinek who have answered so many of my annoying questions about computer and programming.

Dr. Wai-Kin Chan, Dr. Peter Cary and Hugh Geiger have given many helpful discussions and suggestions about statics and migration.

Many thanks also to many CREWES students, among them are Ken Fang, Yong Xu, Sam Sun, Shaowu Wang, Guoping Li, Ye Zheng (a special Chinese geophysics community) and Carlos Rodriguez, Nasser Hamarbitan, Chanpen Silawongsawat, Todor Todorov, Maria Donati, Nicholas Martin, Saul Guevara, Jitendra Gulati. The coffees and beers (sometimes geophysics too) with them have been making my life enjoyable.

Finally, I am profoundly grateful to my wife, Min Xu, for having been a mother and a father to our son, Jason, during most of the time in the past three and a half years in Beijing and in Calgary.

Table of Contents

List of Tables

List of Figures

Chapter 1

Introduction to Residual Statics Analysis

1.1 What is the problem?

What is happening when the seismic waves propagate through the near surface of the earth? This question is important not only for scientists who investigate the geophysical or geological structure or formation of the near-surface (the depth is not more than several hundred meters) layers, but also for those exploration seismologists whose interests are usually in the layers with depth up to thousands of meters. The properties of the seismic waves change much more dramatically in the near-surface weathering layers than in the deeper "solid" layers. The variation of the earth surface elevation and the variation of velocities and thicknesses of the near-surface layers have been problems for seismic data processing since the very beginning of this technology.

It is natural to consider the effects of the near-surface layers as signal filters because they change the amplitudes and phases of the passing seismic waves. The conventional convolution model used for deconvolution processing methods has been very successful in improving the resolution of reflection signals in seismic recordings. The convolution model seems not appropriate for the filtering effects of the near surface, because it seldom deals with the traveltime anomalies caused by near-surface effects. The near-surface "filter" character might be still too complex to investigate, and there is no research or application result available to remove the near-surface effects by estimating the response of such a filter.

The traveltime deviation on recorded seismic traces due to the near-surface anomalies is a more serious problem in seismic data processing than the amplitude and frequency distortions caused by these anomalies. Decades of practical applications have shown that near-surface effects can be virtually corrected by only estimating the resulting traveltime anomalies.

Static corrections (referred to as statics) are widely used to reduce the traveltime anomalies. The methods to estimate statics are often referred to as statics analysis methods. Statics benefit the later processing and the interpretations of the seismic data.

1.2 Basic assumptions

The assumptions applied to traveltime distortions in almost all the statics analysis methods can be expressed as following.

- **The traveltime distortion is frequency and amplitude independent**

  The anomalies caused by the near-surface layers only result in pure traveltime anomalies on seismic traces. Different frequencies and amplitudes may carry different amounts of time shift because of the near-surface filter character, but these differences are usually not the topics of statics analysis.

- **The traveltime distortion is time-invariant**

  The traveltime distortions on seismic traces due to the near-surface effects are independent of the reflection time of an event. It is this time-invariant property that makes the traveltime distortions called "static", which is the contrast to time-variant corrections (called "dynamic"), such as the normal moveout (NMO) correction.

- **The traveltime distortion is surface consistent**

  The "surface consistent" concept is used for those properties of seismic traces that do not change at a given surface source or receiver location. For the static problem, surface consistency means that: the static on a trace contains two parts, a source static and a receiver static. The same source static is shared by all the traces in a shot record, no matter where the receivers are located; the same receiver static is shared by all the traces recorded through the same receiver, no matter where the sources are located.

1.2.1 More on surface consistent assumption

The validity of the surface consistent assumption is illustrated in Figure 1-1, where the wave propagation velocities through the near-surface weathering layers are much lower than the velocities in the deeper layers. The ray paths of seismic waves in the weathering layers are closer to vertical according to the Snell's law. For seismic exploration experiments where the source to receiver offsets are limited within several thousand meters, the reflection seismic signals from the target with certain depth propagate nearly vertical in the near-surface weathering layers. The waves that depart from the same source or reach the same receiver have very little traveltime differences in near-surface layers.

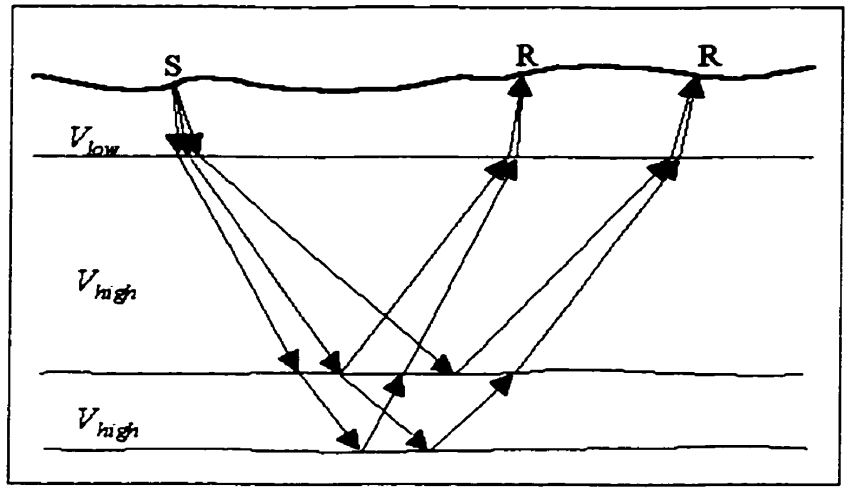

Figure 1-1: The validity of the surface consistent assumption for statics analysis. The ray paths of the seismic waves in the lower-velocity layers are very close to vertical.

If a source and a receiver are located at the same place (this happens routinely in seismic experiments), according to surface consistent assumption, the source static and the receiver static at this location should be the same. This may be correct for some ideal conditions, but in the real world, the sources and the receivers have many different physical properties. For example, the sources may be in holes with depths from 5 to 25 meters, while the geophones are at the surface. A seismic trace is not always recorded through a single geophone, but is usually an averaged signal passing through several geophones (arrays) with certain physical distance between them. In addition, the wave

properties (amplitude and phase) close to a source where the seismic waves are created may be different from those properties after the waves transmit and reflect through the earth.

The surface consistent assumption becomes weaker when the velocities of near-surface layers are not much lower than the velocities in the layers below. However, the traveltime anomalies caused by high velocity near-surface layers will be less serious than those caused by low-velocity near-surface layers. Even in these cases, surface consistent static corrections may still help.

Different from the previous two assumptions, which are mainly for the purpose of simplifying the complexity of the static problem, the surface consistent assumption should be considered as a constraint on the traveltime distortion estimations. This constraint is useful because the traveltime distortion estimations may be incorrect due to the errors in the required information, such as the initial estimates of the near-surface velocities. Static correction with these estimations may cause some undesired traveltime errors.

1.3 Field Static corrections

Static corrections in seismic data processing are practically completed by two different procedures: field static corrections and residual static corrections. The estimation of field statics is based on the earth surface topography and the near-surface velocity and thickness information. Field statics can be estimated using elevation methods or refraction methods, and they are called elevation statics and refraction statics respectively. Uphole information sometimes is used separately for static corrections, which are called uphole statics (Margrave, 1999).

1.3.1 Datum plane

Ideally, we wish that the seismic experiments could be done on a perfectly flat plane, when many techniques in exploration geophysics could be accurately applied. The common midpoint (CMP) stacking technique, for example, is based on flat surface assumption. However, the earth surface is seldom flat in the scale of the range of a 2D

seismic experiment (usually greater than 5 kilometers). Even when the earth surface can be considered flat, the velocities and thicknesses of the near-surface layers may still change significantly. In order to apply data processing techniques properly, seismic traces are shifted to some fixed reference depth level called "datum plane" or shortened as "datum".

There is another important reason for datum correction. The velocity and thickness properties of the deeper layers are usually less variable than those of the near-surface layers. Time anomalies, fundamental in seismic data interpretation, may be caused by near-surface effects rather than the subsurface geological structures themselves. Therefore, correction of the near-surface effects and relocation of the data to a proper datum not only benefit the data processing but also provide more distinct anomaly information for seismic interpretation.

1.3.2 Elevation statics

Elevation statics compensate for the elevation difference between the datum and the elevations of the sources and receivers. Elevation statics methods use source and receiver elevations and uphole information if available. Uphole information that contains uphole time (from the source to the surface) and the hole depth can provide weathering-layer velocity information. If the uphole time is not available or not reliable, a pre-estimated weathering velocity should be provided.

A problem that may occur to elevation statics methods is that the source hole depth is not the real thickness of the weathering layer, and there is no direct way to observe the thickness. This problem is obvious when the sources are located at surface, such as Vibroseis sources. In this case, the elevation static corrections reduce to a surface elevation correction only, and the amount of the time corrections depends very much on the choices of the average near-surface velocity, usually referred to as the replacement velocity.

1.3.3 Refraction statics

Refraction statics analysis methods use the first refraction arrival times (called first breaks) on the seismic traces. The first breaks provide information to estimate the velocities and thicknesses of near surface layers (but not the weathering layer). Not only the traveltimes through these layers can be estimated, a more reasonable replacement velocity can also be selected for the final datum correction.

The quality of the refraction static estimates depends on the quality of the first break picking. High redundancy of the seismic data provides significant improvement on the statistical quality of the first breaks and the static corrections themselves.

The magnitude of elevation statics and refraction statics can be significantly different due to the different choices of datum plane and replacement velocity.

1.4 Residual statics

1.4.1 Why residual statics?

The static corrections estimated by elevation and refraction methods usually leave residual errors. The simplifications of the algorithms and the inaccuracy of the required information rarely allow the field statics to totally remove the near-surface effects. The remaining traveltime errors are usually called residual statics.

Field statics tend to correct the long wavelength contents of the traveltime distortions due to near-surface anomalies. The accuracy and resolution of the near-surface information, such as the wave velocities and the thickness of the near-surface layers, and the first breaks, may be not enough to resolve more detailed short-wavelength portion of the static errors. Reducing the short wavelength static errors may require the utilization of the higher-resolution reflection seismic signals and some other mathematical and statistical techniques. Automatic residual statics methods, such as Hileman et al. (1969), Taner et al. (1974), Wiggins et al. (1976), and Ronen and Claerbout (1985), have been very reliable for compensating for the shortcomings of the field statics analysis methods. Both field statics and residual statics are routinely applied in seismic data processing.

1.4.2 Relativity of residual statics

The physical basis of residual statics analysis is that the wavelets reflected from the same reflector in the subsurface should be aligned smoothly on closely located seismic traces. (That two seismic traces are closely located means their sources and their receivers are closely located.) The residual static corrections can be considered as the *relative* time shifts between traces that tend to align the wavelets of seismic reflection events smoothly. In the common midpoint (CMP) domain, for example, it is often expected that the residual static corrections will produce better normal moveout semblance to improve velocity analysis and obtain superior stacked sections.

The *relativity* of residual statics is strictly limited. For example, continuity of reflection events remains unchanged when all the traces are shifted with the same amount of time (a datum change). However, the stacking velocities will change because they are related to the *absolute* traveltime. If the constant shift is too large, proper stacking velocity will no longer be obtained because the traveltime trajectory may deviate from any possible normal moveout curves. If the field statics have provided a good solution to the long wavelength time anomalies, the residual statics should approximately maintain the *absolute* traveltimes of reflection events.

When there are large elevation changes along the seismic line, static corrections directly to the final datum may cause difficulties to observe appropriate velocity information. In this case, the seismic traces may better be corrected to a variable elevation level called a "floating datum". A floating datum reduces the change of the absolute traveltime on seismic traces. The static corrections for floating datum can be obtained by removing the long wavelength trend from the field statics for final datum. These statics for floating datum might be called residual field statics, and they have the same characteristics of residual statics.

Generally speaking, the residual statics are the plus-minus errors with respect to the long wavelength trend of traveltime anomalies due to the near-surface effects. Their values are statistically expected to be zero, or simply have a zero average.

1.4.3 A short review of previous works

Although many methods of automatic residual statics analysis have been introduced into practical usage since the 60's, estimation of residual statics is still one of the major concerns in seismic data processing.

The earliest published papers are Hileman et al. (1968), Garotta and Michon (1968), Disher and Naquin (1969), Irvine and Worley (1969), Saghy and Zelei (1975), and it is these papers that presented the fundamental concepts of modern technique of automatic residual statics. Taner et al. (1974) and Wiggins et al. (1976) have given excellent comprehensive descriptions of the former methods with their own incisive discussions. Taner et al. (1974) clearly formulated the mathematical model of the statics problem and discussed in detail the standard mathematical algorithm (Gauss-Seidel iteration algorithm) for solving the problem of surface consistent residual statics. Wiggins et al. (1976) extended the discussions to the capability and the limitations of the algorithms used to solve the problem. The well-known conclusion from Wiggins et al. (1976) is that, residual statics analysis can resolve the short-wavelength content of the traveltime distortions, but the estimation of the long-wavelength trend is limited by the spread length of the recording cable (spread length).

Many of the above papers mentioned the importance of forming static reference traces (also called pilot or model traces), but they mainly concentrated on how to obtain better surface consistent source and receiver statics by decomposing the estimated traveltime deviations on seismic. The decomposition process implicitly assumes that the pre-estimated traveltime deviations are accurate, or at least reliable. There are two direct factors that may influence the reliability of the time-shift estimations on seismic traces. First, the reference traces are not really traveltime-error free, and second, the time-shift estimation technique may not be accurate enough. The decomposition of the pre-estimated time-shifts is important, but more attention could have been paid to obtain more reliable time-shift estimates before decomposition.

Ronen and Claerbout (1985) approached the residual statics from a different point of view. Instead of depending on the estimated time-shifts, they developed a method called

stack-power maximization, which updates the reference traces and time-shift estimations every time when a surface consistent static is estimated and applied. In their terms, the previous methods were called traveltime-picking methods, and in contrast, their method was called an optimum-type method.

Almost all the residual statics methods require the seismic data be normal moveout (NMO) corrected. As Taner et al. (1974) mentioned, there are reasons for analyzing residual statics on NMO corrected data. One of them is that the traveltime delays caused by wave velocities and source-receiver offsets are generally much larger than traveltime deviations caused by other factors (such as residual static anomalies). NMO correction by appropriate velocities reduces the size of dynamic delays to smaller scale errors called residual normal moveout (RNMO), and this makes the residual static errors more evident. However, as we will discuss in the next chapter, there are also some shortcomings for residual statics analysis after NMO correction.

There are some methods that estimate residual statics before NMO. As noticed by several authors as early as in 70's (Disher and Naquin (1970), Taner et al. (1974), Waters (1978)), the signal coherency between traces in common offset domain is independent to the velocity influences. Increasing the signal coherency can be a criterion for residual statics analysis, which does not need velocity information and can be applied before or after NMO correction. Chan and Stewart (1996) applied f-x prediction filter in each offset section to enhance the signal coherency and the filtered traces can be used as references for static estimations.

The most recent concept of residual statics analysis may be the one introduced by Tjan et al. (1994) and Larner (1998). The authors presented a method that used prestack depth migration followed by its inverse (called de-migration) as a tool to form reference traces. Some results of this method are obtained from the Marmousi data with synthetic static time-shifts. A difficulty of this method is the high velocity-dependency of depth migration and de-migration process. Larner (1998) suggested that it is possible to estimate both the velocity model and the residual statics in an iterative way.

The method to be presented in the later chapters in this thesis forms reference traces using the principles of equivalent offset migration (EOM). The residual statics are estimated before NMO correction, and a minimum of velocity information is required.

Chapter 2

Principles of Residual Statics Analysis

This chapter discusses in detail the general procedures of the various algorithms for the estimation of surface consistent residual statics. In section **2.1**, a three-step scheme is introduced for comparing different methods. The following sections, **2.2**, **2.3** and **2.4**, discuss each step in the scheme with typical algorithms reviewed. Section **2.5** concentrates on the iterative techniques related to residual statics analysis in seismic data processing.

2.1 The basic methodology

The main scheme of most algorithms of automatic residual statics analysis can be simply expressed as the following steps:

Step1: Use the reflection information on seismic traces to form reference traces that have less or no traveltime deviations due to near-surface anomalies.

Step2: Compare each seismic trace and its corresponding reference trace to estimate the time-shift between them.

Step3: Decompose the estimated time-shifts on every seismic trace into surface consistent source statics and receiver statics.

This three-step procedure is also illustrated in Figure 2-1. The starting point of the whole process is the seismic reflection data itself. Reference traces are formed in Step 1. Both the seismic traces and the reference traces are input to Step 2, and they are correlated to estimate the possible traveltime shifts on seismic traces. This correlation is usually performed for every seismic trace to take advantages of the high redundancy of seismic experiments. Step 3 uses the estimated time shifts from Step 2 as input to decompose the time shifts into surface consistent source and receiver statics.

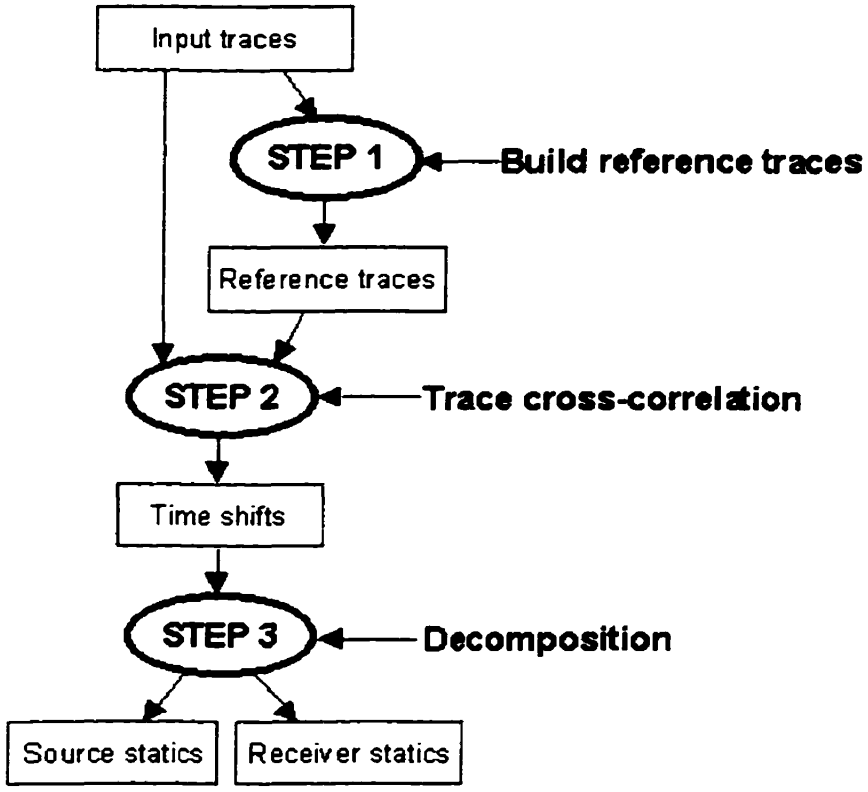

Figure 2-1: Three-step procedure for general methods of residual statics analysis

The algorithm for each step can be different and theoretically it does not influence the performance of other steps. Different methods of residual statics analysis may use different approaches for step 1 and/or step 3, while most methods use the same tool (cross-correlation) for step 2. In many methods, the algorithms for step 1 and the algorithms for step 3 are closely related. For example, most conventional methods require correlating NMO corrected traces, so the NMO errors should be considered during the decomposition of surface consistent statics. On the other hand, if the reference traces are formed before NMO correction (Step 1), then the surface consistent decomposition (Step 3) should not contain the term related to NMO errors.

The estimated time shifts from Step 2 are usually not directly applied to the seismic traces, because these estimates may contain some errors caused by improper reference traces or inaccurate time-shift estimation techniques. The surface consistent assumption

utilises the high redundancy of the seismic data to reduce the statistical errors in the time-shift estimations.

CMP trim static correction is usually the final step in aligning reflection events for the CMP stacking. In this technique, the time shifts estimated by correlation (Step2), which are not surface consistent, are directly applied inside each CMP gather. The reflection events after NMO correction are artificially aligned in time. Usually, the maximum amount of trim statics is limited to a much smaller range, 10 milliseconds, for example, than that of surface consistent statics. The application of trim statics must assume that the NMO velocities are accurate enough and surface consistent residual statics can not provide a better solution of traveltime corrections. The trim statics are often event-dependent (time-variant), and become a compensation of the inaccuracy of time-independent assumption for statics analysis.

2.2 Reference traces

Almost every residual statics analysis method has its own way to find or form reference traces. Instead of discussing each specific way to form reference traces, I present some aspects in which these algorithms may be different or similar to each other.

2.2.1 Internal or external reference model

Some methods choose one trace or several traces from the same dataset as the reference trace(s) for a given trace. These reference traces are called *internal* reference traces. In contrast, reference traces that are not directly selected from the dataset, such as spatial-filtered CMP stacked traces, are called *external* reference traces.

Many earlier methods, such as Hilman et al. (1968), use internal reference traces for statics analysis. The validity of choosing an internal reference is based on the assumption that the traces in one CMP gather after proper NMO correction are similar to each other. The meaning of this similarity is that the reflection signals from the same subsurface reflector should (1) reside at the same traveltime location and (2) have the same (at least close) phase information. The time differences, among the NMO corrected traces in the same CMP gather, are considered the effects of static shifts. Statistically, any trace can be

the reference of the other trace in the same CMP gather. The estimations may be different due to different reference-trace selections, but this reference-trace dependence can be statistically removed by subtracting the mean value from the all time-shift estimations.

As a natural extension, a CMP stacked trace can be a reference trace for all the NMO corrected traces in this gather. The brute or intermediate stacked-sections are the mostly used external model data for residual statics analysis. This is consistent to the original purpose of residual statics analysis, which is to obtain the best stacked-sections.

Any two traces may contain different traveltimes for a given event before NMO correction. In a source, receiver or CMP gather, the differences caused by offset differences always exist; while in the common offset section, any dipping structure related to a reflector results in traveltime differences. This implies that NMO correction makes internal reference traces possible in source, receiver or CMP gathers. However, NMO may not be necessary for methods using external model data. For example, the f-x statics method (Chan and Stewart, 1996) creates reference data by applying f-x prediction filter in common-offset sections, where no velocity information is involved in the entire process. Another external-model method is the one discussed by Tjan et al. (1994) and Larner (1998) which uses prestack depth migration and its inverse process (called de-migration) to create reference traces.

The method to be presented in this thesis is an external-model method, where reference traces are created using the prestack time migration equivalent-offset concept (Bancroft and Geiger, 1994 and Bancroft et al., 1998).

2.2.2 NMO correction: necessary or not

Why NMO correction has been a default requirement for conventional residual statics methods can be explained in following different but relevant ways:

- The original aim of residual statics correction is to obtain the best possible stacked sections and NMO is always needed for CMP stacking.

- NMO correction is a direct way to enhance the similarity between prestack seismic traces. It is easier to form reference traces (such as stacked traces) after NMO correction.
- Dynamic traveltime differences caused by velocity and offset differences are much larger than the size of residual statics. NMO reduce these dynamic differences to the minimum possible and the residual statics are easier to identify.

Because of these advantages, NMO correction is still the standard process for preparing data for residual statics analysis. However, some limitations of NMO correction should be considered when applied to residual statics analysis:

- NMO correction is based on the assumption that the CMP moveout trajectory is approximately hyperbolic. This assumption is violated in areas where subsurface velocity structure is complex.
- NMO correction requires velocity information, which is sometimes difficult to observe when residual statics are significant. Improper NMO correction may in turn cause incorrect static estimations. Even when the residual NMO errors are considered during the statics analysis, the influence from these errors can not be perfectly removed.
- Statics are assumed to be a time-invariant property of seismic traces, while NMO correction is a time-variant (dynamic) operation. The NMO correction slightly changes the time-independence of the statics on seismic traces. NMO stretch is an example of the dynamic effects of NMO correction. It dramatically changes the spectrum and phase information of the events at the shallow or far-offset parts of the seismic reflection signals, and makes these parts not appropriate for being traveltime reference.

As early as in 60's and 70's, many authors, such as Disher (1970), Taner et al. (1974) and Waters (1978), mentioned the possibility of velocity independent approach of residual statics analysis by utilising the signal coherency in common offset domain. The f-x statics method by Chan and Stewart (1996) is a practical example. The limitation of

common offset domain methods is that dramatic lateral velocity variation or faulted structures may destroy the lateral continuity of reflection signals. In these cases, forming reference traces using migration concepts may have its advantages as discussed in the following section.

2.2.3 Migration and de-migration

Tjan, Larner and Francois (1994) presented a method for residual statics estimation using prestack depth migration and de-migration. This de-migration is the inverse operation of depth migration, and can be considered as a modelling process using the depth image as the known reflection coefficients. The concept of this method can be interpreted as:

- If the migration velocity is accurate enough (main assumption), depth migration should be able to produce reliable subsurface structure image because the randomness of the residual statics is statistically destructive. This destructive property is similar to that of CMP stacking that makes stacked traces less affected by the randomness the residual statics on the NMO corrected traces.
- From the migration image, whose amplitude at any location may be considered as a reflection coefficient, a seismic modelling process is performed as the inverse of the depth migration. This modelling process has much less near surface effects than the real seismic experiment. Thus a new set of pre-stack multi-offset modelling data is formed.
- This modelling data can be used as the reference data for residual statics analysis, because the traveltime information should be more reliable due to the destructiveness of the random static shifts during migration.

Tjan et al. (1994) and Larner (1998) showed some results of applying this method to the Marmousi model data. The results demonstrate that the statics can be estimated with certain accuracy, as long as the depth migration velocity profile is accurate.

The requirement of an accurate velocity model is not always valid for field seismic data. The velocity model building actually becomes an integrated part of depth migration

itself, especially for the data from complex-structure areas. An iterative approach was suggested to improve the estimation of the residual statics and the migration velocity.

The computation cost of this depth migration followed by de-migration process is a disadvantage even when the migration velocity can be observed. Instead of using full depth prestack migration and its inverse process (multi-offset modelling), it is possible to formulate an inverse process (still call it de-migration) for more efficient time migration process. The EOMAP method to be presented in chapter 4 is one example.

2.3 Cross-correlation

In this section, some basic concepts of cross-correlation and its applications to residual statics analysis are discussed. In seismic data processing, cross-correlation may be used to

- estimate the time difference between two traces;
- detect quantitatively the similarity between two traces;
- tell how reliable time-shift estimations are;
- detect if a time series have the correct signal polarity (for example, if a seismic trace is reversed due to some acquisition reasons).

Almost all the methods for residual statics analysis use cross-correlation as the tool to compare two traces for their possible traveltime difference, and it has been proved simple and efficient. Usually, it is assumed that the reference traces are similar to their corresponding original traces, so cross-correlation is used mainly for time-shift estimation. However, if the similarity is not good enough or the maximum value of the cross-correlation function cannot be well defined, the reliability of the traveltime difference estimations becomes a problem.

2.3.1 Mathematical definition

The cross-correlation of two traces (time series) $X(t)$ and $Y(t)$ is another time series $R(\tau)$, and it is defined as

$$R(\tau)=\sum X(t+\tau)\cdot Y(t). \tag{2-3-1}$$

The time variable τ is usually called lag time or time shift. The summation is over all the possible time ranges of X and Y of interest.

This definition directly implies the following property of cross-correlation,

$$R(\tau)\le\frac{1}{2}\left[\sum X^2(t)+\sum Y^2(t)\right]. \tag{2-3-2}$$

If there is a time location τ_0 such that $X(t+\tau_0)$ equals to $Y(t)$ for all the t, then R reaches its maximum value at this shifted time τ_0, because

$$R(\tau_0)=\sum X(t+\tau_0)\cdot Y(t)=\sum X^2(t)=\sum Y^2(t)=\frac{1}{2}\left[\sum X^2(t)+\sum Y^2(t)\right]. \tag{2-3-3}$$

On the other hand, if trace Y is known as a time-delayed version of trace X, but the lag time is unknown, then cross-correlation between X and Y can tell this delay time amount by the time where R reaches its maximum value.

The amplitudes of correlation traces are not essential if only the time-shift between them is interested. Cross-correlation between trace aX and trace bY will give the same lag-time estimation as the cross-correlation between X and Y, where a and b are any positive numbers. However, the amplitude information of the cross-correlation function R can be very useful if the two correlation time series X and Y are normalised as

$$\tilde{X}(t)=\frac{X(t)}{\sqrt{\sum X^2(t)}} \text{ and } \tilde{Y}(t)=\frac{Y(t)}{\sqrt{\sum Y^2(t)}},$$

or define the normalised cross-correlation (denoted as R_N) as

$$R_N(\tau)=\frac{\sum X(t+\tau)\cdot Y(t)}{\sqrt{\left(\sum X^2(t)\right)\left(\sum Y^2(t)\right)}}. \tag{2-3-4}$$

The normalization makes the amplitudes of cross-correlation function R_N limited between -1.0 and 1.0, i.e., $-1.0\le R_N\le 1.0$. If at some τ_0, $R_N = 1.0$, then equation $X(t+\tau_0)=cY(t)$ (c is a constant) must hold at any time t in the relevant time range. Practically, two different seismic traces never yield a cross-correlation value equal to 1.0 (or -1.0) at any shift time because of noise, time-range limitation and other reasons. Two traces are

considered very similar if the cross-correlation has value close to *1.0*. The cross-correlation function not only tells how much one trace is possibly time shifted from the other, the amplitudes of R_N also quantitatively tells how similar the two traces are.

The following sections discuss some practical considerations when using cross-correlation as a tool to estimate possible time difference between two seismic traces: a major step in residual statics analysis.

2.3.2 Correlation domains

In seismic data processing, a set of prestack data can be processed and analysed in the following four domains:

- common source domain;
- common receiver domain;
- common mid-point (CMP) domain and
- common offset domain.

Cross-correlation between traces in different domains provides time difference estimation with different components, such as dynamic or static components as in Table 2-1. These time differences always contain the contribution from source or receiver statics, thus, for residual statics analysis, cross-correlation can be performed between traces in any one of the four domains as long as those components other than residual statics can be separated properly.

Comprehensive discussions about traveltime differences between traces in these four domains by Taner et al. (1974) are summarised in Table 2-1.

The traveltime difference of a reflection event on two traces from a common source gather may be caused by

- the difference between receiver statics,
- the difference at different CMP locations caused by the structure of the corresponding reflector, and

- the influence from wave velocity because of the offset difference.

Similarly, the traveltime difference between two traces in the same common receiver gather is caused by different source statics, reflector dips and offset. For two traces in the same CMP gather, the traveltime difference between them contains both the source and the receiver statics, and the influence from velocity. The traveltime difference between two traces with the same offset contains both the source and receiver statics and the effect from reflector dips.

Table 2-1: The influences of dynamic factors and static factors to traveltime differences

	DYNAMIC		STATIC	
Domains	Dip	Velocity	Source	Receiver
Common Receiver	✔	✔	✔	✖
Common Source	✔	✔	✖	✔
Common Offset	✔	✖	✔	✔
Common Mid-Point	✖	✔	✔	✔

* "✔" means influence exists and "✖" means no influences. (after Taner et al., 1974)

Practically, the following two assumptions are widely accepted.

- The differences caused by reflector dips and the offset differences are the long-wavelength content of the traveltime differences;
- The source and receiver statics are relatively the short wavelength content of the traveltime difference.

The cross-correlation between traces in a common *shot* gather can produce receiver static estimations, and cross-correlation between traces in a common *receiver* gather can produce source static estimations, as long as proper filters are applied to remove the long wavelength content of the static estimations (sometimes might be impossible). Similarly, cross-correlation between traces in a CMP gather or common offset section provide traveltime differences that contain both source and receiver statics as the short

wavelength content. In these two domains, surface consistent decomposition is needed to separate source and receiver statics along with the long wavelength content removal.

2.3.3 Maximum possible time shift

The range of time-shift variable τ is limited for residual statics analysis, and cross-correlation beyond these limits are not evaluated. In P-P wave seismic data processing, the possible maximum residual statics are usually limited within 30 milliseconds.

The cross-correlation function may sometimes have more than one local positive maximum values. This happens more often when the dominant frequency of the correlating traces is relatively high. For example, if the maximum possible time shift on seismic traces is from –30 ms to 30 ms, then the dominant frequency of the correlation traces may be better less than $1000/60=16.7Hz$ to avoid multiple maximum values.

Lowpass filtering of the correlating traces and/or reducing the time-shift range can prevent the possibility of multi-maximum–value cross-correlation function. However, there are still some cases in which the wrong maximum value is picked and the estimated time-shift skips one more (or even more) cycles. Cycle-skipping usually happens when one of the events on one correlating trace is occasionally highly correlated with a different event on the other correlating trace. Some authors invented special algorithms to avoid cycle-skipping problem, such as the envelope method introduced by Deng et al. (1996).

The cross-correlation functions should have reasonable positive values if the correlation traces have certain similarity within the limits of the time shifts. (Otherwise, the reference traces are considered improper.) In this case, the maximum value of a cross-correlation function can be picked and the time shift can be estimated. The shift time, τ, is usually automatically sampled with the same rate as the correlation traces, but the maximum value of the cross-correlation may not happen to be at the sampled grid nodes. In practice, interpolation of the second or higher order of the cross-correlation is needed to obtain more accurate shift time estimates.

2.3.4 Trace windowing for correlation

In the definition of cross-correlation function in 2.3.1, the time range over which the summation is performed was assumed as large as it is needed. In practice, the cross-correlation is usually performed between segments of seismic traces. The length of these trace segments is important. The following items are some aspects that may need to be considered for this matter.

Higher signal-to-noise ratio: it is better to select the time range where both correlation traces have higher signal to noise ratios. This will give more reliable estimates of the time shifts. Choosing a time window containing one of the strongest and most stable events may also increase the stability of the statics estimations.

Large time range: the time range should always be large enough to contain several recognisable events. Practically it should be many times longer than the maximum time shifts allowed. Theoretically, the longer the correlation traces, the better the static estimates fitting the static property in the whole trace range. In practice, because of the quality of reference traces and the signal quality of the reflection data itself, some parts of the traces may not be good for cross-correlation. For example, the shallow part of the NMO corrected traces are usually not used because of the NMO stretch effects.

2.4 Decomposition procedure

Many residual statics analysis methods, especially those before Ronen and Claerbout (1985), concentrated on how to decompose the estimated time shifts on the seismic traces into surface consistent source and receiver statics.

2.4.1 The initial mathematical model

The decomposition is mainly a mathematical process, and it is convenient to express our geophysical problem as a mathematical model used by general decomposition algorithms. The mathematical analysis of residual statics begins with the expression of

the traveltime model based on a simplified seismic ray-path geometry illustrated as in Figure 2-2. Suppose that there is a trace with its source located at S and its receiver located at R, then the total traveltime for some given reflection event can be written as

$$T_{SR} = T_{SS_D} + T_{S_DR_D} + T_{R_DR}. \tag{2-4-1}$$

Where (Wiggins et al. 1976):

- T_{SR} is the total traveltime for this event on this trace;
- T_{SS_D} is the traveltime from the source to a reference plane, which may be the base of the weathering layer;
- $T_{S_DR_D}$ is the traveltime from the reference plane down to the reflector corresponding to the event and the traveltime from the reflector back to the reference plane;
- T_{R_DR} is the traveltime from the reference plane back to the receiver.

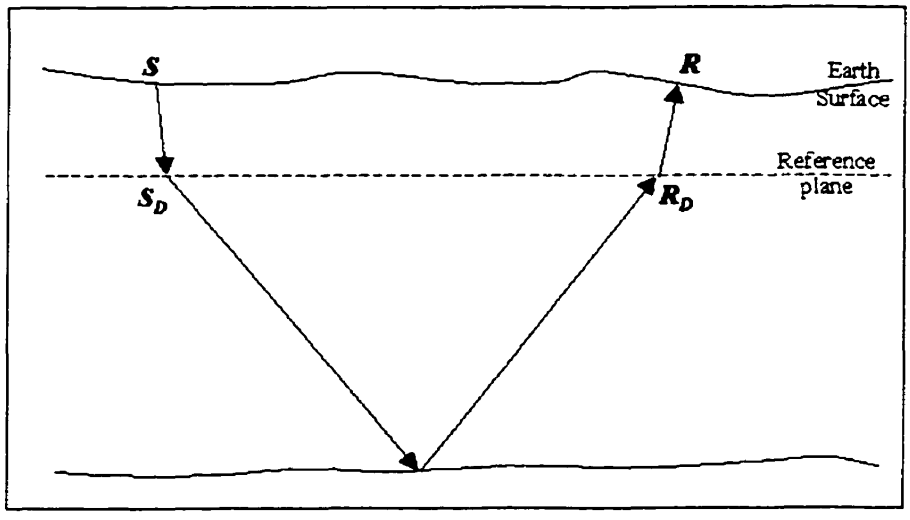

Figure 2-2: Ray-path geometry for the mathematical model of residual statics problem. S and R are the source and receiver locations, and S_D and R_D are at some reference plane beneath the source and receiver.

Suppose ΔT_{SR} be the traveltime anomaliy on this trace due to the near surface effects (which implies that there are no errors in term $T_{S_DR_D}$), it should contain a source related term (source static shift) ΔT_S, a receiver static shift ΔT_R and some errors, i.e.,

$$\Delta T_{SR} = \Delta T_S + \Delta T_R + Error. \qquad (2\text{-}4\text{-}2)$$

The error term can be caused by many factors, such as:

- The error left from field static corrections,
- The possible error due to surface consistent assumption itself.

Decomposition of the estimated time-shift ΔT_{SR} into source and receiver statics is based on the assumption that the error term in equation (2-4-2) is statistically much smaller than the statics themselves. The decomposition process tends to put as much of ΔT_{SR} as possible to the sum of ΔT_S and ΔT_R, i.e., it tries to obtain a set of source and receiver statics so that the error terms become as small as possible.

Suppose there are N_S source locations and N_R receiver locations in a seismic experiment, and all the receivers are active for all the sources. From equation (2-4-2) (without the error term), a system of linear equations can be formed as,

$$\Delta T_{S_i R_j} = \Delta T_{S_i} + \Delta T_{R_j}, \qquad (2\text{-}4\text{-}3)$$

where $i = 1, 2, \ldots, N_S$, and $j = 1, 2, \ldots, N_R$. The N_S+N_R unknowns in this system are

$$\{\Delta T_{S_i}, i = 1,2,\cdots,N_S; \Delta T_{R_j}, j = 1,2,\cdots,N_R\}.$$

Equation (2-4-3) is the initial mathematical model for residual statics decomposition, which is derived from the basic assumptions in Chapter 1. It is different from the equation systems discussed by many other authors (Taner et al. (1974), Wiggins et al. (1976) and Ronen and Claerbout (1985)) because they used additional assumptions of the subsurface consistency and offset consistency. These two additional assumptions can be used to further analyze the error terms in the linear equation system, and will be discussed in later sections (**2.4.3** and **2.4.4**).

The next section discusses two properties of the linear equation system (2-4-3), i.e., over-deterministic and under-constrained. These two properties, however, also apply to the more general linear systems as discussed in sections **2.4.3** and **2.4.4**.

2.4.2 Over-determined and under-constrained

The equation system built by (2-4-3) can be expressed in matrix form as

$$\mathbf{A}\cdot\mathbf{P}=\mathbf{T}, \tag{2-4-4}$$

where **P** and **T** are column vectors with length N_S+N_R and $N_S\times N_R$ respectively,

$$\mathbf{P}=\begin{bmatrix}\Delta T_{S_1}\\ \Delta T_{S_2}\\ \vdots\\ \Delta T_{S_{N_S}}\\ \Delta T_{R_1}\\ \vdots\\ \Delta T_{R_{N_R}}\end{bmatrix}_{(N_S+N_R)\times 1} \quad \text{and} \quad \mathbf{T}=\begin{bmatrix}\Delta T_{S_1R_1}\\ \Delta T_{S_1R_2}\\ \vdots\\ \Delta T_{S_1R_{N_R}}\\ \Delta T_{S_2R_1}\\ \vdots\\ \Delta T_{S_2R_1N_R}\\ \vdots\\ \Delta T_{S_{N_S}R_{N_R}}\end{bmatrix}_{(N_S\times N_R)\times 1},$$

and the coefficient matrix **A** is

$$\begin{bmatrix}
\left.\begin{matrix}1&0&0&\cdots&0&1&0&0&\cdots&0\\1&0&0&\cdots&0&0&1&0&\cdots&0\\ \vdots& & & &\vdots&\vdots& & & &\vdots\\1&0&0&\cdots&0&0&0&0&\cdots&1\end{matrix}\right\}N_R\\
\left.\begin{matrix}0&1&0&\cdots&0&1&0&0&\cdots&0\\ \vdots& & & &\vdots&\vdots& & & &\vdots\\0&1&0&\cdots&0&0&0&0&\cdots&1\end{matrix}\right\}N_R\\
\vdots\\
\left.\begin{matrix}0&0&0&\cdots&1&1&0&0&\cdots&0\\ \vdots& & & &\vdots&\vdots& & & &\vdots\\0&0&0&\cdots&1&0&0&0&\cdots&1\end{matrix}\right\}N_R
\end{bmatrix}_{(N_S\times N_R)\times(N_S+N_R)}$$

(N_S columns | N_R columns)

There are usually many more equations, ($NS\times NR$), than the unknowns, ($NS+NR$), so this linear equation system is called over-determined. On the other hand, the number of independent equations, which is the rank of the matrix **A**, is less than the number of

unknowns, so this system is also called under-constrained. The under-constrained property can be proved by linear algebra theory (See the following boxed text).

PROOF of under-constrained property:

The $N_S \times N_R$ row vectors in matrix **A** can be denoted as $\{V_1, V_2, \ldots, V_{(NS \times NR)}\}$ for simplicity. All these vectors can be grouped for source locations numbered as $s=1,2, \ldots, N_S$. In each group, subtracting the first vector ($r=1$) with any other vector ($r=2, \ldots, N_R$) results in a vector independent to the source number s. That is, equation

$$V_{(s \times N_R+1)} - V_{(s \times N_R+r)} = [0 \ \cdots \ 0 \ \ 1 \ \ 0 \ \cdots \ 0 \ \ -1 \ \ 0 \ \cdots \ 0] = V_1 - V_r$$

holds for any $s = 1, 2, \ldots, (N_S-1)$. For each r, This vector has only two non-zero elements, which are 1 at (N_S+1) and -1 at (N_S+r). By rearranging the equation as

$$V_{(s \times N_R+r)} = V_{(s \times N_R+1)} + V_r - V_1,$$

it can be seen that the vectors $\{V_{(s \times N_R+r)} : s = 1,2,\ldots,(N_S-1), r = 2,3,\ldots,N_R\}$ (totally $(N_S-1) \times (N_R-1)$) can be linearly expressed by the other (N_S+N_R-1) vectors,

$$\{V_1, V_2, \ldots, V_{N_R}, V_{N_R+1}, V_{2N_R+1}, V_{3N_R+1}, \ldots, V_{(N_S-1)N_R+1}\}.$$

This means the rank of the matrix can not be more than (N_S+N_R-1), therefore it is always less than (N_S+N_R), which is the number of unknowns.

END-OF-PROOF

The discussions above are based on the assumption that all the receivers are active for all the sources. However, the number of traces recorded is much more than the total number of source and receiver locations for most seismic experiments, and this ensures the over-determined property of the linear system. On the other hand, when some receivers are not active for some sources, the number of traces is reduced, but the total number of source and receiver locations does not change. This implies that, in the linear equation system discussed above, some equations are dropped but the number of unknowns remains the same. Thus, the system is still under-constrained.

The rank of the coefficient matrix **A** is always less than (N_S+N_R), and this makes the (N_S+N_R) by (N_S+N_R) square matrix $(\mathbf{A}^T\mathbf{A})$ (the superscript **T** means matrix transposition) still under-constrained. Therefore the least-square-error technique can not be directly

applied to solve linear system (2-4-4). For clarity, let NS = 3 and NR =2, and simplify the symbols in (2-4-4) as $\Delta T_{Si} \rightarrow S_i$, $\Delta T_{Ri} \rightarrow R_j$, and $\Delta T_{SiRj} \rightarrow T_{ij}$, then the least square normal equation becomes

$$\left(\mathbf{A}^{\mathrm{T}}\mathbf{A}\right)\mathbf{P} = \mathbf{A}^{\mathrm{T}}\mathbf{T},$$

and can be explicitly expressed as

$$\begin{pmatrix} 2 & 0 & 0 & 1 & 1 \\ 0 & 2 & 0 & 1 & 1 \\ 0 & 0 & 2 & 1 & 1 \\ 1 & 1 & 1 & 3 & 0 \\ 1 & 1 & 1 & 0 & 3 \end{pmatrix} \begin{pmatrix} S_1 \\ S_2 \\ S_3 \\ R_1 \\ R_2 \end{pmatrix} = \begin{pmatrix} T_{11}+T_{12} \\ T_{21}+T_{22} \\ T_{31}+T_{32} \\ T_{11}+T_{21}+T_{31} \\ T_{12}+T_{22}+T_{32} \end{pmatrix}.$$

The fact that the matrix $(\mathbf{A}^{\mathrm{T}}\mathbf{A})$ is not full rank can be easily checked by summing the first three (row or column) vectors and summing the last two (row or column) vectors. A direct way to solve this equation system is to add a small positive number λ to the diagonal of the coefficient matrix $(\mathbf{A}^{\mathrm{T}}\mathbf{A})$, which allows the equation system have a unique solution. This solution is close to the desired statics as long as number λ is small. Some details can be found in Taner et al. (1974).

The values of N_S and N_R are usually much larger than *3* and *2*, and large (N_S+N_R) makes the direct solution of the equation system not practical. Another method that is more often used is the Gauss-Seidel iterative method, which will be discussed in more detail in section **2.5.1**, and in Appendix A.

2.4.3 Subsurface consistent assumption

Theoretically, there are no traveltime errors related to $T_{S_D R_D}$ of equation (2-4-1). In practice, there are always some errors left in $T_{S_D R_D}$ because of the inaccuracy of field statics accuracy, quality of reference traces, and the limitations of the surface consistent assumption. These errors can sometimes be significant enough to influence the accuracy of the decomposition of surface consistent statics.

It is reasonable to consider that a part of the error in equation (2-4-2) may be caused by the anomalies residing in the traveltime through the subsurface. To investigate these subsurface errors, one more assumption is introduced into the mathematical model of residual statics analysis. That is:

> The subsurface traveltime distortions on seismic traces are independent of the source-receiver offset, i.e., they are assumed to be the same for all the traces in one same CMP gather.

This is called subsurface consistent assumption, which is considered by many residual statics analysis methods (Taner et al. (1974), Wiggins et al. (1976) and Ronen and Claerbout (1985)).

The validity of this assumption is rather difficult to verify. However, from the discussion of correlation domains in section **2.3.2**, some traveltime differences may be caused by the existence of dipping reflectors (This depends on how the reference traces are formed). Removal of the subsurface consistent traveltime differences (not errors) from the time-shift estimation should more or less help the estimation of the surface consistent residual statics.

With subsurface consistent assumptions, the traveltime errors on a seismic trace can be further decomposed as

$$\Delta T_{SR} = \Delta T_S + \Delta T_R + \Delta T_G + error\,, \tag{2-4-5}$$

where the new term ΔT_G (comparing to (2-4-2)) represents the subsurface consistent part of the traveltime distortions related to $T_{S_D R_D}$, and it is often called the *geological structure term*. One equation (2-4-5) for each seismic trace leads to a linear equation system as

$$\Delta T_{S_i R_j} = \Delta T_{S_i} + \Delta T_{R_j} + \Delta T_{G_{k(i,j)}},\ i=1,2,\ldots,N_S, \text{ and } j=1,2,\ldots,N_R. \tag{2-4-6}$$

Comparing to equation (2-4-3), this system has the same number of equations but more unknowns. Assume that there are N_G CMP locations in a seismic experiment, a coefficient matrix (denoted with $\underline{\mathbf{A}}$ for distinction) with ($N_S \times N_R$) rows and ($N_S+N_R+N_G$) columns can be built by extending the matrix **A** in equation (2-4-4). The first (N_S+N_R)

columns of $\underline{\mathbf{A}}$ are exactly the same as the columns in **A**. Because the rank of **A** is less than (N_S+N_R) as proved in **2.4.2**, the rank of $\underline{\mathbf{A}}$ must be less than $(N_S+N_R+N_G)$. This means that system (2-4-6) is always under-constrained. The over-determined property is usually true because the number of traces in a seismic experiment is much larger than the number of surface locations, including source, receiver and CMP locations.

2.4.4 After NMO correction

The decomposition equations for residual statics analysis in the previous sections, (2-4-3) and (2-4-6), are independent of NMO correction. If the reference traces are built from NMO corrected data, the estimated time shifts may contain errors due to improper NMO correction. This introduces another assumption: these residual NMO errors are assumed to be offset dependent only. Thus, the decomposition contains one more term for residual NMO, i.e.,

$$\Delta T_{SR} = \Delta T_S + \Delta T_R + \Delta T_G + E_{nmo} \cdot \overline{SR}^2 + error, \qquad (2\text{-}4\text{-}7)$$

where $\overline{SR}$ is the source to receiver offset. The offset term is squared because the error term E_{nmo} should be the same for either positive or negative offset, so the Taylor series expansion has zero first order term. The higher order Taylor expansion of the error is again ignored. E_{nmo} is called the residual NMO (RNMO) term.

The linear equation system based on (2-4-7) is also over-determined and under-constrained as shown by Taner et al. (1974) and Wiggins et al. (1976).

Offset dependent errors could be considered with data before NMO, although they are not the residual NMO errors. The ray paths at near surface may deviate away from vertical direction when source-to-receiver offset is large and/or the wave velocities in near-surface layers are not significantly lower than the deeper-layer velocities. In these cases, the surface consistent assumption is weaker, and the traveltime errors tend to be offset dependent.

2.5 Iterative technique

Iterative techniques are usually used for residual statics solutions because the residual statics problem is rarely totally solved by the first attempt of any algorithm. The iterative concepts and the residual statics analysis are related in many different ways.

2.5.1 Iterative decomposition algorithms

The coefficient matrices of the linear equation systems discussed in the previous sections are usually very large and sparse. This makes iterative algorithms preferred for the decomposition of the surface consistent statics. The most discussed iterative algorithm for residual statics analysis purpose may be the one called the Gauss-Seidel iterative algorithm (Taner et al., 1974 and Wiggins et al., 1976). Without losing generality, the linear system (2-4-6) with simplified symbols is used to explain the Gauss-Seidel algorithm,

$$T_{ij} = S_i + R_j + G_k . \qquad (2\text{-}5\text{-}1)$$

The starting point of the iteration is to obtain some pre-estimated values for any two of the three terms at the right side of equation (2-5-1). A convenient condition for residual statics analysis is that the source statics and receiver statics are usually assumed to have zero mean value, even at each CMP location (indexed by k). That is,

$$\sum_G S_i^{(0)} = \sum_G R_j^{(0)} = 0.0 .$$

The superscript (0) represents the starting level of the iterative process, and the summation over G means the summation of all the numbers at the same G-location, i.e., CMP location. Then the results of the next level (first level, denoted by superscript (1)) in the iteration can be written as,

$$G_k^{(1)} = \frac{1}{N(G_k)} \sum_{G_k} T_{ij} ,$$

$$S_i^{(1)} = \frac{1}{N(S_i)} \sum_{S_i} \left(T_{ij} - G_k^{(1)} \right) \text{ and}$$

$$R_j^{(1)} = \frac{1}{N(R_j)} \sum_{R_j} \left(T_{ij} - G_k^{(1)} - S_i^{(1)} \right).$$

Where the summation over S_i means a summation of all the numbers at the same source location indexed by i, and the summation over R_j means the summation of all numbers at the same receiver location indexed by j. $N(G_k)$ is the number of T_{ij}'s (number of traces practically) in the k-th CMP gather; $N(S_i)$ is the number of T_{ij}'s in the i-th source gather and $N(R_j)$ is the number of T_{ij}'s in the j-th receiver gather. Typically, the source statics S_i are solved before receiver statics R_j because the source fold is usually much higher (i.e., $N(S_i) > N(R_j)$), and the estimates S_i should be more stable.

For any later level (n-th level) of the iteration, the process can be expressed as

$$G_k^{(n)} = \frac{1}{N(G_k)} \sum_{G_k} \left(T_{ij} - S_i^{(n-1)} - R_j^{(n-1)} \right), \tag{2-5-2a}$$

$$S_i^{(n)} = \frac{1}{N(S_i)} \sum_{S_i} \left(T_{ij} - G_k^{(n)} - R_j^{(n-1)} \right) \text{ and} \tag{2-5-2b}$$

$$R_j^{(n)} = \frac{1}{N(R_j)} \sum_{R_j} \left(T_{ij} - G_k^{(n)} - S_i^{(n)} \right). \tag{2-5-2c}$$

The iterative results, $S_i^{(n)}$, $R_j^{(n)}$ and $G_k^{(n)}$, maybe with some conditions, converge to a solution of the equation system (2-4-6) (Taner et al. (1974) and Wiggins et al. 1976). In practice, some mathematical technique may be needed to ensure the faster convergence of this iterative algorithm (See Taner et al. (1974) for more detail).

Note that the most recent estimations of G_k and S_i are immediately used in each iteration. It is this property of the Gauss-Seidel method that makes the algorithm converge faster than the original Jacobi method, where the updated results are not used until the next iteration (Carnahan et al., 1969). However, this property may also cause instability of the algorithm, and some combinations with Jacobi algorithm may help.

In general, iterative algorithms have advantages over some direct methods for residual statics analysis. Iterative methods leave more chances to update the estimated time shifts T_{ij} at any iteration level. The present estimations of T_{ij} may be not accurate enough and further decomposition with these T_{ij} may cause incorrect statics

decomposition. Ronen and Claerbout's maximum stack power method is an example of updating T_{ij} during decomposition. This will be discussed in more detail in the next section.

2.5.2 Iteration with reference-trace updating

A practical problem with residual statics analysis is that there are always some traveltime errors in the reference traces. No matter what method is used for forming reference traces, the reference traces just tend to have less traveltime deviation than the original seismic data. One way to make reference traces more error-free is to update the reference data every time when a reasonable amount of statics have been corrected. After new reference traces are obtained, a new round of cross-correlation can be performed to get a new set of estimations of the time shifts. These time-shift estimations should be more accurate because the new reference traces contain more reliable traveltime information. Finally, the surface consistent statics decomposition will be more accurate.

Ronen and Claerbout's stack-power maximization method is an excellent example for updating the reference traces (stacked traces) each time a set of source statics or receiver statics are estimated and corrected. Every time source statics or receiver statics are estimated, the traces are corrected and new stacked traces (reference traces) are formed for the next iteration of cross-correlation and decomposition.

Many other methods can also be applied in an iterative manner by updating the reference model data. For example, the f-x statics method (Chan and Stewart, 1996) can be applied again by re-applying f-x filter on previous statics corrected common offset sections to obtain a new set of prestack reference data volume. The prestack depth migration plus de-migration method by Tjan et al. (1994) and Larner (1998) is suggested to be used iteratively, because of its dependence on migration velocity.

2.5.3 Iteration with velocity updating

Most conventional residual statics methods require preliminary velocity information for NMO correction. More reliable NMO velocity should result in more reliable statics estimation. On the other hand, reliable residual statics correction helps more accurate

velocity analysis. This relation between residual statics and NMO velocity introduces another iterative concept in residual statics analysis, which can be expressed as:

Velocity analysis: The velocity function may not be accurate enough for final stacking or migration, but maybe good enough for creating reasonable reference data for ***residual statics analysis***.

Residual statics analysis: Using present velocity to form reference traces and estimate residual statics. These static estimations are not perfect because that the reference traces may still contain some traveltime errors, but they may be good enough to correct some significant traveltime deviations on seismic traces and then ***better velocities*** can be observed.

If this "better velocity" is accurate enough for final stacking or migration, the job of residual statics analysis is done. Otherwise, this better velocity can be used to form a new set of reference data from seismic data with statics partly corrected. The new reference data should be more reliable as well as the resulting new residual statics.

The iterative approach with velocity updating can be considered for any residual statics method that uses velocity information to form reference traces, such as the depth migration method (Tjan et al., 1994).

2.5.4 Convergence and other limitations

The iterative techniques discussed in the previous three sections can not totally solve all the problems involved in residual statics analysis. The automatic residual statics analysis technique itself has limitations. Besides the validity limitation of the assumptions in Chapter 1 and section **2.4**, there are also some physical limitations from the seismic experiments themselves.

Wiggins et al. (1976) found out that the resolving capability of residual statics analysis methods is very much limited by the seismic field configuration parameters such as CDP fold multiplicity and the cable length (in terms of number of traces along the cable). If the CDP fold multiplicity is too low, the statistical reliability of the statics solution will be a problem. Longer cable length will enhance the capability of residual

statics to resolve the longer wavelength content of the traveltime distortions. In terms of iterative technique, if the cable length is not long enough or the CDP fold is too low, some long wavelength contents of the traveltime distortion will practically never be resolved no matter how many iterations one performed for reference data building or decomposition or velocity updating.

The limitations of seismic field configuration parameters have different influences on CMP processing and migration processing as indicated by Claerbout (1987). The cable length limits the capability of CMP processing, such as stacking velocity analysis and CMP stacking itself, but theoretically it does not limit the performance of migration. Migration processing utilizes all the data within the migration aperture, which is theoretically independent to the cable length and is only limited by the geographical limits of the seismic experiments. From this point of view, the residual statics methods utilising migration concepts can be more reliable because

- they may involve *more traces* for reference trace formation and then increase the statistical reliability and stability of reference data;
- they can have more control on the *long wavelength* contents of the statics because the reference traces contains information from all the traces within migration aperture which is usually larger than the cable length;
- they increase the possibility of the *uniqueness* of the statics solution because traces within migration aperture are always coupled, while CMP statics methods may have independent static solutions for certain kind of field configuration.

Chapter 3

Equivalent Offset Prestack Migration

Equivalent offset migration (EOM) method was first introduced by Dr. John Bancroft and his co-workers at the University of Calgary (Bancroft and Geiger, 1994, Bancroft, et al., 1998). EOM is a Kirchhoff type prestack migration algorithm, it is easier to implement and it is faster than conventional Kirchhoff prestack migration algorithm. The EOM method is reviewed here with focus on the related topics for the development of a new method of residual statics analysis in the next chapter.

3.1 Kinematics of prestack migration

Migration of seismic data is a process that attempts to reconstruct the image of the subsurface reflecting structure from recorded seismic wavefields. Different migration methods can be categorized by whether they are designed for surface seismic or vertical cable data, prestack or poststack data, 3D or 2D data, and whether they are depth or time migration methods. In this thesis, migration related discussions focus on 2D Kirchhoff prestack time migration for pure-mode (no mode conversion) surface seismic data.

3.1.1 The scatterpoint model: from depth to time

In seismic data processing, the earth subsurface is often modelled as a layered medium with each layer having uniform acoustic properties. The reflection energy from the interfaces between the layers can be considered as the sum of the scattered energy from a large number of points "closely" located on the interfaces. The reflection amplitude at each point is taken as proportional to the reflection coefficient of the interface at this point location. This subsurface model is called the *scatterpoint model*, which forms the basis of Kirchhoff migration methods. The points that may not be at any recognizable layer interfaces can still be considered as scatterpoints with zero or very small reflection amplitudes. This makes the whole subsurface an arrangement of scatterpoints.

The earth subsurface is initially considered as a one-layer isotropic medium where the seismic compressional wave propagation velocity is a constant (V). A scatterpoint at (x, z) and a source-receiver pair at surface locations x_s and x_r are given, as in Figure 3–1. The traveltime of a seismic wave starting from the source to the scatterpoint then to the receiver can be expressed as

$$T = \frac{1}{V} \cdot \left[\sqrt{z^2 + (x_s - x)^2} + \sqrt{z^2 + (x_r - x)^2} \right]. \qquad (3\text{-}1\text{-}1)$$

The traveltime T is a function of source and receiver locations x_s and x_r, and it is called the *traveltime response* of the scatterpoint (x, z).

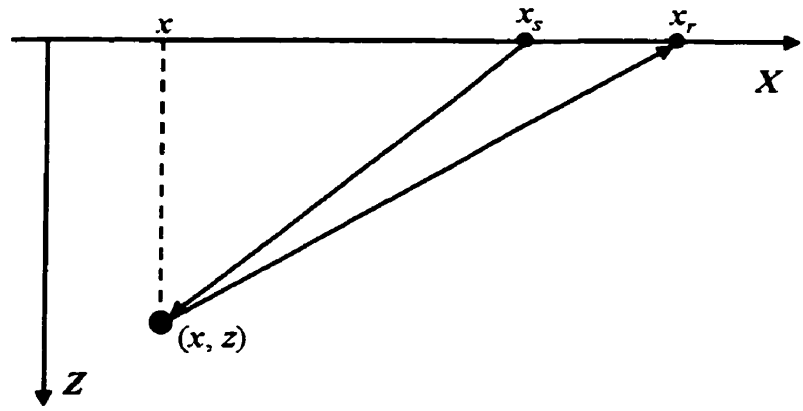

Figure 3-1: The geometry of a scatterpoint. A scatterpoint, at (x, z), scatters incoming energy back in any direction.

Introducing two-way vertical traveltime

$$\tau = 2\frac{z}{V},$$

which is proportional to the depth z when the velocity is constant, equation (3-1-1) can be expressed as

$$T = \sqrt{\frac{\tau^2}{4} + \frac{(x_s - x)^2}{V^2}} + \sqrt{\frac{\tau^2}{4} + \frac{(x_r - x)^2}{V^2}}. \qquad (3\text{-}1\text{-}2)$$

Subsurface images are expected to be 2D functions of spatial coordinates (x, z), and they ideally represent the reflection coefficients at all subsurface points. Practically, it is easier to obtain a subsurface image in x-τ space than in x-z space. These x-τ domain

images are called time migration sections. Each point on a time migration section, (x, τ), can also be called a scatterpoint, because of its correspondence with the spatial domain scatterpoint (x, z). This extension of the scatterpoint concept, from depth to time, (same as the extension of migration concept, from depth to time), is exact when the wave velocity is constant. When velocity varies only with depth z, the one-to-one relation between scatterpoints in depth and scatterpoints in time domain still holds. However, when the velocity changes significantly in the horizontal spatial direction (x), the time domain scatterpoint (x, τ) may not have exact one-to-one correspondence with some physical spatial position (x, z). Example 3-1 shows a simple case where one depth domain scatterpoint may have two different correspondences on a time migration section.

Example 3-1: Scatterpoint concepts in depth domain and time domain

By the image ray theory introduced by Hubral (1977), a depth domain scatterpoint (x_0, z) as in Figure E3-1-1(a) may have many different time domain correspondences (x_0, τ_0), and (x_1, τ_1), as shown in Figure E3-1-1(b). The values of τ_0 and τ_1 are the two-way traveltimes along two image rays, one from $(x_0, 0)$ to (x_0, z) and from $(x_1, 0)$ to (x_0, z), respectively.

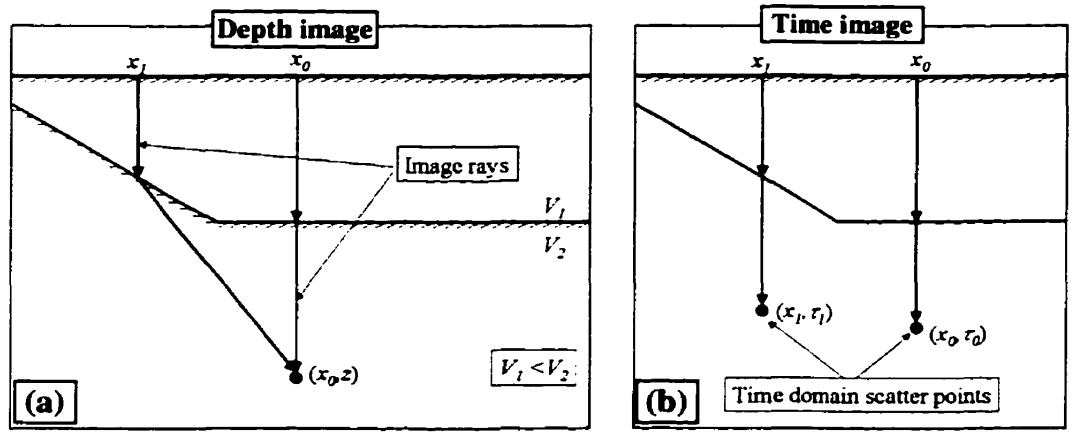

Figure E3-1-1: Time domain scatterpoints may not have exact one-to-one relation when there is lateral velocity variation.

When the subsurface structure is not very complex, or the lateral velocity variation is fairly "smooth", equation (3-1-2) can still approximate the traveltime response of a scatterpoint with properly defined velocity, V. The migration velocity for prestack

Kirchhoff time migration, denoted as V_{mig}, is in fact defined by the following generalized version of equation (3-1-2),

$$T=\sqrt{\frac{\tau^2}{4}+\frac{(x_s-x)^2}{V_{mig}^2(x,\tau)}}+\sqrt{\frac{\tau^2}{4}+\frac{(x_r-x)^2}{V_{mig}^2(x,\tau)}}. \qquad (3\text{-}1\text{-}3)$$

In other words, the migration velocity V_{mig} is a function of (x,τ) such that equation (3-1-3) best fits the traveltime response of some corresponding scatterpoint. For vertical velocity variation and small offsets, the RMS velocity is a often used approximation, as in following Example 3-2.

Example 3-2: RMS velocity as approximate migration velocity

When velocity changes only with depth z, the traveltime response of a given time domain scatterpoint (x, τ), as a function of the source and receiver coordinates, can be approximated by (Bancroft, 1997)

$$T=\sqrt{\frac{\tau^2}{4}+\frac{(x_s-x)^2}{V_{rms}^2(\tau)}}+\sqrt{\frac{\tau^2}{4}+\frac{(x_r-x)^2}{V_{rms}^2(\tau)}},$$

where $V_{rms}(\tau)$ is called root-mean-square (RMS) velocity, and it is defined as

$$V_{rms}^2(\tau)=\frac{1}{\tau}\int_0^{\tau}V^2(\tau')d\tau'.$$

3.1.2 Prestack migration based on scatterpoint model

Equation (3-1-2) is called the double-square-root (DSR) equation, and it is often expressed in CMP-offset domain as

$$T=\sqrt{\frac{\tau^2}{4}+\frac{(x_{off}-h)^2}{V^2}}+\sqrt{\frac{\tau^2}{4}+\frac{(x_{off}+h)^2}{V^2}}, \qquad (3\text{-}1\text{-}4)$$

where h denotes the half source-receiver offset, x_{off} denotes the horizontal distance (which is called *migration distance*) between a CMP location $x_{cmp}=(x_r+x_s)/2$ and the related scatterpoint surface location x, i.e., $x_{off}=|x_{cmp}-x|$.

In 3D (x_{off}, h, T) space, equation (3-1-4) describes a surface called *Cheop's pyramid* (Claerbout, 1985).

In terms of the scatterpoint model and Cheop's pyramid, the migration process can be interpreted in two different ways. Claerbout (1985) discussed these two interpretations for poststack migration as "hyperbola summation and semicircle superposition methods".

3.1.2.1 Migration: collect energy scattered from a scatterpoint

In terms of a scatterpoint at (x, τ), the migration process attempts to collect all the energy scattered from this point as a way to estimate the reflection "strength" at this point. That is:

1. (Traveltime computation) Locate where in seismic recordings the energy has been scattered to. For prestack Kirchhoff time migration, this step is practically a process to find the right migration velocity V_{mig} to best fit the traveltime response by a Cheop's Pyramid described by the DSR equation.
2. (Amplitude correction) Estimate how much energy has been scattered to each position on the Cheop's pyramid. Usually the geometrical spreading and obliquity factors are considered. Phase correction should also be considered.
3. (Imaging) Sum the energy at all the positions on the Cheop's pyramid, and put it back at the scatterpoint.

3.1.2.2 Migration: distribute recorded energy back to scatterpoints

Consider a recorded sample at some arrivaltime (traveltime) T with half source-receiver offset h and CMP surface location x_{cmp}, migration is now interpreted as a process that distributes the energy at the sample (x, T) back to all the scatterpoints (x, τ) that might have scattered seismic energy to this sample. This process can be decomposed into three steps as following:

1. (Traveltime calculation) Locate where (which scatterpoints) the energy at this sample could have come from.
2. (Amplitude factor) Estimate how much energy has been scattered to this sample from each scatterpoint located by the first step.

3. (Superposition) Scale and sum the input sample to each scatterpoint.

Example 3.2 shows the migration response curve of a recorded sample when the velocity is constant.

Example 3-3: elliptical migration response

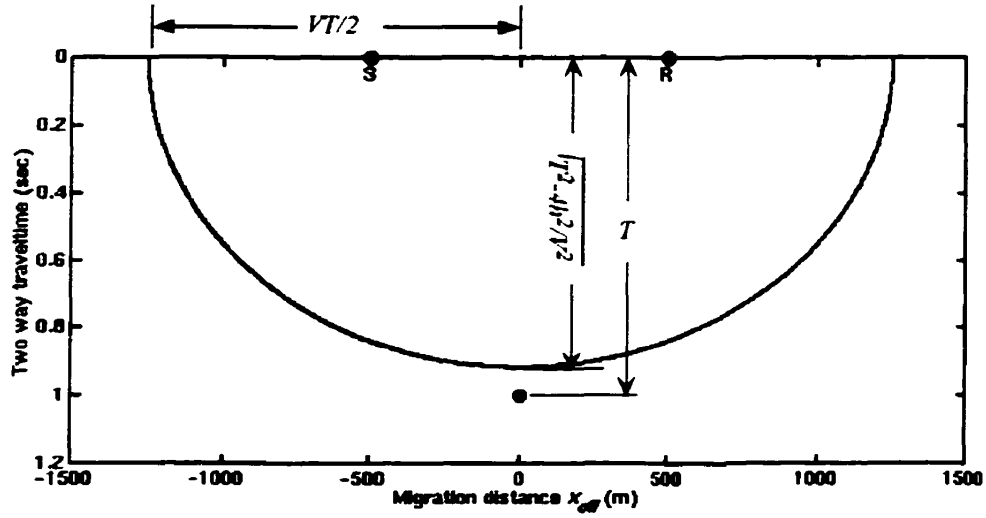

Figure E3-3-1: The migration response of a recorded sample is an ellipse when the velocity is constant. The dot at (x_{off}, T)=(*0, 1.0*) indicates the input sample. The dots '**S**' and '**R**' represent the source and receiver locations respectively. The source to receiver offset is 1000 meters.

Ignoring the amplitude considerations, the migration of the energy at one input sample is to find the positions of all scatterpoints (x, τ) that have scattered energy to this sample. When the migration velocity is constant, DSR equation (3-1-4) provides an x-τ relation that defines the possible scatterpoint locations. This relation can be expressed as

$$\frac{\tau^2}{T^2 - \frac{4h^2}{V^2}} + \frac{4(x - x_{cmp})^2}{T^2 V^2} = 1,$$

which, as shown in Figure E3-3-1, expresses an ellipse in (x, τ) space.

3.1.3 Prestack migration versus NMO, zero-offset migration and DMO

A new form of the DSR equation (Bancroft, Geiger and Margrave, 1998),

$$\tau^2 = T^2 - \frac{4h^2}{V^2} - \frac{4x_{off}^2}{V^2} + \frac{16x_{off}^2 h^2}{V^2 (VT)^2}, \tag{3-1-5}$$

provides convenient comparisons between prestack migration and some related processes in seismic data processing, such as NMO correction, DMO and poststack migration.

The first two terms on the right hand side of equation (3-1-5) represent a time quantity T_N as

$$T_N^2 = T^2 - \frac{4h^2}{V^2}. \tag{3-1-6}$$

Equation (3-1-6) expresses the NMO correction process, and it is also equation (3-1-5) when the migration distance x_{off} is set to 0. This means NMO correction can be kinematically considered as a part of the prestack migration process.

Some more processes have to be performed after NMO correction to obtain the desired migration result. These processes can be expressed by inserting equation (3-1-6) into equation (3-1-5), i.e.,

$$\tau^2 = T_N^2 - \frac{4x_{off}^2}{V^2}\left(1 - \frac{4h^2}{(VT)^2}\right). \tag{3-1-7}$$

Notice that this relation still contains the influence from source-receiver offset. This implies that, even for constant velocity cases, NMO corrected non-zero-offset traces are not the same as the zero-offset traces at the corresponding CMP locations. Let $h = 0$ in equation (3-1-7), it becomes

$$\tau^2 = T_N^2 - \frac{4x_{off}^2}{V^2}, \tag{3-1-8}$$

which is the migration process for zero-offset cases.

The difference between (3-1-7) and (3-1-8), which is shown in Figure 3-2, shows the inaccuracy of poststack migration applied on NMO corrected traces. DMO is a process designed to eliminate or minimize this difference. DMO combined with NMO attempts to transform non-zero-offset traces into zero-offset traces, and this is why sometimes DMO plus NMO is called the "migration to zero offset (MZO)".

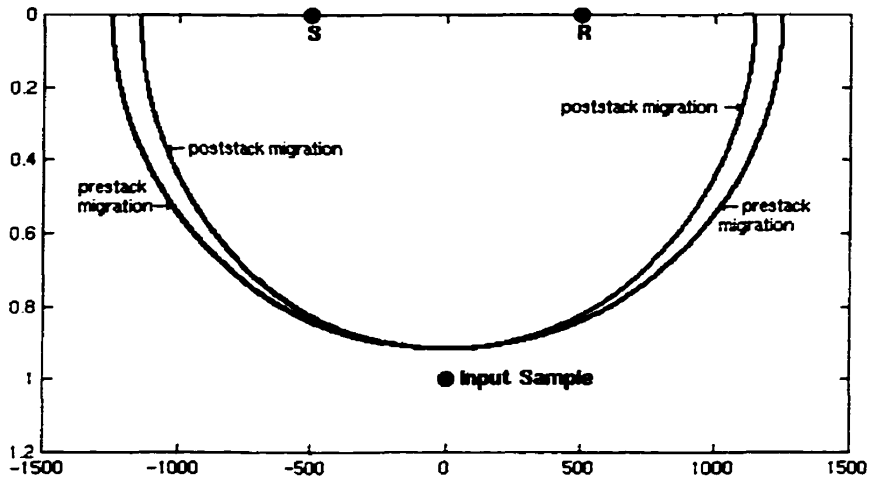

Figure 3-2: The difference between the prestack migration response and the result of poststack migration directly after NMO correction for constant velocity cases. The input sample is at 1.0 second, and is on a trace with 1000-meter source receiver offset and $x_{cmp}=0$. The velocity is constant, 2500 m/s, for prestack migration, NMO correction and poststack migration.

Prestack migration can be analyzed as the following three "energy-moving" processes separately, although they are not separable during migration.

1. migration in time direction (T to τ) where NMO is a special case,
2. migration in horizontal spatial direction (CMP location to scatterpoint), and
3. migration in offset direction (non-zero to zero) where DMO is an example.

Poststack migration on NMO corrected traces simplifies the full migration process by using NMO correction (which is just part of the time direction migration) to approximately complete the offset-direction migration. Practically, this simplification greatly reduces the computation cost of migration process, and this perhaps is the only advantage of poststack migration.

Many DMO methods can accurately migrate the non-zero-offset energy to zero-offset only when the velocity is constant. When velocity varies, DMO is usually an approximation to the full offset direction migration.

Besides conventional Kirchhoff prestack migration methods and NMO plus DMO followed by poststack migration, there are some other approaches to complete the full

migration process expressed by equation (3-1-5) (Fowler, 1987 and 1988). Equivalent offset migration (EOM) technique is a successful example.

3.2 Equivalent offset and CSP gathering

The EOM process is based on the concepts of equivalent offset and CSP gathering, which will be analyzed in detail in this section.

3.2.1 Equivalent offset

There are different ways to introduce equivalent offset concept. For the continuity of the discussion, the equivalent offset is defined from equation (3-1-5). Another definition with some geometric explanation will also be discussed.

Equation (3-1-5) can be re-arranged by splitting the time-related term and the space-offset term as

$$\tau^2 = T^2 - \frac{4}{V^2}\left(h^2 + x_{off}^2 - \frac{4x_{off}^2 h^2}{(VT)^2} \right). \qquad (3\text{-}2\text{-}1)$$

Then the *equivalent offset* h_e can be defined as

$$h_e^2 = h^2 + x_{off}^2 - \frac{4x_{off}^2 h^2}{(VT)^2}, \qquad (3\text{-}2\text{-}2)$$

and equation (3-2-1) can then be expressed as a simple NMO equation

$$\tau^2 = T^2 - \frac{4h_e^2}{V^2}. \qquad (3\text{-}2\text{-}3)$$

Equation (3-2-2) defines an equivalent offset for each sample in the prestack seismic data volume. The equivalent offset changes with the output scatterpoint location and the related velocity.

Figure 3-3 shows the equivalent offsets (as function of traveltime T) for one trace at variant migration distance x_{off}, where the migration velocity is constant. Equation (3-2-3) determines that the equivalent offset is defined at times below the straight line $T=2h_e/V$. Times above the line represents energy that would be migrated above the zero depth, which is physically impossible.

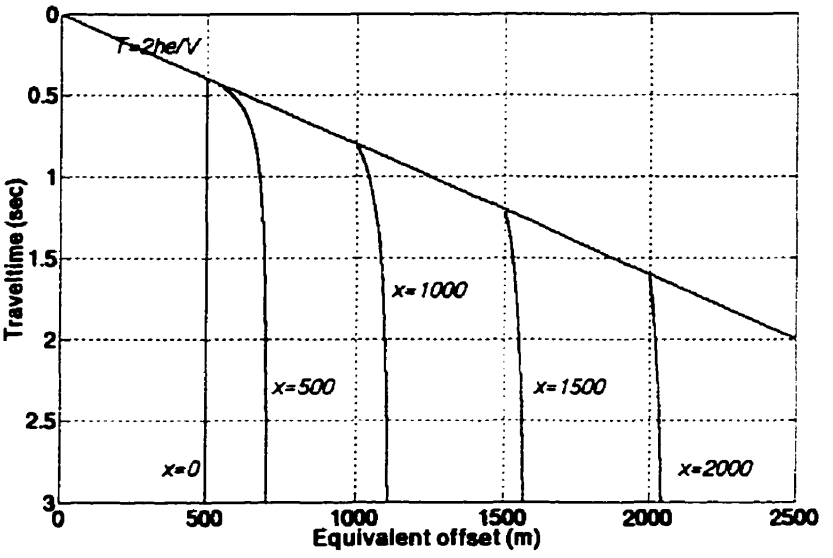

Figure 3-3: Equivalent offsets as functions of traveltime T at different migration distance x_{off}. In this example, h=*500* m and V=*2500* m/s.

Some basic properties of equivalent offset can be derived from equation (3-2-2) and they can be observed from Figure 3-3 as well.

1. The equivalent offset h_e can not be smaller than the half source-receiver offset h, i.e., $|h_e| \geq |h|$, because physically VT can not be smaller than $2h$.
2. The equivalent offset usually increases with traveltime T, but this may not be the case when the migration velocity decreases with τ.
3. The equivalent offset is absolutely limited, i.e., in any case, $|h_e| \leq \sqrt{x_{off}^2 + h^2}$.
4. When VT is relatively large comparing to x and h, i.e., $VT >> xh$, the equivalent offset tends to be independent of velocity and traveltime, $|h_e| \rightarrow \sqrt{x_{off}^2 + h^2}$.

Equivalent offset concept has an intuitive geometric explanation. As in Figure 3-4, for source-receiver pair located at x_s and x_r, and a scatterpoint at (x, z), there is always one surface location, x_e, such that the two-way traveltime from (x_e, *0*) to (x, z) and the traveltime from (x_s, *0*) to (x, z) then to (x_r, *0*) (with the same velocity) are the same, i.e.,

$$\frac{1}{V}\left[\sqrt{(x_s - x)^2 + z^2} + \sqrt{(x_r - x)^2 + z^2}\right] = T_s + T_r = T = \frac{2}{V}\sqrt{(x_e - x)^2 + z^2} \quad (3\text{-}2\text{-}4)$$

The horizontal distance between $(x_e, 0)$ and the scatterpoint, i.e., $|x_e - x|$, is defined as equivalent offset h_e. Replacing z with $V\tau/2$, the last equation in (3-2-4) can be written as

$$T^2 = \tau^2 + \frac{4h_e^2}{V^2},$$

which is exactly the same as (3-2-3).

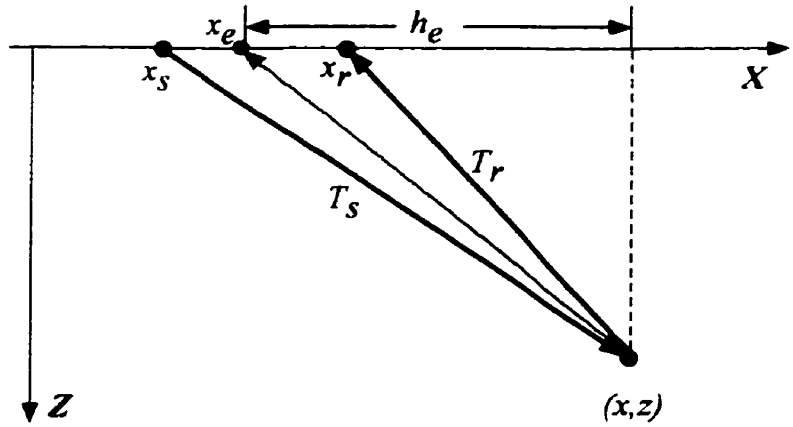

Figure 3-4: Geometrical explanation of equivalent offset. Where, the scatterpoint is located at (x, z), the source and receiver are located at x_s and x_r.

3.2.2 Common scatterpoint (CSP) gathers

Any seismic trace may contain scattered energy from any scatterpoint in the relevant range. If the energy can be sorted by scatterpoint locations instead of CMP locations, migration related problems should be much easier to solve. The equivalent offset concept based on scatterpoint model introduces a convenient measure for gathering reflection and scattered energy in seismic data.

A common scatterpoint (CSP) gather at a certain surface location (called CSP location) is defined as a two-dimensional re-arranging of the seismic energy in equivalent offset and traveltime. In a CSP gather, the energy from those scatterpoints vertically aligned at this CSP location will be gathered, and the Cheop's pyramids corresponding to these scatterpoints will be collapsed to hyperbolas as expressed by equation (3-2-3). Energy from scatterpoints that are not below the CSP location will also be summed, but the energy will be destructively dispersed.

CSP gathers can be formed at any surface location from data with arbitrary acquisition geometry. Once the CSP gathers are formed, kinematically only NMO correction (3-2-3) and CMP stacking applied on these CSP gathers are left for a full prestack migration. A very important property of CSP gathers is that they provide a direct method to observe migration velocity using conventional velocity analysis tools.

It is important to mention that during the CSP gathering process, no time-shifting is involved. The time-direction energy-moving process for the final migration is left for the NMO correction at each CSP locations. This no-time-shift property of CSP gathering significantly reduces the velocity dependence in the process, and this will be discussed in more detail later in section **3.4**. The no-time-shift and velocity insensitive properties are also essential for the statics analysis method we will introduce in the next chapter.

3.2.3 Energy distribution during CSP gathering

To further clarify how CSP gathering works, the following discussions focus on what it does to one recorded sample and a hyperbolic event on CMP gathers.

3.2.3.1 From point sample to equivalent offset hyperbola

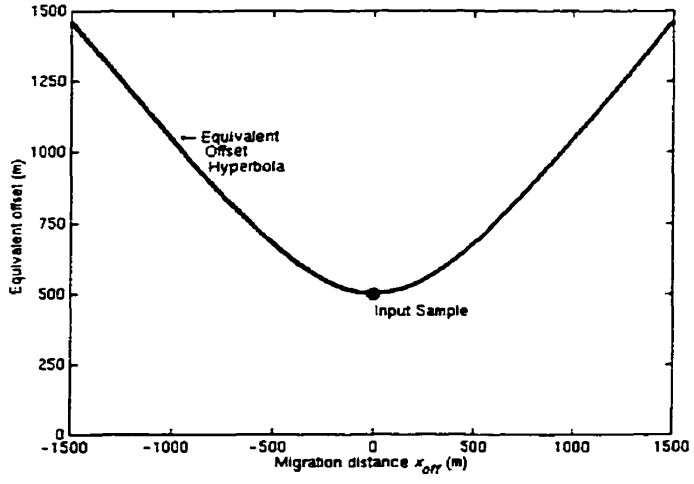

Figure 3-5: Equivalent offset hyperbola. The input sample is at *1.0* second, and on a trace with *1000* m source-receiver offset (*h=500* m). The migration velocity is *2500* m/s.

Equation (3-2-2) expresses a hyperbolic relation between x_{off} and h_e with given T, V and h. This is to say that, when the migration velocity is constant, CSP gathering

distributes the energy at a seismic sample to a hyperbola in a constant T plane. This hyperbola is called *equivalent offset hyperbola* (Bancroft, et al., 1998), as shown in Figure 3-5. The elliptic migration response of this sample is found when NMO correction (using the migration velocity) is applied to the equivalent offset hyperbola.

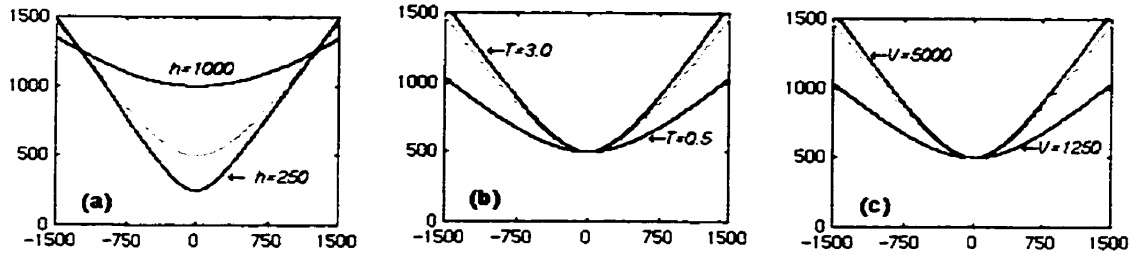

Figure 3-6: Equivalent offset hyperbolas for (a) different offsets h, (b) different traveltimes T, and (c) different migration velocities V.

The equivalent offset hyperbola changes its shape and/or position when h, T, or V changes. Figure 3-6 shows some equivalent offset hyperbolas for (a) different offsets, (b) different traveltimes, and (c) different migration velocities. The light grey curve is the equivalent offset hyperbola shown in Figure 3-5, where $h = 500$ m, $T = 1.0$ sec, and $V = 2500$ m/s. In (a), the three curves have the same T and V, but different h's. In (b), the three curves have the same h and V, but different T's. In (c), the three curves have the same h and T, but different V's.

From Figure 3-6 (b), it can be seen that, if the traveltime T is larger (not less than 1.0 in this example), the equivalent offset hyperbola changes very little with increasing time. Similarly, as shown in Figure 3-6(c), the equivalent offset hyperbola changes very little when velocity is higher. These properties are related to the sensitivity of the equivalent offset versus the errors of h, T and V, which will be discussed in more detail in **3.4**.

3.2.3.2 From hyperbola to a "pro w" shape

Assume that the earth surface is horizontally flat, and the subsurface contains only one reflector parallel to the surface, the reflected seismic energy from the interface should follow the same moveout curves at all CMP locations. For simplicity, it is assumed that all the related CMP gathers have same number of traces and same offset range, as shown in Figure 3-7(a).

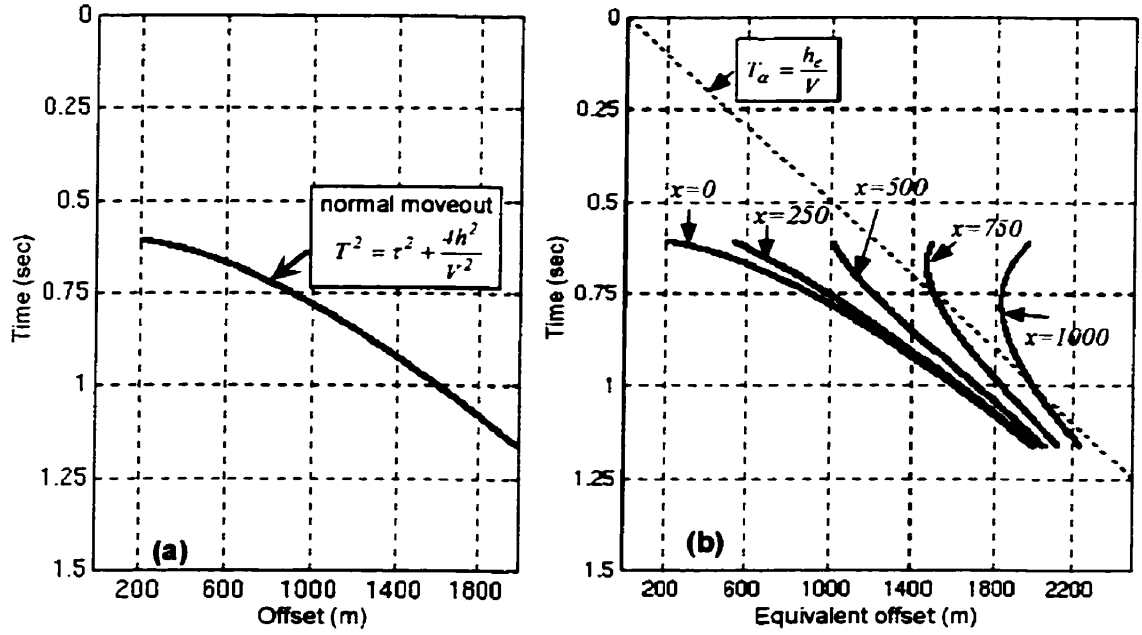

Figure 3-7: (a) shows a CMP gather with one event from a flat reflector. (b) shows a CSP gather with energy from some neighbor CMP's, and these neighbor CMP gathers are the same as the one shown in (a).

Re-write the equivalent offset equation (3-2-2) as

$$h_e^2 = x_{off}^2 + h^2 \cdot \left(1 - \frac{4x_{off}^2}{V^2T^2}\right),$$

h_e^2 can be considered as a linear mapping from h^2. This mapping contains a "compressing" (multiply by a number smaller than 1.0), which narrows the offset range, and a "shifting" (plus certain value), which increases all the offset values. Both compressing and shifting are mainly determined by x_{off}^2, although the "compressing" factor also depends on VT. It can be seen from Figure 3-7 (b) that, the larger the migration distance x_{off}, the narrower the equivalent-offset range and the more the equivalent offset increase. The dashed line denotes a boundary of the first possible traveltimes for different offset at the CSP location.

In CSP gathers, the compressed and shifted hyperbolas from all the CMP gathers are linearly superposed. The resulted constructive interfered energy forms a "prow" shape (Bancroft and Geiger, 1997) which is the "envelop" of all the compressed and shifted

CMP hyperbolas. The coherent energy at the top of the prow emerges from the near offset. The coherent energy at the bottom of the prow emerges after the maximum source receiver offset, and it is the effect of the cable ends.

The following Example 3-4 shows some CSP gathers formed from a set of synthetic data generated over a two-reflector subsurface model, with one reflector flat and the other dipping.

Example 3-4: CSP gathering of the energy from hyperbolic events in CMP gathers.

A set of synthetic data is acquired from the subsurface model shown in Figure E3-4-1. The offset ranges from 100 meters to 1000 meters.

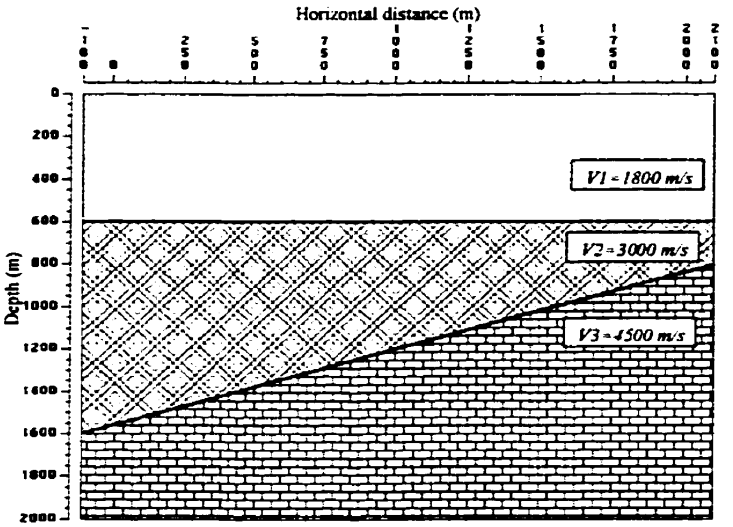

Figure E3-4-1: A simple subsurface model with two reflectors.

Four CSP gathers at the same surface location are formed in order to show how the hyperbolic moveout energy on neighboring CMP gathers is migrated. These four gathers are shown in Figure E3-4-2.

The gather in Figure E3-4-2 (a) only contains the energy from five CMP gathers located 0, 125, 250, 375 and 500 meters ***left*** to the CSP location. The gather in Figure E3-4-2 (b) contains energy from five CMP gathers located 0, 125, 250, 375 and 500 meters ***right*** to the CSP location. It can be seen from (a) and (b) how the hyperbolas from CMP gathers are "compressed" and "shifted" in the CSP gather at different migration distances. The earlier-time and far-offset parts of the two gathers look different because of the asymmetric acquisition geometry. The CMP gathers at the left

end of the line contains only near offset traces and the CMP gathers at the right end of the line contains only far offset traces.

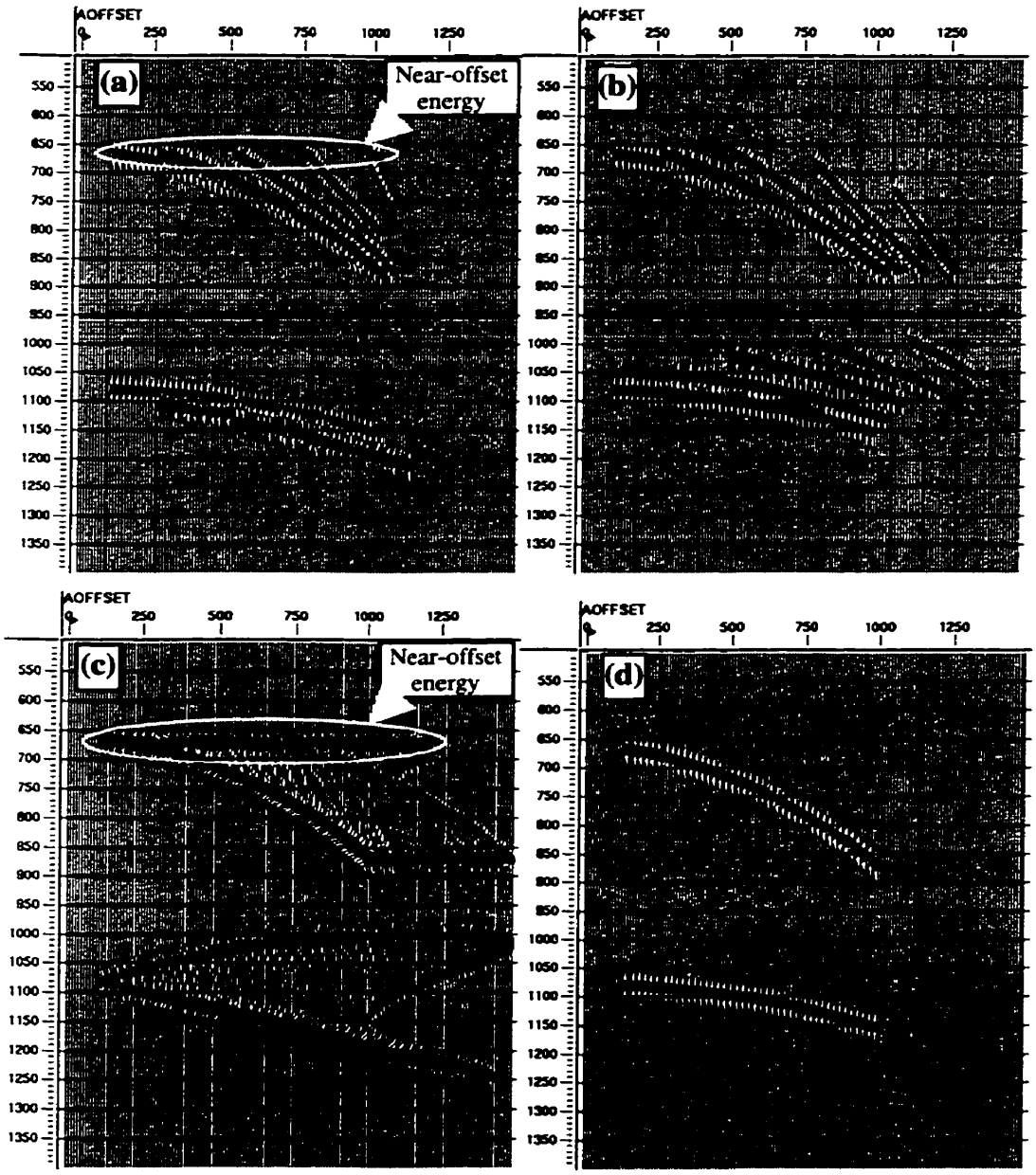

Figure E3-4-2: 4 CSP gathers formed at the same location. (a) contains contributions from 5 left-side CMP's. (b) contains energy from 5 right-side CMP's. (c) contains all possible energy. (d) contains only the energy from the CMP gather at the same location.

Figure E3-4-2 (c) shows the CSP gather with all possible energy collected from the data set. The constructive and destructive interference of the energy results in a "prow" shape for the flat event, and a skewed prow shape for the dipping event.

Figure E3-4-2 (d) shows the CSP gather containing only the energy from the CMP gather at the same surface location, i.e., the migration distance is zero. The CSP gathering process does not change the energy arrangement (offset versus time) in this case. Comparing (d) with (c), the moveout curves for the flat event remain the same location before and after CSP gathering, while for the dipping event, the hyperbola is mapped into a new moveout curve corresponding to a lower semblance velocity. It is the new hyperbolic moveout trajectories, which are dip-independent, on CSP gathers that provide convenient migration velocity analysis.

3.2.4 Amplitude scaling

The above discussions of prestack time migration are mainly kinematics, where no amplitude considerations are included. In general, Kirchhoff type migration methods can be called diffraction summation methods. For 2D poststack data, the diffractions (the traveltime responses of scatterpoints) are hyperbolas, and for prestack data, the diffracted energy forms Cheop's pyramids. The amplitude and phase information along the diffractions is not uniformly distributed. According to Yilmaz (1987), the following factors must be considered before diffraction summation:

1. The obliquity factor or the directivity factor.
2. The spherical spreading factor.
3. The wavelet shaping factor, which mainly is a constant 45-degree phase shift for 2D migration

3.2.4.1 Obliquity factor

The amplitude obliquity factor of diffracted energy can be approximated by the cosine of the angle between the direction of the wave propagation and the vertical axis (Yilmaz, 1987). For poststack migration with constant velocity, this cosine value is equal to the ratio of migration output time to input time (Bancroft, 1997). However, it is not apparent what is exactly the amplitude obliquity factor for prestack Kirchhoff migration.

In a conventional Kirchhoff migration algorithm, the amplitude obliquity factor tends to zero at the farthest possible migration distance, and tends to maximum when the

migration distance is zero. Between these two extreme cases, the scaling factor should change "smoothly". By this simple principle, some simplified amplitude scaling factors can be efficiently applied to CSP gathering process.

The definition of equivalent offset, equation (3-2-2), implies a simple relation between migration distance x_{off} and equivalent offset h_e. That is, when $x_{off} = 0$, the x_{off}-to-h_e ratio, x_{off}/h_e, is zero, and it equals to 1.0 when $x_{off} = h_e$, which corresponds to the maximum possible migration distance. Thus the following two scaling functions

$$S_{amp-1} = 1 - \frac{x_{off}}{h_e} \text{ and } S_{amp-2} = 1 - \left(\frac{x_{off}}{h_e} \right)^2, \tag{3-2-4}$$

can be used as two approximations to the amplitude obliquity factor.

These two scaling factors are not accurate, but they help to minimize the coherent energy emerging from the near offset as illustrated in Example **3-5**. This near-offset energy on CSP gathers is needed for the final imaging, but it influences the seismic data reconstruction from CSP gathers to CMP gathers. Reconstruction of the seismic data is the key concept for the EOMAP method of residual statics analysis introduced in the next chapter.

Example 3-5: CSP gathering with amplitude scaling S_{amp-1} and S_{amp-2}

Figure E3-5-1 shows a CSP gather at the same location as the CSP gathers shown in Example **3-4**. This gather also collects all the possible energy as the one shown in Figure E3-4-2(c). The difference is, during the CSP gathering of this gather, the amplitude-scaling factor S_{amp-2} is used. It can be seen that, the constructive near-offset energy shown in Figure E3-4-2(c) is removed.

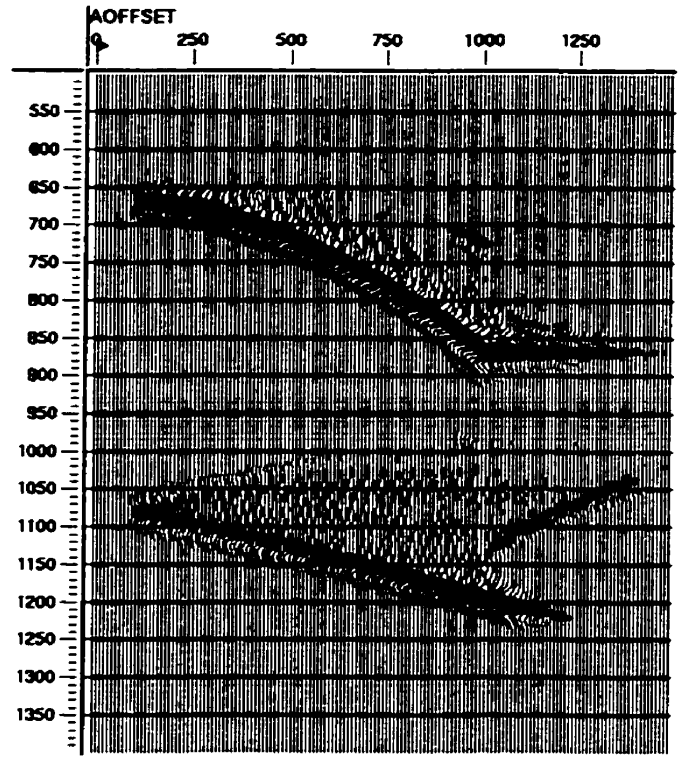

Figure E3-5-1: A CSP gather with amplitude scaling factor applied during the mapping from CMP gathers to CSP gathers. The coherent energy constructively superposed from near-offset energy, i.e. the top of the prow shape, is attenuated.

More accurate amplitude obliquity scaling factor is possible with more detailed analysis of the relation between prestack migration and poststack (zero-offset) migration, where more accurate amplitude scaling factor is available.

The ratio of migration output time τ to the zero-offset time T_N approximates the amplitude obliquity factor for zero-offset migration (Bancroft, 1997). This ratio, τ/T_N, should also be a good approximation for prestack migration, at least for constant velocity cases. It should be noticed that, the non-zero offset obliquity may also be different from the zero-offset cases, the obliquity factor can also be approximated by the ratio of τ directly with the traveltime T, i.e., τ/T. For EOM method, these two obliquity factors can be expressed as

$$S_{amp-3} = \frac{\tau}{T_N} = \sqrt{\frac{T^2 - \frac{4h_e^2}{V^2}}{T^2 - \frac{4h^2}{V^2}}} = \sqrt{\frac{V^2T^2 - 4h_e^2}{V^2T^2 - 4h^2}}, \quad \text{(3-2-5a)}$$

$$S_{amp-4} = \frac{\tau}{T} = \frac{\sqrt{T^2 - \frac{4h_e^2}{V^2}}}{T} = \frac{\sqrt{V^2T^2 - 4h_e^2}}{VT}. \quad \text{(3-2-5b)}$$

A very important property of scaling factor S_{amp-4} in (3-2-5b) is that both τ and T do not change in the process of CSP gathering. It implies that this approximation of the obliquity scaling factor can equivalently applied after CSP gathering, which is much more efficient because it avoids the same factor being applied every time when the energy at same traveltime level (on a Cheop's pyramid) is migrated.

3.2.4.2 Spherical spreading factor

The spherical spreading amplitude factor depends on the distance from certain source to certain receiver within given traveltime T. The distance used for time migration can be approximated by the value of VT, where V is the migration velocity for relevant scatterpoint. This VT value does not changing during the CSP gathering process. Thus, similar to the obliquity factor S_{amp-4}, instead of applying spherical spreading amplitude correction for each input sample every time when its energy is migrated, the correction can be applied more efficiently on CSP gathers.

Applying amplitude correction factors on CSP gathers, rather than on each input traces every time they are migrated, is one reason why EOM method is faster than conventional Kirchhoff migration algorithms.

3.3 EOM: the algorithm and application

The main part of the computer implementation of EOM is CSP gathering. The conventional NMO correction and the CMP stacking methods can be conveniently applied on CSP gathers to obtain the final image. Some additional processing needed for

CSP gathers, such as 45-degree phase-shift and amplitude scaling, can be implemented separately.

3.3.1 The algorithms for forming CSP gathers

The equivalent offset concept is originally defined in a sample-by-sample manner, but in practice, it is unnecessary to compute the equivalent offset for each sample. The computation of equivalent offset can be transformed to an equivalent process of computing the traveltimes corresponding to certain equivalent offset values. This transformed algorithm is accurate and efficient (Li and Bancroft, 1996b).

3.3.1.1 Knowns and unknowns

Before any computation begins, the velocity field V should be available at all relevant scatterpoints coordinated by CSP surface locations x, and two-way vertical traveltime τ.

To compute equivalent offset h_e for an input sample with traveltime T, half source-receiver offset h and CMP location x_{cmp}, the knowns and the unknowns should be identified in equation

$$h_e^2 = h^2 + x_{off}^2 - \frac{4x_{off}^2 h^2}{(VT)^2}, \tag{3-3-1}$$

where x_{off} is the migration distance and V is the migration velocity for related scatterpoint. The values of h and T are known, and $x_{off} = |x - x_{cmp}|$ are known for each CSP x. The only quantity that needs to be calculated is the migration velocity V. The migration velocity is a known two-variable function of x and τ, but τ is unknown and has to be computed.

Although there is another known relation between h_e and τ (and V), i.e.,

$$\tau^2 = T^2 - \frac{4h_e^2}{V^2}, \tag{3-3-2}$$

there is no apparent way to remove the dependence of V from equation (3-3-1) or remove the dependence to both V and τ from equation (3-3-2) to get a explicit expression of h_e by exactly known quantities, T, h and x_{off}.

3.3.1.2 The algorithms

A natural numerical solution of computing h_e for a sample (h, x_{cmp}, T) might be an iterative technique as following:

Step 1: Take the velocity V at some pre-determined initial τ value.

Step 2: Calculate h_e using equation (3-3-1).

Step 3: Calculate a new τ value using equation (3-3-2), and go back to Step1.

It is a question that how many iterations are needed for each sample to obtain an accurate equivalent value. This question does not need to be answered because another algorithm that does not require iteration is available, and it is accurate and efficient.

Practically, CSP gathers have to be sampled in both offset and time directions. CSP gathering is a binning process, such that, a trace in a CSP gather with an equivalent offset value also contains the energy of samples with equivalent offsets very close to this value. The equivalent offset bin size and the equivalent offset range determine how the energy in a CSP gather is arranged and superposed. Suppose the equivalent offset bin centers are given by

$$\{h_e(i): i = 1,2,\cdots,N_{he}\} = \{0, \Delta h_e, \cdots, h_{e\text{-}max}\},$$

where Δh_e is the equivalent offset bin size and $h_{e\text{-}max}$ is the maximum equivalent offset of interest, then any sample with its equivalent offset falling in the interval

$$(h_{e-}(i), h_{e+}(i)] = \left(h_e(i) - \frac{1}{2}\Delta h_e, h_e(i) + \frac{1}{2}\Delta h_e \right] \qquad (3\text{-}3\text{-}3)$$

will be (fully or partly) summed into the trace with assigned equivalent offset value $h_e(i)$.

Because of the physical continuity of the equivalent offset function, if some sample on a trace at traveltime T_1 has equivalent offset $h_{e-}(i)$, and another sample on this trace at traveltime T_2 has equivalent offset $h_{e+}(i)$, then all the samples on this trace with traveltimes between T_1 and T_2 will have equivalent offsets falling in the interval $(h_{e-}(i), h_{e+}(i))$.

From this point of view, a new algorithm can start from the equivalent offset boundary values, $h_{e-}(i)$ or $h_{e+}(i)$, and then find the corresponding boundary traveltimes T_1 and T_2. This is to say, h_e, h and x in equations (3-3-1) and (3-3-2) are known, the

unknowns are T (explicitly) and τ (implicitly). Although this algorithm also involves V as a "half-unknowns", V and τ, V and T can be easily combined together as two separable unknowns (VT) and $(V\tau)$. Expressions of the common term $(VT)^2$ in equations (3-3-1) and (3-3-2) lead to

$$\frac{4x^2h^2}{h^2+x^2-h_e^2} = (VT)^2 = (V\tau)^2 + 4h_e^2,$$

and the unknown $(V\tau)$ is then expressed directly by known quantities as,

$$(V\tau)^2 = \frac{4x^2h^2}{h^2+x^2-h_e^2} - 4h_e^2. \qquad (3\text{-}3\text{-}4)$$

It can be proved that $(V\tau)^2$ is an absolutely increasing function of τ, as long as V is of (or close to) RMS type (Li and Bancroft, 1996b). An accurate τ value can be obtained by inverting the function $(V\tau)^2$ from the right hand side of equation (3-3-4), and the traveltime T can be computed using the migration velocity V at this τ through either equation (3-3-1) or (3-3-2).

The function inversion process can be very efficiently done by creating τ versus $(V\tau)^2$ table at all output CSP locations before inputting any seismic traces (Bancroft and Li, 1998).

For clarity, the process of CSP gathering by equivalent offset can be explicitly expressed in following steps:

Loop 1: For each CSP location,

The migration velocity array is available

Loop 2: For each equivalent offset,

The equivalent offset boundaries are available

Loop 3: For each input seismic trace,

The CMP location and half source-receiver offset are available

The migration distance can be computed

- Use equation (3-3-4) and the inversion function table to compute the traveltime boundaries on the present trace
- Sum (with scaling if needed) the present trace segment defined by the time boundaries to the trace segment at the present CSP location and the present equivalent offset

End Loop3

End Loop2

End Loop1

3.3.2 Application considerations

In the practical computer implementation of EOM method, there are some factors, such as migration dip limits, migration aperture limits, anti-aliazing filter, need to be considered.

The migration dip limitation in EOM method can be considered during the formation of CSP gathers as conventional Kirchhoff migration methods do. In the EOM method, the obliquity factor S_{amp-4} in (3-2-5b) does not change during CSP gathering, allowing the migration dip limitations to be applied to the CSP gathers (Bancroft, 1998a). This is an advantage because the migration dip limits can be designed laterally variant with no extra effort, and this can be done interactively using conventional mute-time-picking techniques.

Migration aperture limitation is the limitation of migration distance. Aperture limitation can also be used along with the limits on migration dips as in conventional Kirchhoff methods, and it is an efficient way to save the computation cost.

CSP gathering process is a natural anti-aliazing filter (Bancroft, 1996a). Although the performance of this filter depends on equivalent offset bin size, the summation of samples with close equivalent offsets forms an automatic boxcar filter for the traces being binned into CSP gathers.

There are two special factors related to equivalent-offset concept. They are the maximum equivalent offset and the equivalent offset bin size. The selection of these two parameters is essential to the quality of CSP gathers and the final imaging.

The equivalent offset bin size usually should not be larger than the CMP spacing of the input data, because the difference between samples from two different CMP gathers should always be properly differentiated. As mentioned above, the equivalent offset bin size is proportional to the length of an anti-aliazing boxcar filter for the migration. Too large equivalent offset bin size may lose desired signal resolution without differentiating certain amount of traveltime differences. Offset bin size that is too small may result in

- increasing memory requirement to store the large CSP gathers;
- additional anti-aliazing filter to be designed;
- more computation cost.

The maximum equivalent offset should never be smaller than the maximum source-receiver offset of the seismic experiment, because the equivalent offset of a sample is never smaller than its source-receiver offset. How large the maximum equivalent offset may be depends on the necessary maximum migration distance (aperture), as in equation (3-3-1). By the equivalent offset NMO equation (3-3-2), the maximum equivalent offset can be estimated roughly by

$$|h_e| \le \frac{1}{2} V_{\max} T_{\max},$$

where V_{max} is the maximum possible migration velocity for the whole seismic line, and T_{max} is the maximum traveltime recorded or of interest. When the maximum migration distance x_{max} is determined, h_e should always be limited by $\sqrt{h_{\max}^2 + x_{\max}^2}$.

3.3.3 Why is EOM faster?

Bancroft (1998b) presented a detailed analysis of the computational cost of the EOM method relative to standard Kirchhoff migration methods. The EOM method is faster mainly because of the following strategy:

The samples on each input trace are considered as a "group" when they have very close equivalent offset values, this may be equivalent to some algorithms for conventional Kirchhoff migration where traveltime and scaling factor tables are pre-computed. However, EOM method further combines all possible traces with close equivalent offset values at each CSP location as a "group", i.e., a trace in the CSP gather. According to the discussions in previous sections, many time-consuming computations, such as time direction correction (moveout correction), amplitude scaling factor (obliquity and spherical spreading) and phase correction, can be done just once for one such group.

As an example, Bancroft and Wallace (1997) shows how the application of equivalent offset and CSP gather concepts saves the computation cost for poststack 3D Kirchhoff migration.

3.4 Velocity dependence analysis

The error in the computation of equivalent offset is caused by the inaccuracy of migration velocities, because all other related quantities, traveltime, offset and migration distance, are accurately known in the computation. However, velocity dependence is not sensitive. This velocity-insensitive property of CSP gathering is one of the major advantages of the EOM method. The following sections focus on some detail analysis of the velocity dependence of the equivalent offset.

The sensitivity of equivalent-offset error versus the migration-velocity error can be expressed as the ratio of relative error of equivalent offset to the relative error of migration velocity, i.e., (Bancroft and Geiger, 1995 and 1996b)

$$S(h_e,V)=\left|\frac{dh_e/h_e}{dV/V}\right|=\left|1.0-\frac{x^2+h^2}{h_e^2}\right|=\frac{4x^2h^2}{h_e^2V^2T^2}. \qquad (3\text{-}4\text{-}1)$$

The following properties,

$$max(|x|,|h|)\le\frac{1}{2}VT, \text{ and } he\ge max(|x|,|h|),$$

imply that the sensitivity is always limited, i.e.,

$$S(h_e, V) \leq 1.$$

This means when the velocity error is 10%, the relative error of the equivalent offset can not be greater than 10%. In fact, the following detail analysis tells that the sensitivity is usually much smaller. In some cases, the errors can be practically ignored.

The sensitivity may behave differently when the migration distance x, the half source-receiver offset h, the traveltime T and the accurate migration velocity V are different. The values of x and h are symmetric relative to both equivalent offset and the migration velocity, therefore the following results show the behavior of sensitivity versus different x, T and V.

Instead of directly giving the values of the sensitivity, in the following analysis, the relative equivalent offset errors are shown as functions of relative velocity errors. The relative velocity errors are expressed as percentage of the accurate velocity, which ranges from −100% to 100%, where −100% means that the wrong velocity is half of the accurate velocity and 100% means the wrong velocity is twice of the accurate velocity.

3.4.1 Sensitivity changing with migration distances x

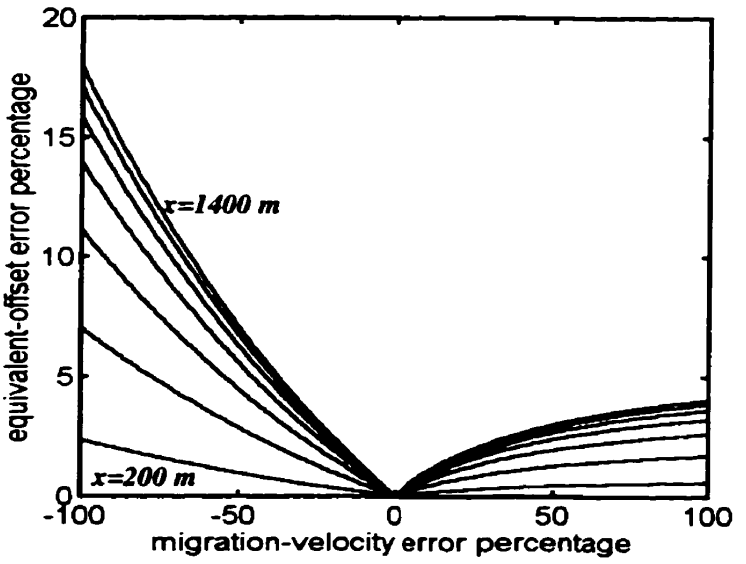

Figure 3-8: Relative equivalent-offset-error (percentage) versus the relative velocity-error (percentage) shown as curves for different migration distances.

Figure 3-8 shows some curves for different migration distances. Each curve represents the relative equivalent-offset-error (percentage) as a function of the relative

velocity-errors. The half source-receiver offset h is *500* meters, the accurate velocity V is *3000* meters per second and the traveltime T is *1.0* second for all the curves. The migration distance is sampled from *0* to *1500* meters (which is the largest possible) by every 200 meters.

The sensitivity, as defined in (3-4-1), is less than 0.2 (20%) in this case. There are significant differences between the sensitivities at higher velocities and lower velocities relative to the accurate velocity. In this example, when velocity changes from 3000 m/s down to 1500 m/s, the equivalent offset percentage error is 18%, and when velocity goes from 3000 m/s up to 6000 m/s, the equivalent offset percentage error is less than 4%. This suggests that, when the velocity is only known between two velocities, the higher value will usually give better approximations.

Figure 3-9 shows only the percentage of equivalent-offset-error for those velocities higher than the accurate one (the positive percentages of the velocity errors). It is a zoomed version of the right-side half of Figure 3-8. The later analysis will only show the results with higher wrong velocities.

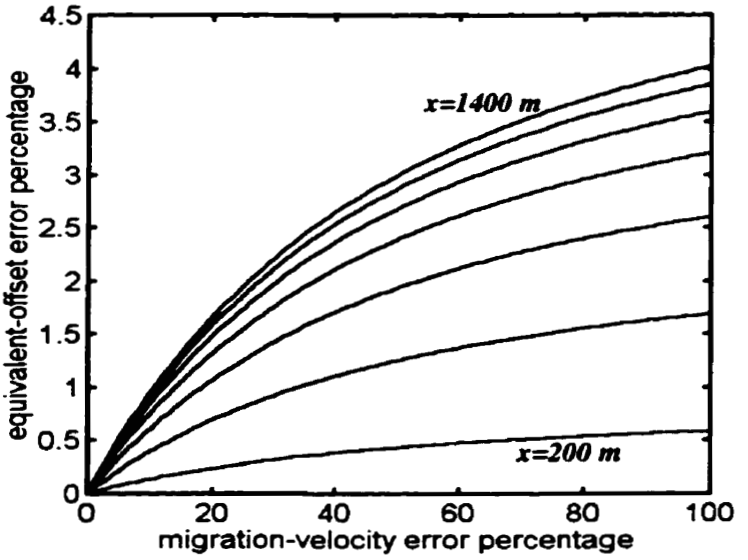

Figure 3-9: This is half of Figure 3-8 with only the relative equivalent offset error curves at positive velocity error percentages shown.

3.4.2 Sensitivity versus traveltime T

Figure 3-10 shows some equivalent-offset-error curves for different traveltimes T. As in Figure 3-9, only the values at positive percentage velocity errors are shown. For all the curves, x, h and the accurate velocity V are given as 600 meters, 500 meters and 3000 meters per second respectively.

The sensitivity of equivalent-offset-error versus velocity-error decreases as the traveltime T increases. The equivalent offsets of the samples with large traveltimes, the velocity error does not result in significant differences In Figure 3-10, it decreases very rapidly at the first one second or so, from 2.6% down to 0.6% at 100% wrong (double valued) velocity. Usually, for data after two or three seconds, the equivalent offset error due to velocity-error is practically zero (less than 0.5%).

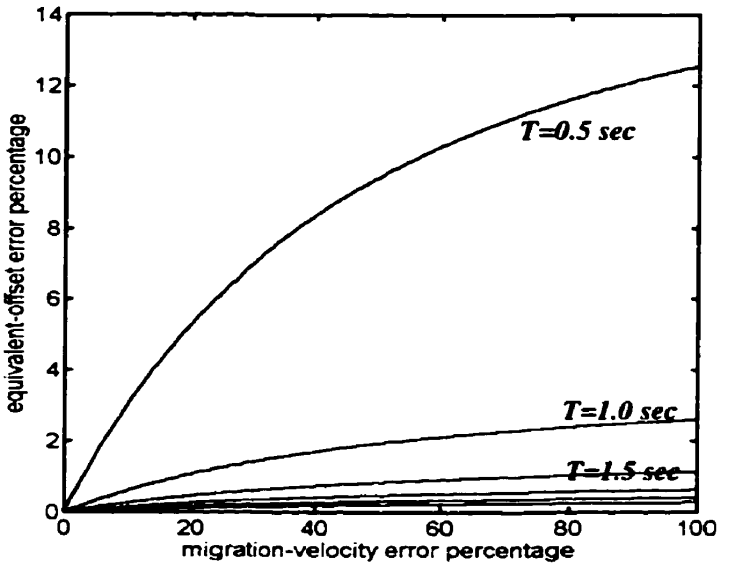

Figure 3-10: Relative equivalent offset error versus relative velocity error for different traveltime T's.

3.4.3 Sensitivity versus accurate velocity V

Figure 3-11 shows some equivalent offset error curves for different accurate migration velocities V. For all these curves, x, h and T are fixed at 600 meters, 500 meters and 1.0 second respectively.

The sensitivity of equivalent offset error versus input velocity error decreases as the migration velocity V increases. For example, in Figure 3-11, when the accurate migration velocity is 2000 m/s, if 4000 m/s (100% error) is used, the equivalent offset will be 6.5% more than the accurate value. While if the accurate velocity is 4000 m/s, an 8000 m/s (also 100% error) velocity is used, the equivalent offset will be only 1.5% more than the accurate value.

As a summary, when the migration distance is relatively small relative to offset, the sampled traveltime is relative large and the migration velocity is large, the velocity (larger than accurate) error may not be a serious problem. This is true at least for forming static reference traces by the EOMAP method, which will be discussed in the next chapter.

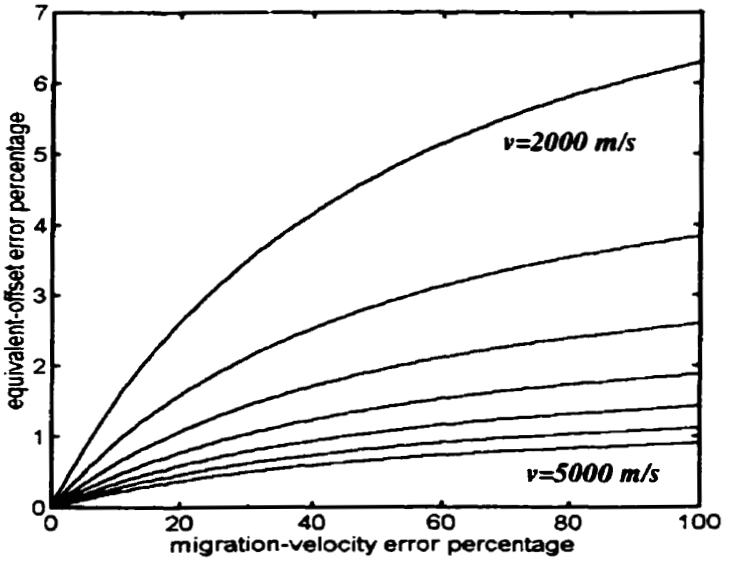

Figure 3-11: Relative equivalent offset error versus relative velocity errors for different accurate migration velocities V.

Chapter 4

Residual Statics Analysis by Equivalent Offset Mapping

Many new methods for residual statics analysis concentrate on how to build more reliable reference traces for traveltime distortion estimation, especially when hyperbolic moveout assumption is violated by either the significant statics or high complexity of the subsurface structure. The depth migration plus de-migration method by Tjan, et al. (1994), and Larner (1998), and the f-x static method by Chan and Stewart, (1996) are the examples. This chapter focuses on the development of a new method of forming reference traces for residual statics analysis using the concepts of equivalent offset and CSP gathering. Many concepts involved in this chapter are based on the related definitions of the previous two chapters.

4.1 Relation between prestack migration and residual statics analysis

Normal moveout (NMO) correction and CMP stacking together can be considered as a simplified intermediate step for seismic prestack migration. Residual statics analysis is originally a technique developed for obtaining better CMP stacked sections by estimating and correcting the random traveltime anomalies on seismic traces. Because of this relationship between NMO-plus-stacking (NMOPS) and residual statics analysis, a natural relationship between residual statics analysis and prestack migration is introduced. In this case, residual static correction may be considered as a process for enhancing the quality of migrated stacked sections, instead of the CMP stacked sections.

4.1.1 NMO, CMP stacking and residual statics

When the subsurface structure is not very complex, the reflection traveltime of a seismic wave from a reflector follows approximately a hyperbolic trajectory along the offset direction at each CMP location. The hyperbolic traveltime trajectory is called *normal moveout* (NMO). NMO correction is the process attempting to align the normal moveout energy to zero-offset traveltime with proper velocity information. The aligned

(NMO corrected) energy in all the CMP gathers will be constructively enhanced by the CMP stacking process to produce an interpretable image (stacked section) of the subsurface structure.

Residual statics, as random traveltime distortions on seismic traces, make the normal moveout trajectories more or less deviated from hyperbolas. These statics still exist after NMO correction, and become random errors deviated from the zero-offset times. The CMP stacking process and some spatial filtering attenuate the effect of the randomness of the residual statics. The CMP stacked traces should contain statistically more reliable traveltime information.

The higher reliability of the traveltime information on CMP stacked traces allows these stacked traces to be the reference traces for estimating the possible traveltime distortions on the traces before stacking. Conventional methods of residual statics analysis using stacked sections as model data can be illustrated as a scheme in Figure 4-1.

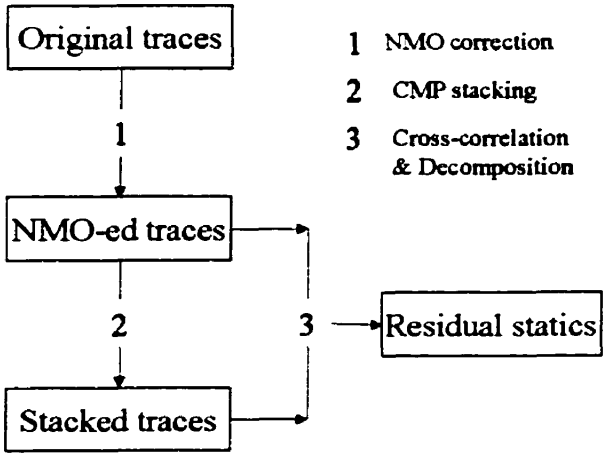

Figure 4-1: Many conventional residual statics analysis methods compare CMP stacked traces with the NMO corrected traces before stacking to estimate the possible traveltime deviations.

When using a stacked section as model data, cross-correlations are performed between stacked traces and NMO corrected traces. This is because NMO is required for CMP stacking instead of a requirement by statics analysis. The stacked traces can "equivalently" be used as the references for the original pre-NMO traces by removing the NMO corrections. That is, for each seismic trace in a CMP gather, its reference trace can

be formed by applying inverse NMO (INMO) to the stacked trace with the appropriate offset and velocity information that are the same as that used to NMO correct the seismic trace. This process is illustrated in Figure 4-2.

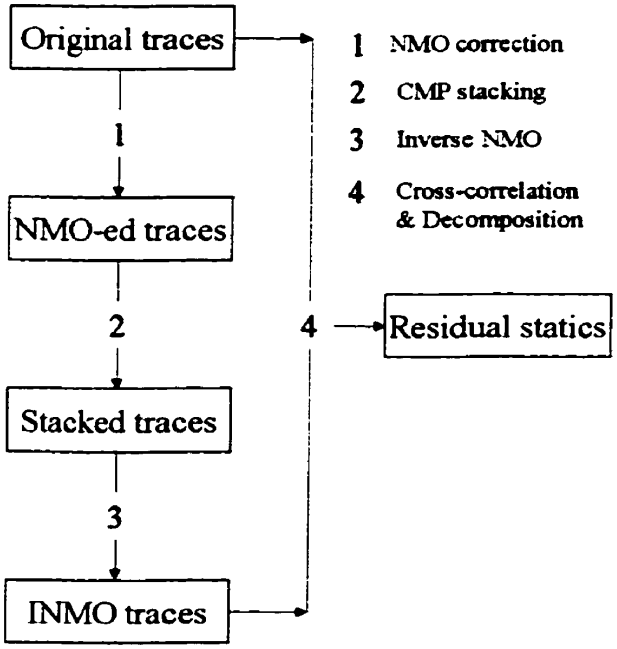

Figure 4-2: Residual statics can also be estimated by comparing the original seismic traces before NMO with the stacked traces INMO-ed by the proper offset and velocity information.

Statics analysis using the scheme shown in Figure 4-2 should have less velocity dependence and less influence from improper NMO correction. Unfortunately, INMO can not exactly reverse the NMO operation applied on seismic traces. In addition, the velocity errors involved with NMO correction can usually be reasonably removed by proper approximation of the residual NMO (RNMO) errors during statics estimation, the INMO step seems unnecessary in practice.

For the purpose of forming reference traces, it is the statistical property of the stacking process that really contributes. The NMO correction, as a deterministic process, is used only because it is required for CMP stacking. If there are other methods that can also utilize the stacking property to reduce the randomness of traveltime deviations, NMO may not be necessary.

The residual statics analysis methods requiring NMO correction are based on the assumption that the reflection events follow normal moveout hyperbolic trajectories in CMP gathers. This assumption is not valid when the earth subsurface structure is complex. Example 4-1 shows an example.

Example 4-1: Non-hyperbolic moveout trajectories

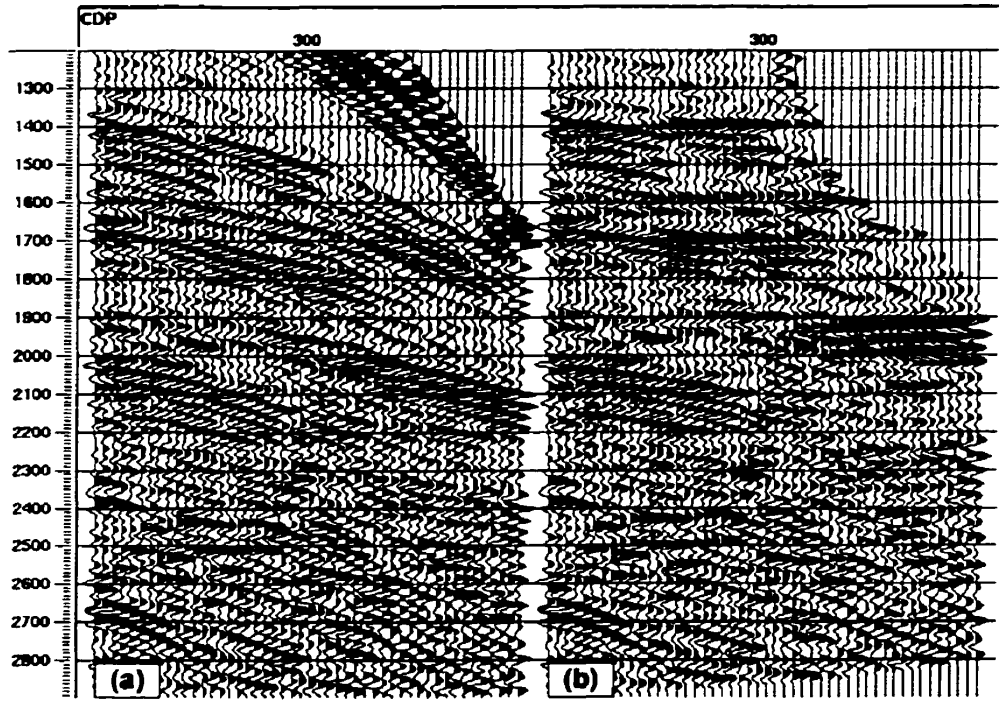

Figure E4-1-1: A CMP gather (a) from the raw Marmousi model data with its NMO corrected version (b).

The CMP gather shown in Figure E4-1-1a is taken from the raw Marmousi data, which was numerically generated and no statics are present. From the time range of 1200 ms to 2900 ms, there are few energy trajectories of the reflection events that can be fitted in portions of the offset range with normal moveout (hyperbolic) curves. Virtually none of them can be flatted in the entire offset range by NMO correction (Figure E4-1-1b). Some more experiments with the Marmousi model data will be discussed in detail in Chapter 5.

4.1.2 Prestack migration and NMO-stacking process

Prestack migration and NMO plus stacking (NMOPS) have at least two aspects in common. They both start from the seismic data before NMO correction, and they both produce "pictures" of the Earth's subsurface.

The following discussions analyze the similarities and differences of these two processes (prestack migration and NMOPS) in more detail.

First, prestack migration can be decomposed into two separable steps: moveout time correction and trace stacking. The moveout correction in the migration processes can be called migration moveout (MMO) correction, and the stacking process after MMO can be called common scatter point (CSP) stacking or common image point (CIP) stacking. Reflection events on NMO corrected traces in a CMP gather are assumed aligned at the same zero-offset times cross the offset direction. MMO corrected traces at certain CSP or CIP location are also assumed similar to each other. MMO corrected energy at samples with the same time or depth should come from the same scatter point. Similar to CMP stacking, the CSP or CIP stacking process can be considered as a tool for signal enhancement, and it also attenuates the randomness of traveltime deviations on the seismic traces.

Second, in NMOPS, each input trace only contributes to one output location, and only one NMO correction is applied on this trace. In the migration process, an input seismic trace theoretically contributes to all the output CSP or CIP locations, and different MMO corrections may be applied for different output locations (Figure 4-3).

Third, the total number of traces that contribute to each CMP stacked trace is the fold of the present CMP gather. Theoretically all traces in the prestack data volume have contribution to a migrated trace (Figure 4-4). A CMP stacked trace only collects the energy from one CMP gather, while a migrated trace contains energy from all the traces within related migration aperture.

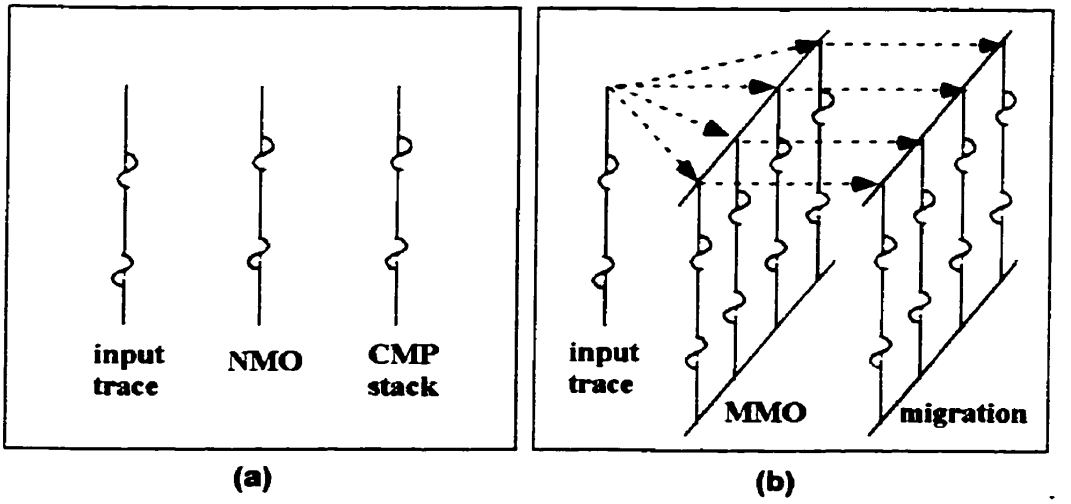

Figure 4-3: The difference between the energy contributions of an input trace to the output locations of (a) NMOPS and (b) prestack migration.

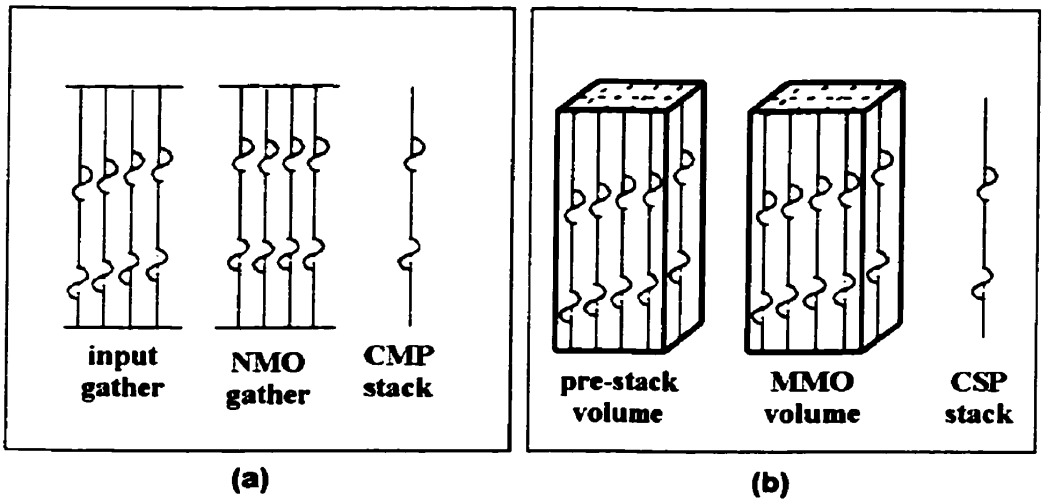

Figure 4-4: The difference between CMP stacked traces (a) and the migrated traces (b) in terms of collecting energy from input prestack data volume.

These similarities and differences between NMOPS and prestack migration imply that prestack migration can be considered as an extension of NMOPS, and some applications related to NMOPS, such as residual statics analysis, can be naturally related to prestack migration.

4.1.3 Static reference model by prestack migration and de-migration

As discussed in **4.1.1**, NMOPS plus INMO process forms reference traces for residual statics analysis. For later comparison, the reference-trace-forming part of Figure 4-2 is reformatted as Figure 4-5.

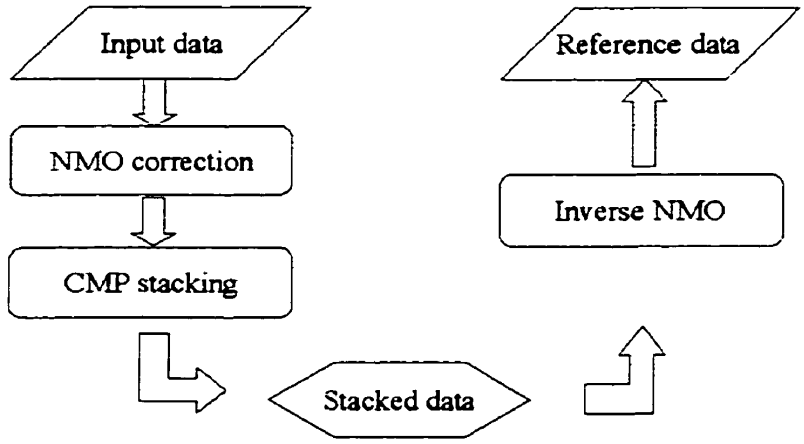

Figure 4-5: NMO plus CMP stacking followed by inverse NMO forms prestack dataset as a reference model for residual statics analysis.

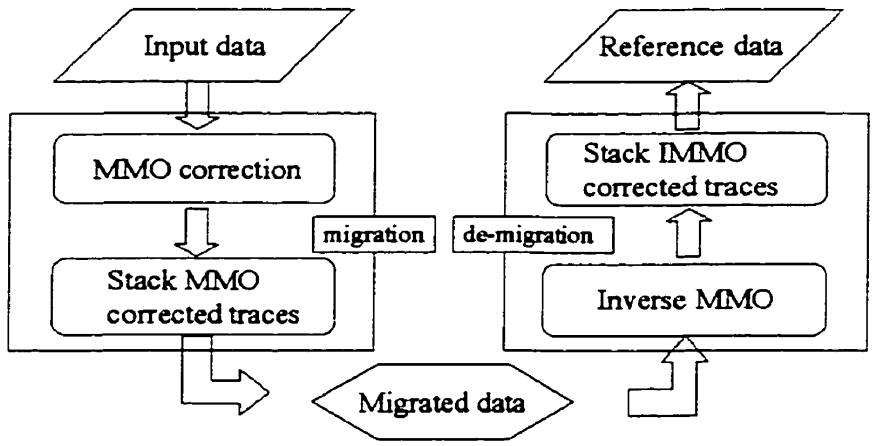

Figure 4-6: Prestack migration and its inverse (de-migration) can form reference data for residual statics analysis.

Prestack migration, including MMO and CSP (CIP) stacking, can form reference data for statics analysis by introducing an inverse operation for the migration process (called de-migration). As shown in Figure 4-6, this de-migration should contain an

inverse of MMO correction (IMMO) and an inverse for the stacking process, which can be a stacking process applied to IMMO corrected traces.

Migration followed by de-migration has some advantages over NMOPS plus INMO in terms of forming reference traces. Both the migration and the de-migration include stacking processes involving many more traces than CMP stacking, so the process shown in Figure 4-6 should better attenuate the random traveltime errors. At least, the processes should be less influenced by low CMP fold, where traveltime errors may not be attenuated in CMP stacking process.

The migration process involves more traces than NMO and CMP stacking, therefore it may also introduce more errors due to inaccurate MMO corrections. The accuracy of migration moveout (MMO) correction depends on the accuracy of migration velocities, which are usually more difficult to observe than NMO stacking velocities. The velocity dependence restricts the practical applications of migration plus de-migration method to form static reference traces (Larner, 1998)

Fortunately, EOM, as a prestack time migration, provides a convenient algorithm to form reference data for residual statics analysis with little velocity dependence. This will be presented in later sections.

4.2 Equivalent offset mapping and residual statics

Forming CSP gathers from CMP gathers in the EOM process can be considered as a mapping from source-receiver offset to equivalent offset and it can be called equivalent offset mapping (EOMAP).

4.2.1 EOMAP's: forming static reference data

Instead of direct MMO and CSP or CIP stacking in conventional Kirchhoff migration process, a full prestack time migration can be performed through the following steps:

1. Forming CSP gathers by EOMAP,

2. Amplitude correction, filtering and NMO correction (Kirchhoff NMO) on each CSP gather,

3. Stacking each CSP gather.

EOM method uses two separated steps (1 and 2 above) to complete the MMO correction. Therefore the process shown in Figure 4-6 can be interpreted using EOM concepts, and it becomes a scheme illustrated in Figure 4-7.

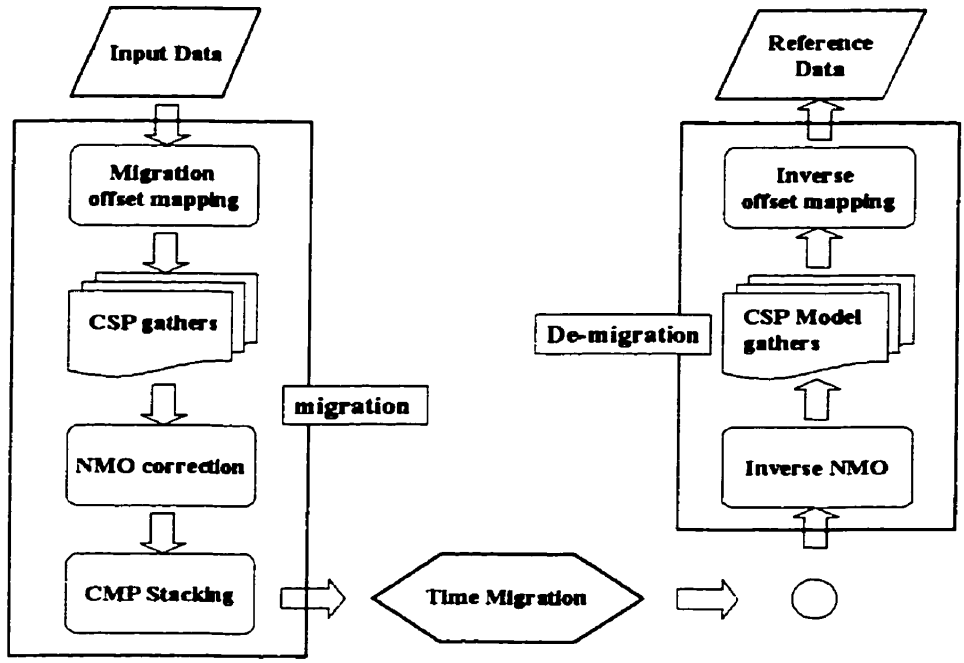

Figure 4-7: Full migration and de-migration processes with EOM process involved.

Note that in the de-migration process in Figure 4-7, a set of "model" CSP gathers is formed by applying multi-offset INMO on migrated traces. The entire scheme can be simplified by

- replacing model CSP gathers with the CSP gathers formed in the migration process, and
- ignoring the NMO and stacking applied to CSP gathers and the INMO process.

The new scheme becomes very simple as shown in Figure 4-8. This scheme forms a new algorithm for building residual statics reference traces based on the migration equivalent offset mappings. This method will be referred as EOMAP statics method later in this thesis.

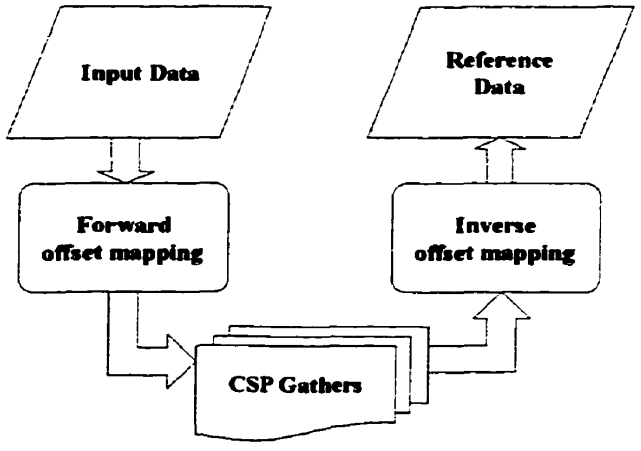

Figure 4-8: Reference traces for residual statics analysis can be more efficiently formed by using just the forward and inverse equivalent offset mappings.

The forward EOMAP (from source-receiver offset to equivalent offset) and the inverse EOMAP (from equivalent offset back to source-receiver offset) both include stacking processes that can attenuate the traveltime random errors. They should make the CSP gathered traces and the final reference traces contain more reliable traveltime information.

4.2.2 Explanations from the scatter point and Cheop's pyramid

Using the concepts of the scatter point model and the Cheop's pyramid, the relation between prestack migration and static reference data can be described graphically. A graphic explanation of EOMAP statics method can also be introduced.

The scatter point model assumes that a recorded 2D seismic prestack volume is a superposition of an arrangement of Cheop's pyramids, and each of these pyramids corresponds to one scatter point on the migration image. For time migration, the location of such a scatter point is simply the apex of the Cheop's pyramid. A pyramid and its

corresponding scatter point for the constant velocity cases are shown in Figure 4-9. In Figure 4-9(b), the Cheop's pyramid is shown in light grey color to emphasize the location of its scatter point. The coordinates are horizontal distance (x) source-receiver offset (h) and the depth (z).

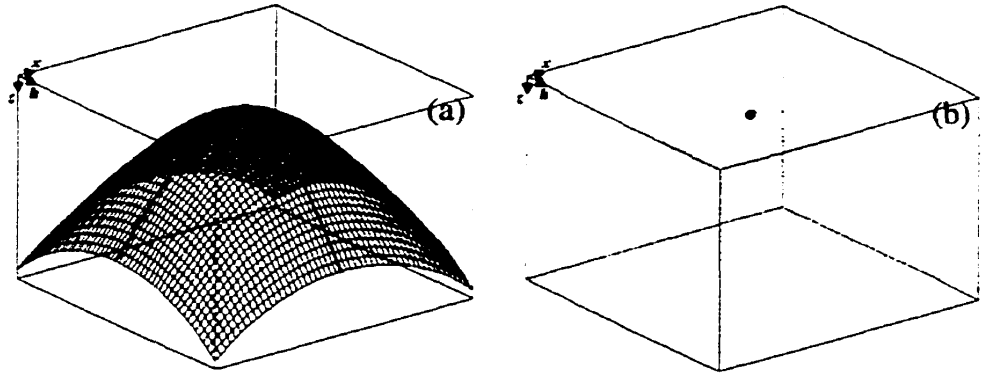

Figure 4-9: A Cheop's Pyramid (a) and its corresponding scatter point, shown as the heavy black dot in (b).

Prestack migration is the process that collapses the energy on every Cheop's pyramid back to its corresponding scatter point (from (a) to (b) in Figure 4-9). Seismic modelling is the inverse process that produces a Cheop's pyramid from a scatter point (from (b) to (a) in Figure 4-9).

EOM is a prestack migration method that introduces an intermediate step of CSP gathering. Instead of directly collapsing a pyramid into a point, this CSP gathering process collapses a Cheop's pyramid of Figure 4-10 (a) to a hyperbola in the offset direction of Figure 4-10 (b). A consequent step then collapses the hyperbola into the desired scatter point in Figure 4-10 (c).

The CSP gathering step (from (a) to (b) in Figure 4-10) can be considered as a partial migration. Its inverse process can be kinematically introduced as a process that produces Cheop's pyramid from each hyperbola in the CSP gathers (from (b) to (a) in Figure 4-10).

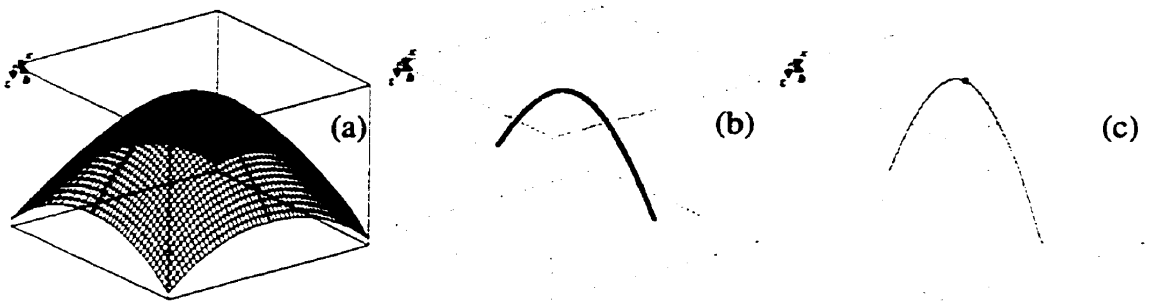

Figure 4-10: EOM collapses a Cheop's pyramid (a) to a hyperbola in the offset direction (b), which is then collapsed to the scatter point (c).

In the EOM method, the pyramid-to-hyperbola process keeps the traveltime constant. Figure 4-11 illustrates both the forward (a) and inverse (b) equivalent offset mappings in terms of the constant traveltime contours of the Cheop's pyramid. The arrows in the figure show the directions of energy collection or distribution. In (a), all the energy at the closed curve of each time level is collected and put to one location (zero horizontal distance in the figure); and in (b), the energy at each CSP location is distributed to a closed curve at each time level. The pyramid-to-hyperbola relationship can be simplified as one between a closed curve and one point at each time level.

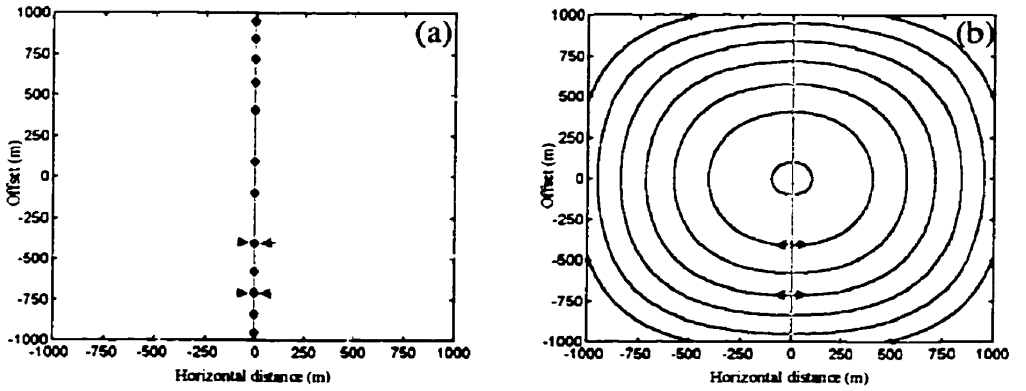

Figure 4-11: Forward equivalent offset mapping (a) and its inverse (b) shown in terms of the constant traveltime contours of Cheop's pyramid.

4.2.3 Computation of Inverse equivalent offset mapping

The formulation of forward EOMAP has been discussed in detail in Chapter 3. The computation of the inverse EOMAP can be directly derived from the forward algorithm because they both are based on the same relationship.

Forward EOMAP distributes the energy at an input sample to different CSP gathers with different equivalent offset values. The inverse EOMAP attempts to collect all the energy back from the CSP gathers and put it back at this sample as shown in Figure 4-12. When the migration velocity is constant, the energy at a sample is distributed to the traces located along the equivalent offset hyperbola in forward mapping. The energy on this hyperbola will be collected back to this sample in the inverse mapping. The hyperbolic function forms the basic relation for both forward and inverse EOMAP's.

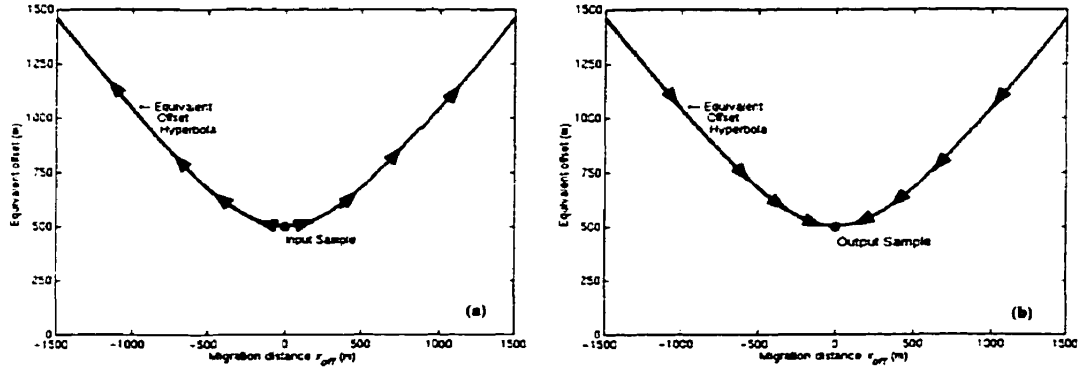

Figure 4-12: Forward (a) and inverse (b) EO mappings in terms of the relation between a recorded sample and its corresponding equivalent offsets hyperbola. The arrows indicate the direction of the energy movement during the mappings.

The major tasks in both forward and inverse EOMAP's are the same: finding the relation between triplets (x_{cmp}, h, T) and (x_{csp}, h_e, T), which is described by the same equation

$$h_e^2 = h^2 + x_{off}^2 - \frac{4x_{off}^2 h^2}{(VT)^2},$$

where $x_{off} = x_{cmp} - x_{csp}$. The variables x_{cmp} and x_{csp} stand for CMP location and CSP location respectively, T the related traveltime, h the half source-receiver offset, and h_e the equivalent offset. The velocity V may vary with different CSP locations.

An efficient algorithm for inverse EOMAP as following is used.

Loop 1: for each pair of source and receiver locations in the acquisition geometry,
the CMP location and half source-receiver offset are computed.
Loop 2: for each CSP gather,
the migration velocity array is available, and
the migration distance is computed.
Loop 3: for each equivalent offset,
the equivalent offset boundaries are available, and

- Use the same algorithm described in Section ***3.3.1.2***, to compute the traveltime boundaries
- Sum (with scaling if needed) the trace segment defined by the time boundaries at present CSP gather and present equivalent offset to the trace segment at present source and receiver locations

End Loop3
End Loop2
End Loop1

4.2.4 Amplitude scaling considerations

Amplitude-scaling factors should be considered during both the forward and inverse EOMAP's.

As mentioned in chapter 3, the near offset coherent energy appearing on farther offset traces of CSP gathers should be attenuated for the purpose of forming static reference traces. This near-offset energy sometimes affects the similarity between seismic traces and their corresponding reference traces, and may result in inaccurate estimations of traveltime distortions on seismic traces.

When applying the scaling factors during the forward and inverse EOMAP's, the following principle should be honored:

> If a sample is scaled by a factor when its energy is summed to a CSP gather in the forward EOMAP, the same factor should be used to scale the energy from this CSP gather for summing back to the original sample location in the inverse EOMAP.

This can be compared with the relationship between migration and modelling. For example, a prestack Kirchhoff migration algorithm should attempt to use the same amplitude scaling factors used by an accurate Kirchhoff diffraction modelling algorithm.

4.3 Total velocity independence: the asymptotic EOMAP's

As in section **3.2** and Figure 3-3, the samples on one seismic trace usually have limited equivalent offset range, especially those samples at later traveltimes. The equivalent offset h_e of some input sample (x_{cmp}, h, T) has been previously stated as

$$h_e^2 = x^2 + h^2 - \frac{4x^2h^2}{V^2T^2}, \tag{4-3-1}$$

where V is the migration velocity at some CSP location x_{csp} for this sample, and $x=|x_{csp}-x_{cmp}|$ is the horizontal distance between the CMP and the CSP locations. When the value of VT is relatively large to x and/or h, the equivalent offset h_e approaches a traveltime independent and velocity independent value $h_{e\omega}$ as

$$h_{e\omega} = \sqrt{x^2 + h^2}. \tag{4-3-2}$$

This $h_{e\omega}$ is called the *asymptotic equivalent offset* of this input sample. The traveltime independence implies that all the samples on an input trace have the same asymptotic equivalent offset for each CSP location.

An asymptotic equivalent offset is accurate when either h or x equals to zero. Therefore, when h is small relative to x, or x is small relative to h, or in other words, when x or h is small relative to the equivalent offset, the asymptotic equivalent offset can

be a good approximation at any traveltime. In addition, The equivalent offsets of samples at finite traveltimes tend to the asymptotic equivalent offset when the migration velocities are very high.

In practice, velocity cannot be infinite, but a maximum possible velocity, V_{max}, can always be estimated for any seismic experiment. Also, there is always a maximum recording T_{max} in any seismic data. By these two "maximum" quantities, a better approximation for equivalent offset h_{em} can be defined as (Bancroft, 1998c)

$$h_{em}^2 = h^2 + x^2 - \frac{4x^2h^2}{V_{max}^2 T_{max}^2}, \tag{4-3-3}$$

which is also velocity and traveltime independent. We call this new approximation *pre-asymptotic equivalent offset*. Because of

$$h_e^2 \le h_{em}^2 \le h_{e\omega}^2,$$

pre-asymptotic equivalent offset h_{em} is always a better approximation to h_e than $h_{e\omega}$.

A detailed analysis of the relations between equivalent offset and its two asymptotic approximations are summarized in Figure 4-13, Figure 4-14 and Figure 4-15. In all three figures, the accurate equivalent offset values are drawn in solid lines, the asymptotic equivalent offset values are shown in dashed lines, and the pre-asymptotic equivalent offset values are shown with dotted lines. The migration velocities used for these examples are the same constant value, 2500 m/s, and all the input samples are assumed to be at the same CMP location for simplicity.

Figure 4-13a shows the equivalent offsets and corresponding asymptotic equivalent offset values of three input samples all at traveltime ***T=1.0*** second. These three samples have half source-receiver offsets 200 m, 800 m, and 1400 m respectively. The solid line (for accurate equivalent offset) at the farthest offset is missing because the input half source-receiver offset (1400 m) is too large for the traveltime (1.0 second) and the velocity (2500 m/s) to have valid equivalent offset values. Figure 4-13b shows the differences between the accurate equivalent offsets and their corresponding asymptotic

approximations for the three samples. Again, the differences for the sample at offset 1400 m is not valid for the traveltime *T=1.0* second.

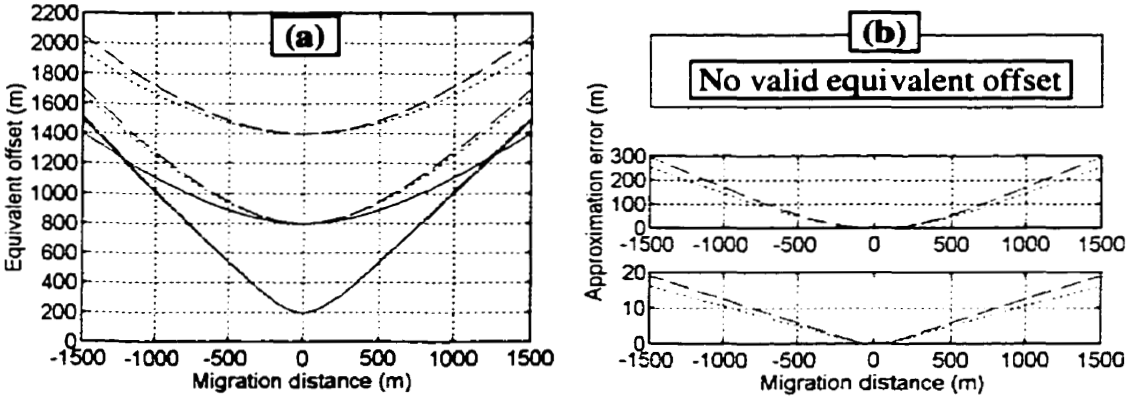

Figure 4-13: (a) Equivalent offsets and their corresponding asymptotic and pre-asymptotic approximations of samples at time *T=1.0* second. (b) The differences between the accurate equivalent offsets and their approximations.

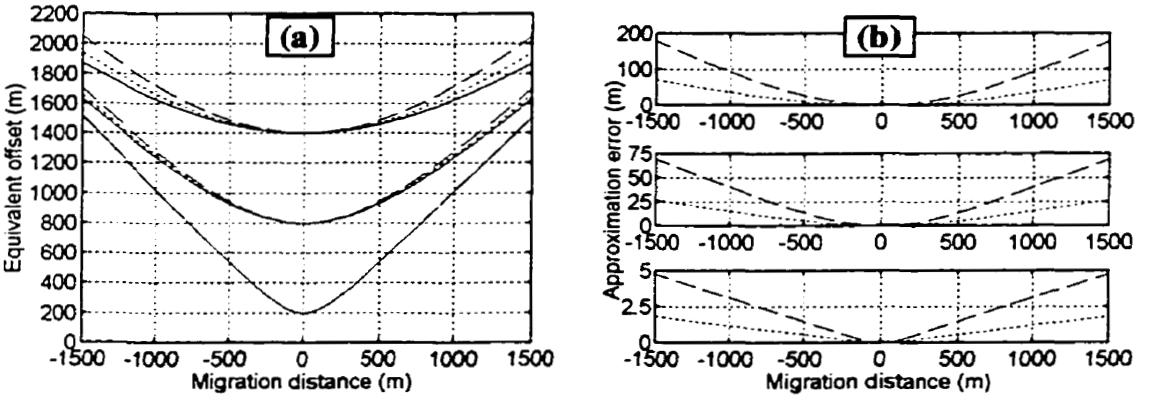

Figure 4-14: (a) Equivalent offsets and their corresponding asymptotic and pre-asymptotic approximations of samples at time *T=2.0* second. (b) The differences between the accurate equivalent offsets and their approximations.

Figure 4-14a illustrates the equivalent offsets and the corresponding asymptotic equivalent offset values of three input samples all at traveltime ***T=2.0*** second. These three samples also have half source-receiver offsets of 200 m, 800 m and 1400 m respectively. Figure 4-14b shows the differences between the accurate equivalent offsets and their corresponding asymptotic approximations for the three samples.

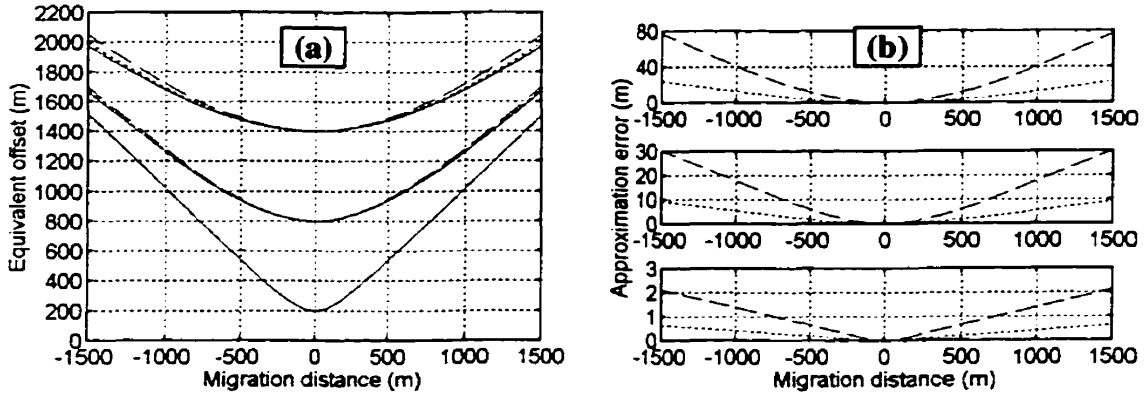

Figure 4-15: (a) Equivalent offsets and their corresponding asymptotic and pre-asymptotic approximations of samples at time *T=3.0* second. (b) The differences between the accurate equivalent offsets and their approximations.

Figure 4-15a illustrates the equivalent offsets and corresponding asymptotic equivalent offset values of three input samples all at traveltime ***T=3.0*** second. These three samples also have half source-receiver offsets of 200 m, 800 m and 1400 m respectively. Figure 4-15b shows the differences between the accurate equivalent offsets and their corresponding asymptotic approximations for the three samples.

The following conclusions can be drawn from the results in the above three figures.

1. The smaller the source-receiver offset, or the larger the traveltime, the better the approximation.
2. For the near-offset samples, the two asymptotic approximations have very high accuracy for any migration distance at any traveltime. The maximum error (shown in Figure 4-13) is less than 1.5% (20/1500) of the accurate equivalent offset. Symmetrically, when the migration distance is small, the two asymptotic approximations also have very high accuracy.
3. At the later time of 3.0 seconds, as in Figure 4-15, the two approximations are fairly accurate for large range of offsets (from 200m to 1400m in the figure), especially the pre-asymptotic approximation h_{em} (less than 2%).

4. At relatively earlier times and larger offsets, for example, 1.0 second and 800m in Figure 4-13 (error is about 20%) or 2.0 seconds and 1400m in Figure 4-14 (error is about 10%), both approximations have lower accuracy.

The asymptotic equivalent offsets are usually not used for the purpose of migration because of their inaccuracy. However, the asymptotic equivalent offsets can be routinely used in forming reference data for statics because of the following reasons.

(1) The computations of these approximations take much less time than the computation of accurate equivalent offsets.

(2) The migration distance can be limited to a relatively smaller range for higher accuracy of the asymptotic approximation, while the randomness of the residual statics can still be attenuated by the forward and inverse asymptotic EOMAP's.

(3) Asymptotic equivalent offsets have higher accuracy at latter times, and residual statics can be well estimated by only using reflection signals from later times.

4.4 Residual statics analysis

The EOMAP statics method is new mainly because of its new way of forming reference traces, which is the first step of residual statics analysis as discussed in Chapter 2. This new method of reference trace forming is different from the conventional methods by

- introducing migration and de-migration concepts and it is theoretically not limited by the assumption of hyperbolic normal moveout, and
- forming an individual reference trace for every trace in the prestack data volume.

It is also different from the method introduced by Tjan et al. (1994) and Larner (1998) where prestack depth migration and its inverse were used to form reference traces. Specifically, the EOMAP method

- uses partial prestack time migration (CSP gathering only) and its inverse instead of full depth migration;
- does not involve any time shift in the forward and inverse EOMAP processes;
- requires the minimal velocity information. If the asymptotic EOMAP is used, the whole process is totally velocity independent.

Theoretically, when the reference data is formed, any methods for Step 2 (cross-correlation) and Step 3 (decomposition) can be used. In the EOMAP applications discussed in this thesis, some specific techniques are used for Step 2 and Step 3.

The first method used in this thesis is a conventional process as follows:

- Cross-correlate between each seismic trace and its corresponding reference trace and obtain the time difference estimations;
- Use these time differences as the known observations and decompose them into surface consistent source and receiver statics using the two-term (source and receiver) linear equation system (the meanings of the symbols are the same as in section **2.5.1**)

$$T_{ij} = S_i + R_j . \qquad (4\text{-}4\text{-}1)$$

- Solve the equation system by the conventional Gauss-Seidel iteration algorithm or its combination with the Jacobi method (Carnahan et al., 1969).

For clarity, detailed derivation and formulation of the Jacobi and Gauss-Seidel iterative algorithms for the two-term linear equation system are described in Appendix A. A Matlab M-file that contains both two-term (source and receiver) and three-term (structure, source, and receiver) algorithms is also provided in the appendix.

The second method of use the reference traces in the EOMAP method is similar to the one introduced by Ronen and Claerbout (1985).

In the stack-power maximisation method (Ronen and Claerbout, 1985), a source super-trace is formed by linking all the traces in one source gather, and the corresponding

reference super-trace is formed by linking the corresponding reference traces. One cross-correlation between these two super traces is performed for each source gather, and it produces a time-lag estimation that is considered as the static shift at this source location. The surface consistent assumption is automatically honoured in this process. Similar super-trace cross-correlation is performed for each receiver location.

The method used here is a little different. Instead of forming super traces for one source (or receiver) gather, a correlating trace is formed for each source (or receiver) gather by stacking (summation) all the traces in the gather. The reference correlating trace is formed in the same way using the reference model source (or receiver) gather at the same location. The cross-correlation between these two traces directly produces the estimation of the source (or receiver) static, and the surface consistent assumption is automatically honoured. The scheme of this method (referred to as summation-trace cross-correlation method for simplicity) is illustrated in Figure 4-16.

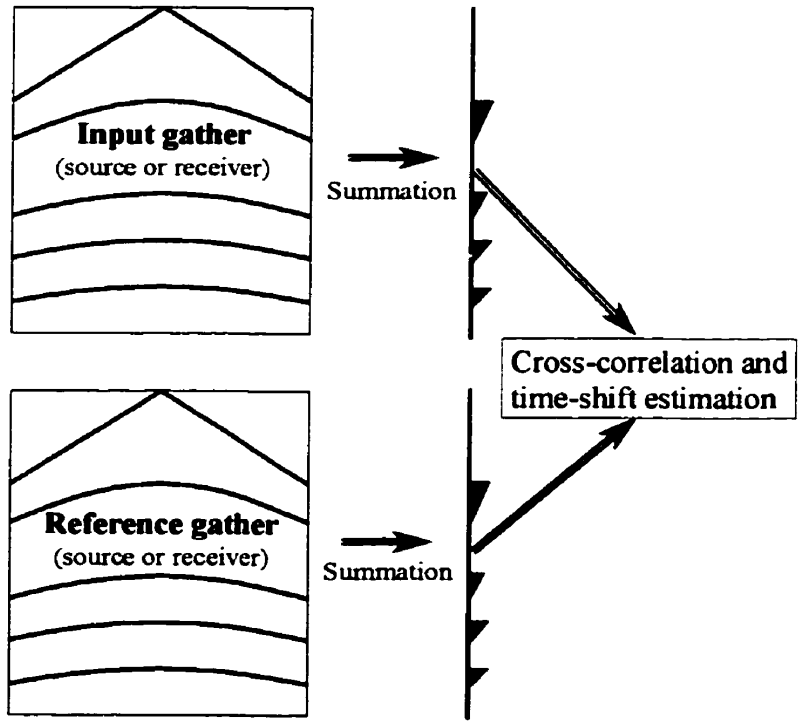

Figure 4-16: The scheme of the summation-trace cross-correlation method.

This method is simpler and faster because only one cross-correlation is needed for a source or receiver gather, and the correlating traces are of the same length of the normal traces (not like the super traces). In addition, the summation process in the scheme may increase the stability of the traveltime information, although the wavelet shape may change and the trace resolution may decrease. Many applications have proved the stability of the summation-trace cross-correlation method, however, more theoretical investigations may be needed for this method.

Comparisons between the results from these two methods (conventional Gauss-Seidel method and summation-trace cross-correlation method) conclude that the estimations with the summation-trace cross-correlation method are usually more stable and have higher accuracy, especially the experiments with the Marmousi model data. The lower-quality estimations from the Gauss-Seidel method may be because of the following reasons: The reference traces may not always have high quality in the trace-to-trace manner, and cross-correlations sometimes fail to provide good quality time difference estimations for the decomposition process.

Figure 4-17 shows the static estimations from both summation-trace cross-correlation method and the Gauss-Seidel method with the synthetic static shifts added to the original Marmousi model data. In general, the estimations from the summation-trace cross-correlation method have higher accuracy, although there are many source and receiver locations where Gauss-Seidel estimations are more accurate.

Figure 4-18 shows the static estimations from the Blackfoot data using both summation-trace cross-correlation and Gauss-Seidel methods. Both source and receiver statics from these two methods are very close. Their differences are always less than 2 ms. The high similarity between the results from these two methods may be because of the very high fold of the data (source fold is 200 and the receiver fold is 189). The high quality and high fold of Blackfoot data also benefit the EOMAP method of forming static reference traces, and high quality individual reference traces significantly benefit the Gauss-Seidel method. The little difference between these two methods on Blackfoot data

also shows that the summation-trace cross-correlation can be used as a general method for surface consistent statics decomposition.

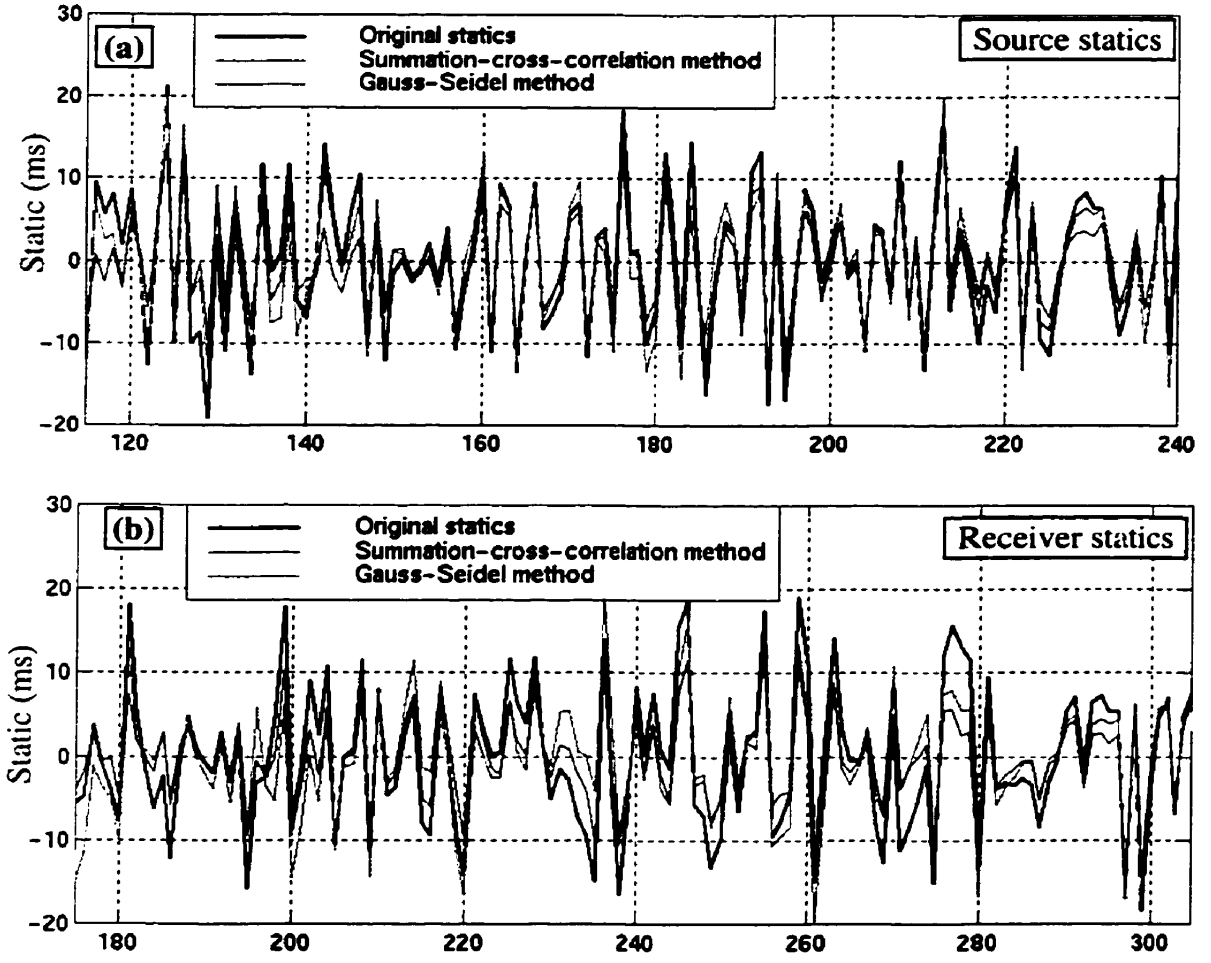

Figure 4-17: Comparisons of the source statics (a) and receiver statics (b) estimated by the summation-trace cross-correlation method and the Gauss-Seidel method from the Marmousi model data.

Almost all the static estimations by EOMAP method in the next chapter are obtained using the summation-trace cross-correlation method. In fact, only the results shown in Figure 5-4 are obtained by the Gauss-Seidel iterative method.

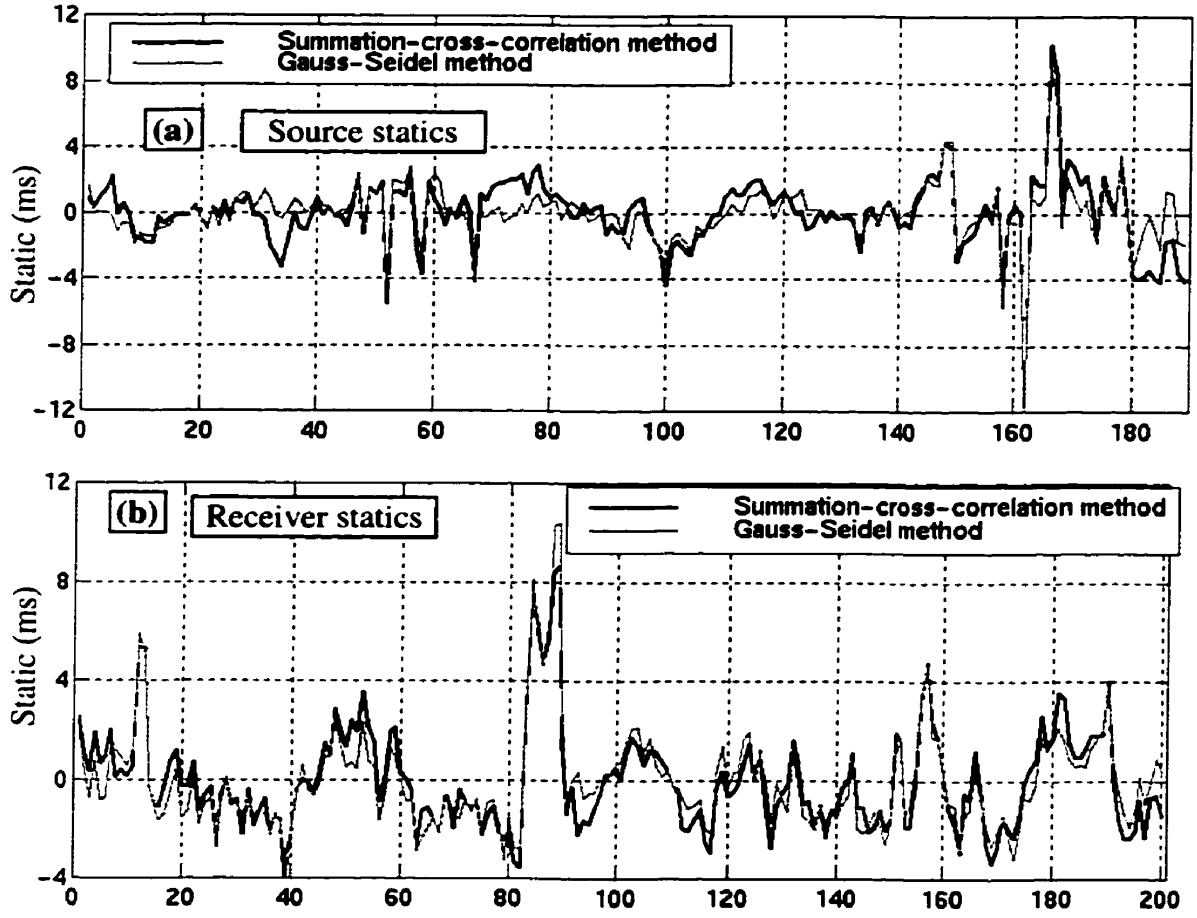

Figure 4-18: Comparisons of the source statics (a) and receiver statics (b) estimated by the summation-trace cross-correlation method and the Gauss-Seidel method from Blackfoot data.

The manner in which the EOMAP's build the reference traces aids the surface consistent decomposition of the traveltime differences on the seismic traces. The decomposition equation system (4-4-1) does not include the structure term and the offset term because the reference traces are formed with exactly the same structure and offset information as their corresponding seismic traces. Ideally, the reference traces formed by the EOMAP method can be considered as the "seismic traces" recorded with the same acquisition process but over a migrated earth subsurface image, which does not contain near-surface anomalies. The traveltime differences between real seismic traces and their corresponding reference traces are only the effects of near-surface anomalies, which are not directly related to offset or deeper subsurface structure.

Another important issue in the EOMAP statics method is the iterative property. Theoretically, any statics method can be iterative including the EOMAP statics method. Practically, with the experiences with synthetic and real data, the EOMAP method usually provides high accuracy statics at the first iteration. More iterations have not shown observable improvement of the static estimations. For example, with Blackfoot data, the first iteration of the EOMAP statics method provides very good static estimation, and there are virtually no statics left. While with the Marmousi model data, the first iteration reduces the size of the static shifts from 20 ms to about 5 ms, and there are still recognizable errors. However, because of the high complexity of the Marmousi model, the 5ms error is about the limit of the resolution of the EOMAP method. This can be seen from the static estimations by the EOMAP method with raw Marmousi data with no static shifts applied (Figure 5-31 of the next chapter).

Chapter 5

Applications and Discussions

This chapter presents some results from the applications of the equivalent offset mapping (EOMAP) statics method to synthetic data and field data. The results show that the EOMAP method can estimate the surface consistent residual statics with plausible accuracy, even for data acquired from area with complex subsurface structure where hyperbolic normal moveout (NMO) assumption is seriously violated.

5.1 Simple synthetic data

The first experiments are based on a set of synthetic data with random surface consistent time-shifts applied. Different residual statics methods are applied to the data under different conditions. A comparison of results illustrates the advantages of the EOMAP statics method.

5.1.1 Earth model and acquisition geometry

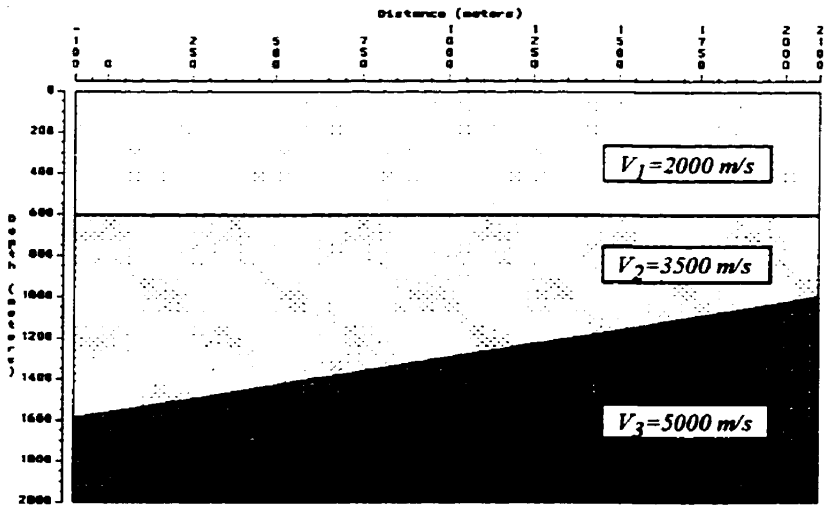

Figure 5-1: A simple two-reflector earth subsurface model with one reflector parallel to the flat earth surface and the other dipping about 15 degrees.

The experiments presented in this section are based on a simple three-layer earth subsurface model shown in Figure 5-1. The three layers are separated by two linear

reflection interfaces with the shallower one parallel to the perfectly flat earth surface and the deeper one dipping about 15 degrees from the right down to the left. The wave propagation velocities in the three isotropic layers are 2000 m/s, 3500 m/s, and 5000 m/s respectively.

A synthetic seismic dataset was generated using the acquisition geometry illustrated in Figure 5-2. The 41 shots range from 500 m to 1500 m (coordinates are as in Figure 5-1) with 25 meter interval. Each shot has 81 receivers (channels) located at –500 m to 500 m relative to the shot point location, and the receiver interval is 12.5 meters. As shown in Figure 5-3, this acquisition geometry results in a maximum CDP fold of 21.

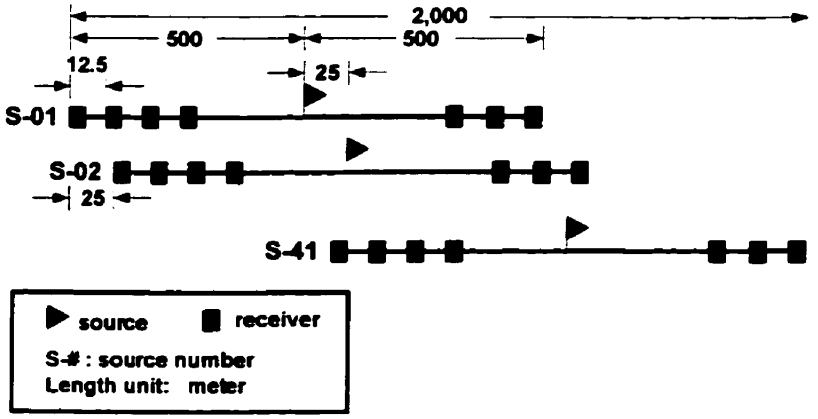

Figure 5-2: Geometry used to acquire a set of seismic data over the earth subsurface model shown in Figure 5-1. There are 41 shots with each having 81 channels.

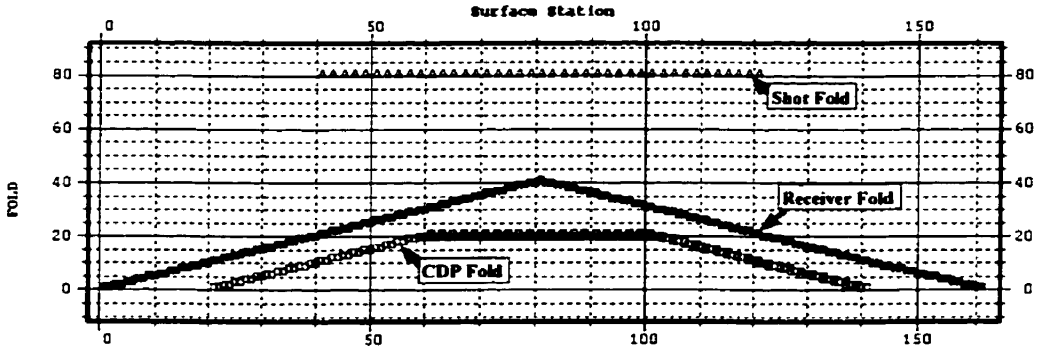

Figure 5-3: The CDP, receiver, and shot fold distributions of the acquisition geometry illustrated in Figure 5-2. The surface location ranges from 1 to 161, which are corresponding to 0 m and 2000 m with a 12.5-meter interval, as in Figure 5-1. The maximum CDP fold is 21.

The synthetic seismic data is numerically generated using GXII (GX Technology, Inc.) with a time-sample rate equal to 4 milliseconds. In the modeling process, the wave

mode conversion and the multiple reflections are ignored. A Ricker wavelet with 30Hz dominant frequency was used. There are 3321 traces in this dataset.

5.1.2 Direct application of EOMAP method to the traveltime-error-free data

One way to verify the reliability of the EOMAP statics method is to directly apply this method to the traveltime-error-free data where the statics should be zero.

Before any velocity analysis, a set of model data is created by using asymptotic EOMAP's (forward and inverse), and normalized cross-correlations are performed between the original traces and the model traces. As expected, the surface consistent source and receiver statics (Figure 5-4) estimated by using EOMAP reference data are very close to zero. The statics are not more than 0.25 ms. Only 2 source locations (two ends) greater than 0.01 ms. The receiver statics have only 5% larger than 0.1 ms and 23% larger than 0.01 ms. Comparing to the 4ms sample rate, 0.25 ms is practically negligible. This result at least shows that, when no statics are present in a set of seismic data, EOMAP method does not create irrational estimations.

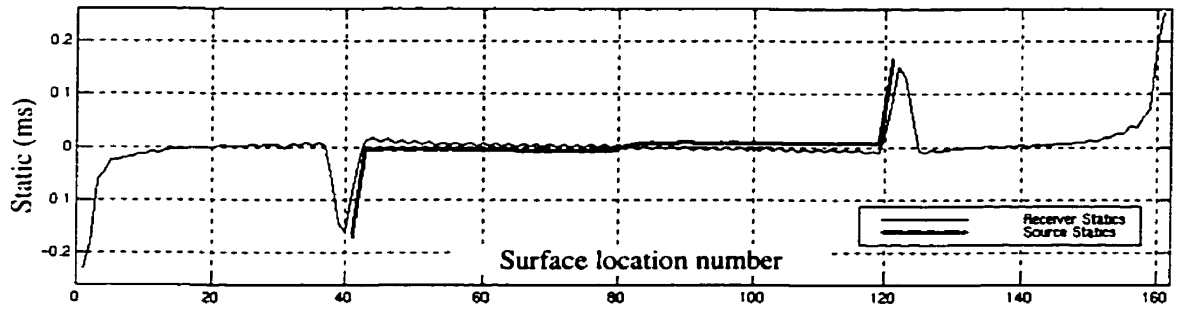

Figure 5-4: The statics estimated from a set of synthetic data without traveltime errors. The vertical axis is in the unit of milliseconds.

Note that there are some edge effects in the static estimations. At the two end receiver locations (ends of the seismic line), the statics estimation error tends to be larger. This is because the receiver folds are very low at the ends of the line. The relatively larger source static errors at the two end source locations are mainly caused by the larger errors of the receiver locations related to them. The receiver static errors at the end source locations are then caused by the edge-errors of the related source statics.

The following statistical analysis of the cross-correlation peak amplitude and peak lag time shows quantitatively the accuracy of the EOMAP method.

The cross-correlation peak amplitude values are all very close to 1.0. Among them,

- 100% (3321) are greater than 0.867;
- 80% (2670) are greater than 0.9;
- and 29.3% (973) are larger than 0.99.

The cross-correlation lag times (absolute values) are all very close to 0.0, and the average of all 3321 absolute values is 0.0216 (only 5% of the 4 ms sample rate). Among the 3321 values,

- only one is larger than 0.4 ms and it is located at the very end of the line;
- 93% are smaller than 0.1 ms;
- 74% of the lag-times are smaller than 0.01ms;
- 69% of them are smaller than 0.005ms.

5.1.3 Synthetic surface consistent time-shifts

From the traveltime-error-free data, another set of synthetic data was created by applying synthetic randomly distributed time shifts to each shot and each receiver. The source and receiver time shifts both range from –24 ms to 24 ms, and this leads to a maximum possible time-shift of 48 ms on each trace and a maximum 96 ms relative shift between two traces.

Figure 5-5 shows two two-sided super CMP gathers (summation of 5 adjacent CMP gathers) at the same location from two datasets, one without and one with the synthetic time-shifts added. It is difficult to observe reliable velocity information from a gather like Figure 5-5 (b). Figure 5-6 shows two stacked sections from these two datasets with the same stacking velocity field estimated from the original traveltime-error-free data. The quality of the stacked section is significantly affected by the synthetic time-shifts.

In the following sections, the residual statics analysis process for the data with synthetic time-shifts will be evaluated using the EOMAP statics method and some traditional methods. The conventional methods used include the maximum stack-power

method and the correlation autostatics method that are modules in Landmark's ProMAX 2D seismic data processing package.

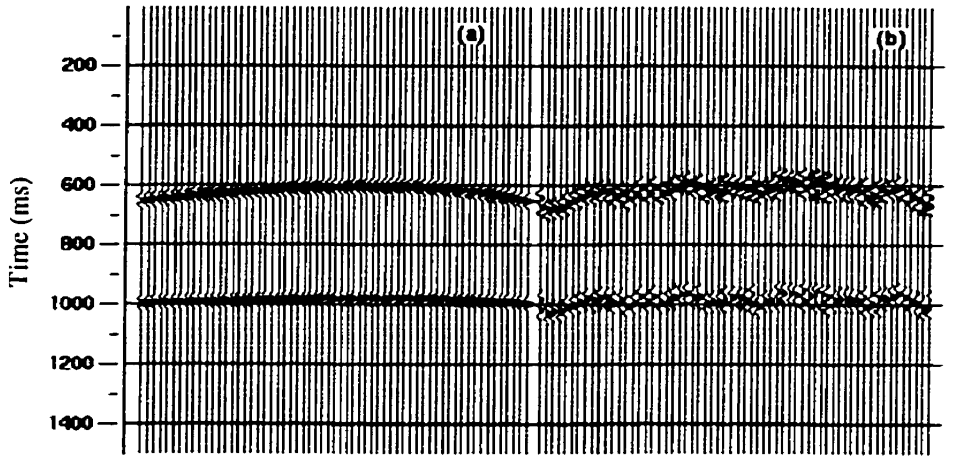

Figure 5-5: Super CMP gathers with 5 adjacent CMP gathers combined where **(a)** is formed from the original data without time shifts, and **(b)** after adding synthetic time-shifts at all source and receiver locations.

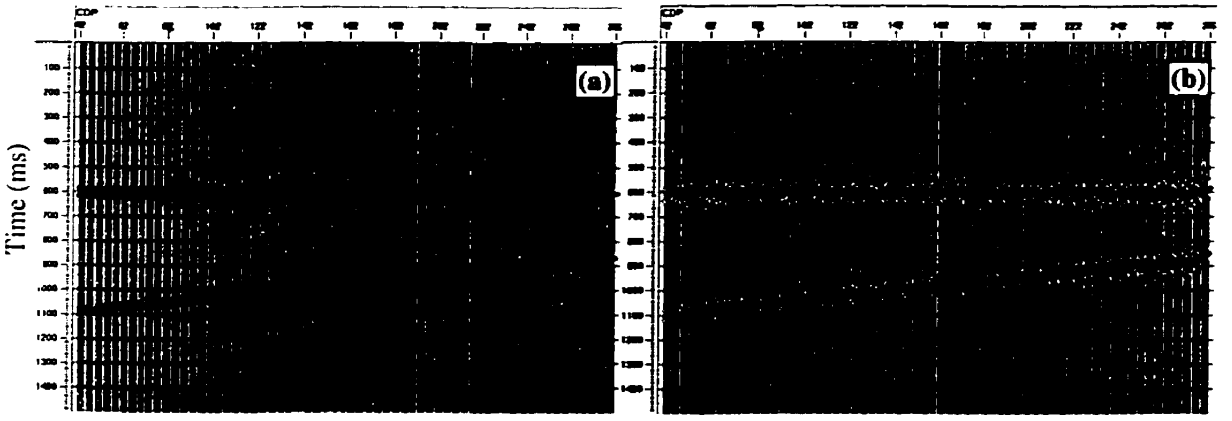

Figure 5-6: **(a)** The stacked section obtained from the data without traveltime errors and **(b)** the stacked section obtained from the data after synthetic time-shifts being added. The same stacking velocity is used for both sections, and it is observed from the error-free data.

5.1.4 Statics estimations and their comparisons

5.1.4.1 Ronen-Claerbout stack-power maximization method

The stack-power maximization method (Ronen-Claerbout, 1985) is one of the broadly used methods for surface consistent residual statics analysis. Like many other conventional methods, it requires that the input data be NMO corrected with proper stacking velocity. Using the accurate stacking velocity observed from the traveltime-

error-free data, the stack-power maximization method produces very accurate estimations of the source and receiver statics. The statics are shown in Figure 5-7, where the heavier lines are the estimations and the lighter lines are the synthetic shifts applied to the shot and receiver locations.

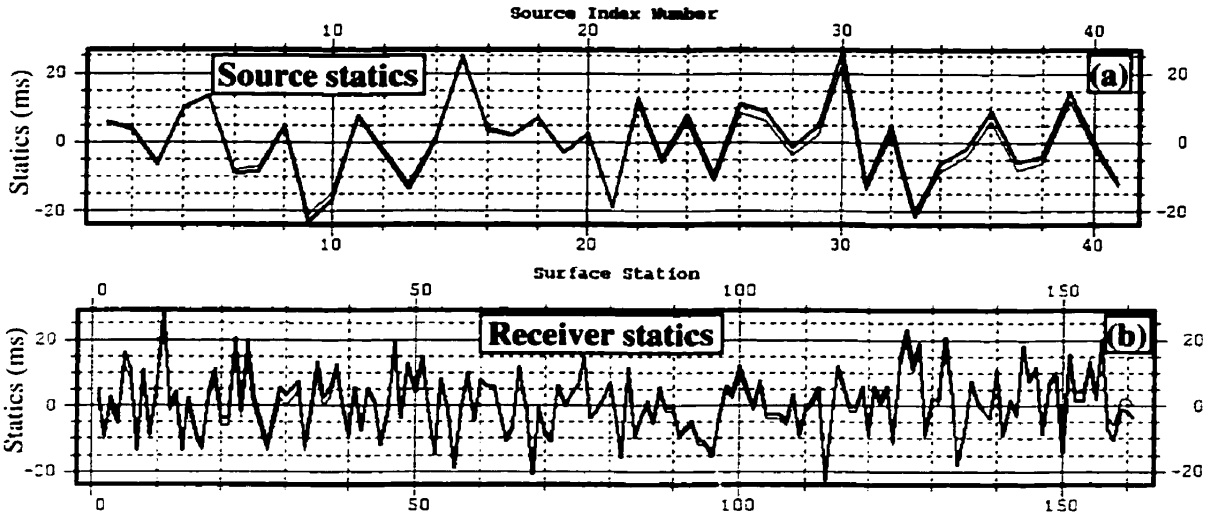

Figure 5-7: Estimations of the source statics (a) and the receiver statics (b) by the maximum stack-power method with accurate NMO velocities.

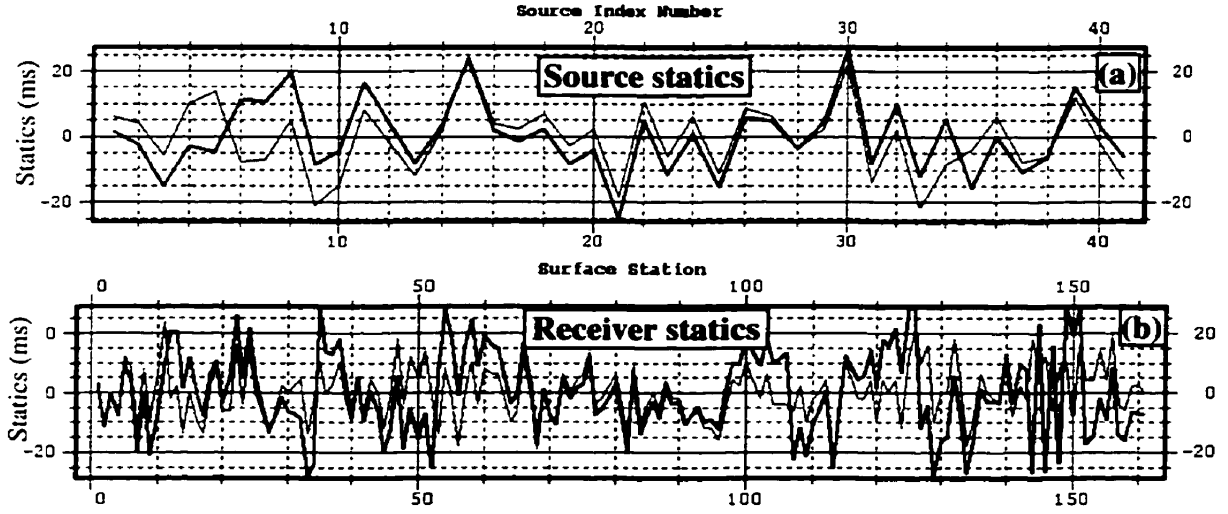

Figure 5-8: Estimations of the source statics (a) and the receiver statics (b) by the stack-power maximization method with a constant NMO velocity equal to 3000 m/s. The heavier lines are the estimations and the lighter lines are the synthetic shifts applied to the source and receiver locations.

Accurate NMO velocities are very difficult to observe when significant statics are present (see Figure 5-5 (b)). To illustrate the effects, the time-shifted traces were NMO corrected by a constant NMO velocity equal to 3000 m/s. The static estimations from this set of NMO corrected data by stack-power maximization method are shown in Figure 5-8. The static estimations are less accurate than those shown in Figure 5-7.

The estimation errors of the two experiments are shown in Figure 5-9, and this shows that the static errors due to the velocity error are significant. The darker lines are the errors from the estimations with constant 3000 m/s NMO velocity, and the lighter lines are the errors from the estimations by accurate NMO velocity.

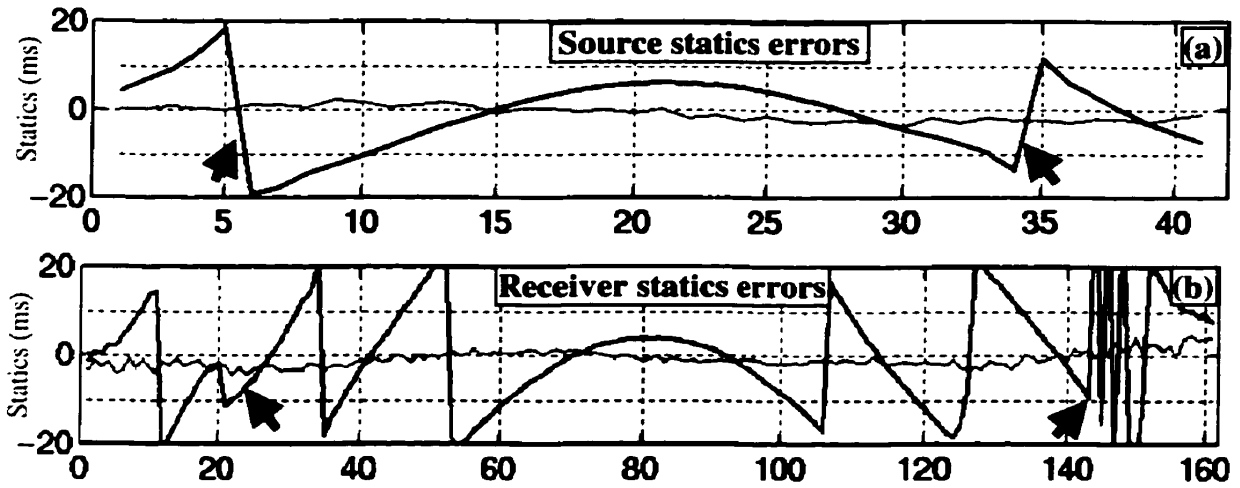

Figure 5-9: Estimation errors of the source statics (a) and the receiver statics (b) by the maximum stack-power method.

It can also be seen from Figure 5-9 that, along with long-wavelength errors, there are some short-wavelength errors (indicated by arrows) in the static estimations, especially in the receiver statics estimations. These short wavelength errors may not be separated easily from the statics themselves.

5.1.4.2 Conventional correlation method

The correlation autostatics method is used here because it considers the possible errors caused by the NMO velocity inaccuracy. As shown in Figure 5-10, the estimations of the source and receiver statics by correlation method with accurate NMO velocities are

almost perfect. The maximum error is not greater than 3 ms. The heavier lines represent the static estimations and the lighter lines are the synthetic time-shifts.

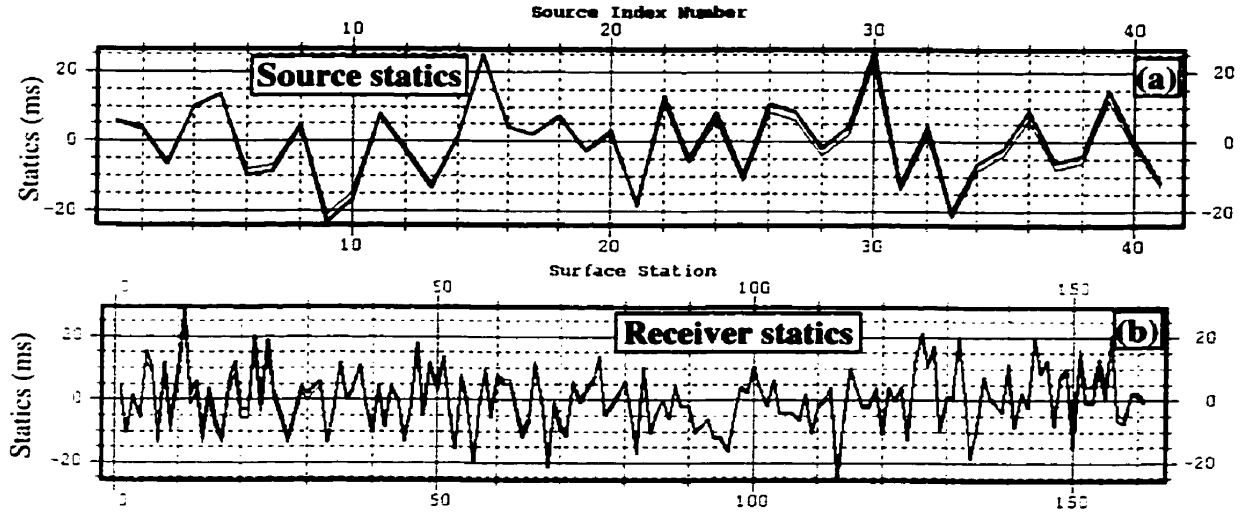

Figure 5-10: Residual source statics (a) and receiver statics (b) estimated by the correlation method with accurate NMO velocity.

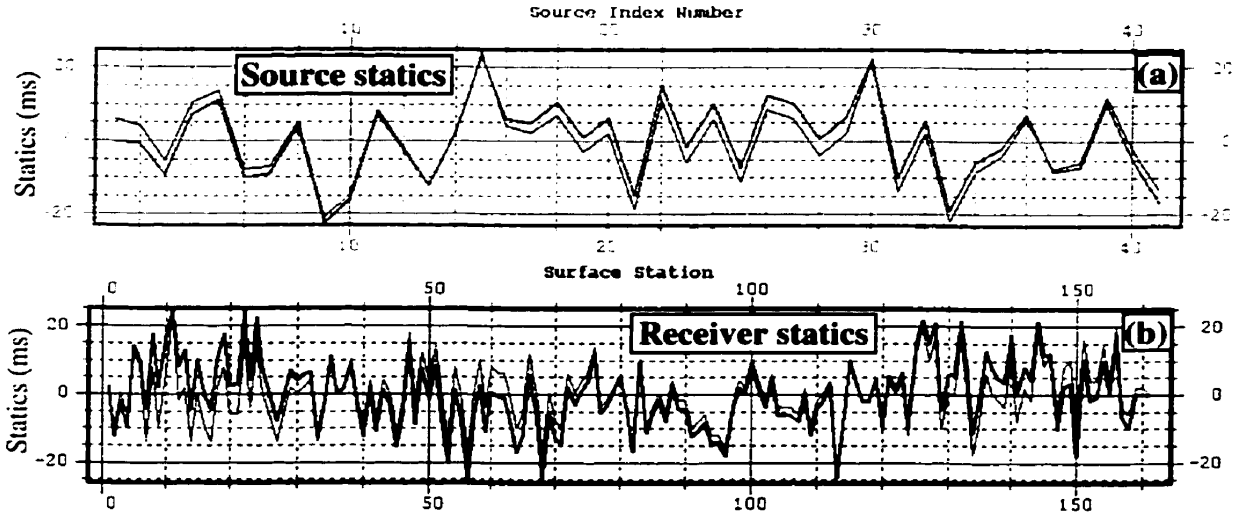

Figure 5-11: Estimations of the source statics (a) and the receiver statics (b) by the correlation autostatics method with a constant NMO velocity equal to 3000 m/s.

Figure 5-11 shows the statics estimated by the correlation method with a constant NMO velocity equal to 3000 m/s. Compared to the accurate estimations in Figure 5-10, the results in Figure 5-11 are affected by the velocity inaccuracy, even though the NMO errors are considered in correlation autostatics method.

However, comparing to the estimations through the stack-power maximization method with inaccurate velocity (Figure 5-8), the estimation errors in Figure 5-11 are much smaller. This can be seen more clearly in the following Figure 5-12, where the estimation errors by correlation method are shown. The darker lines are the errors from the estimations with constant 3000 m/s NMO velocity, and the lighter lines are the errors from the estimations by accurate NMO velocity.

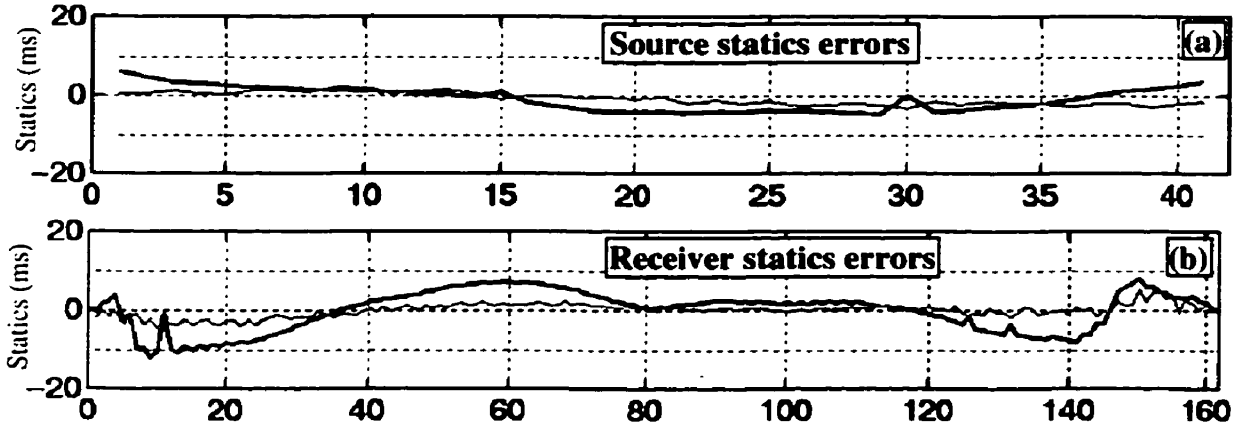

Figure 5-12: Estimation errors of the source statics (a) and the receiver statics (b) by the correlation autostatics method.

5.1.4.3 EOMAP method

The results shown in Figure 5-13 are the estimated residual statics by the EOMAP method, where the dark lines are the EOMAP estimations and the light grey lines are the synthetic shifts applied to the source and receiver locations. The accuracy of the estimations is visually comparable to the one estimated by the correlation statics method as in Figure 5-11. The difference is that, for the EOMAP results, no velocity information is used. In the forward and inverse EOMAP processes, the asymptotic equivalent offset relation is used. In addition, in the process of surface consistent statics decomposition, only the source and receiver terms are considered.

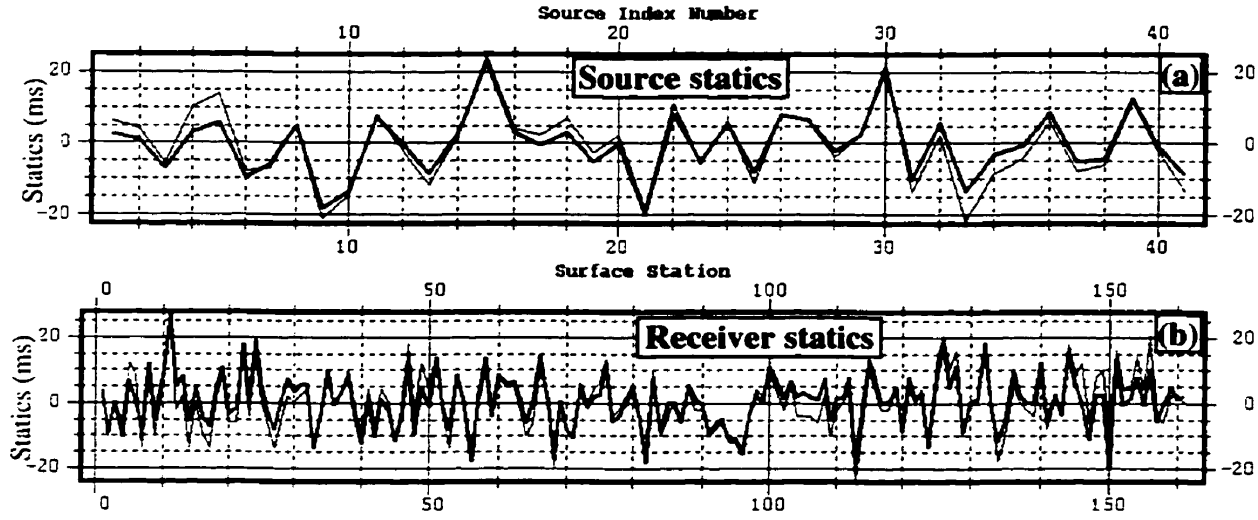

Figure 5-13: Residual source statics (a) and receiver statics (b) estimated by the EOMAP method where no velocity information is needed.

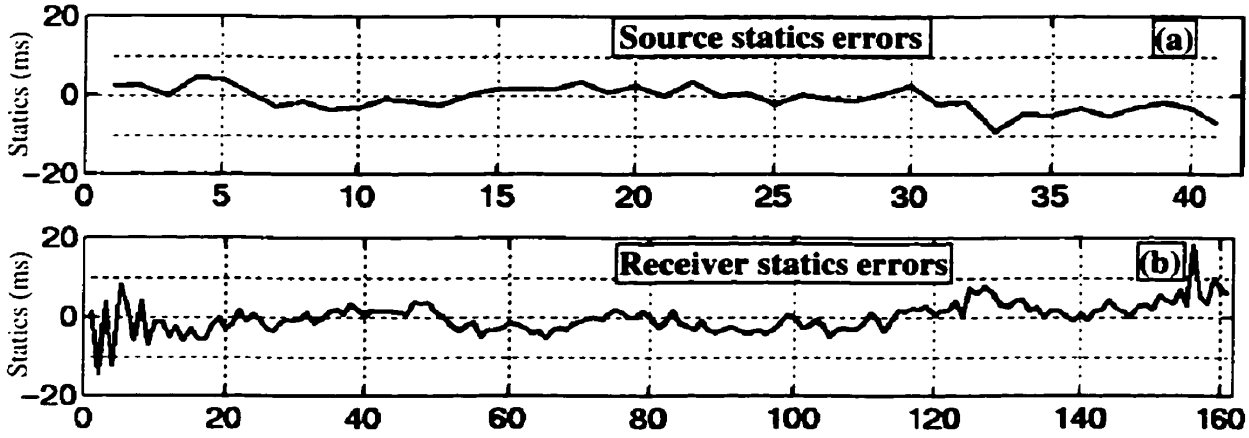

Figure 5-14: Estimation errors of the source statics (a) and the receiver statics (b) by the EOMAP statics method.

The EOMAP static estimation errors are shown in Figure 5-14. Comparing to the errors shown in Figure 4-9 or Figure 4-12, the EOMAP method seems has better control of the long wavelength statics content at least in the sense that the EOMAP method does not create obvious long wavelength errors. However, the estimation errors in correlation method seems have better short wavelength estimations, this may be because the EOMAP reference traces are not perfect as shown in section **5.1.5**.

5.1.4.4 f-x statics method

F-x statics method (Chan and Stewart, 1996) has been applied to this data. It could not provide good statics estimation because the reference data created by f-x prediction filter in common offset sections failed to attenuate the traveltime errors. This can be seen from Figure 5-15, where one of the common offset section and its f-x filtered version are shown.

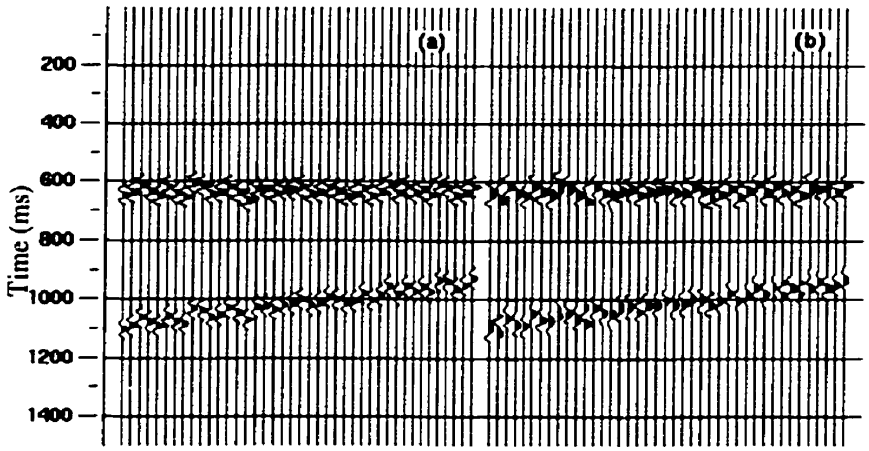

Figure 5-15: A common offset section before (a) and after (b) f-x prediction filter.

5.1.5 Description of the EOMAP procedure

At first, a shot gather and its corresponding model gather by the EOMAP method are shown together in Figure 5-16. The model shot gather contains artifacts that may change the nature of the reflection signals, such as frequency bandwidth, phase and amplitude information. However, the model data is particularly useful for the residual statics analysis because it provides more reliable traveltime information. As shown in Figure 5-16, the "jitter" traveltime differences between the time-shifted traces are "smoothed" out by constructive and destructive superposition of the EOMAP processes. The statics were estimated using the summation-trace cross-correlation method.

Figure 5-17 shows the same shot gather before and after correction by the EOMAP statics. As expected, the improvement is obvious, and more accurate NMO velocity can then be observed. Figure 5-18 shows the stacked sections before and after the EOMAP statics are applied. The improvements in resolution and signal to noise ratio are visible.

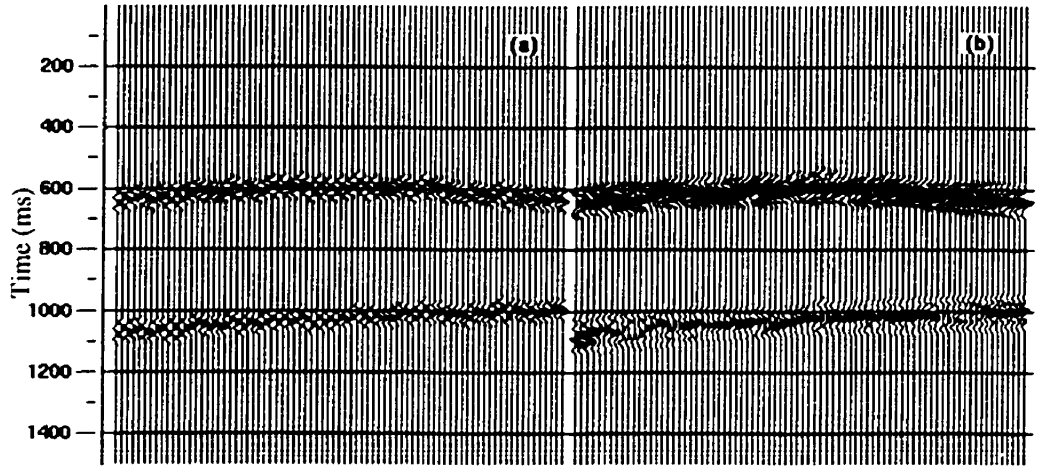

Figure 5-16: A shot gather after synthetic time-shifts (a) and its corresponding EOMAP reference model gather (b).

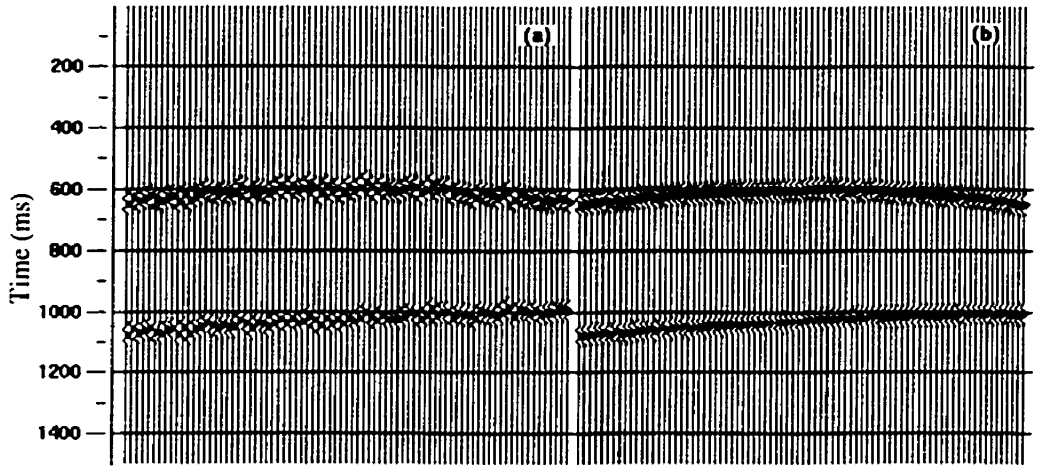

Figure 5-17: A shot gather before (a) and after (b) corrected by the statics estimated by the EOMAP method.

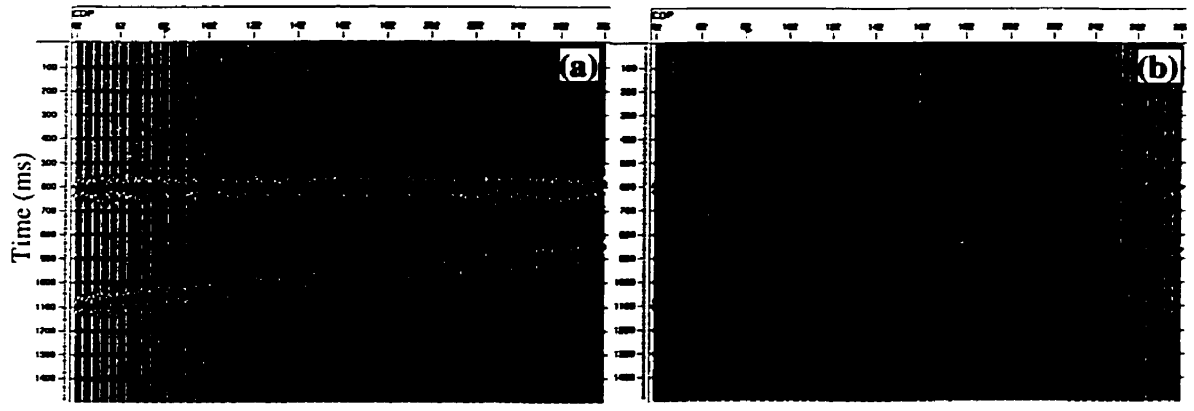

Figure 5-18: Stacked section before (a) and after (b) EOMAP statics applied.

5.2 Blackfoot data

The Blackfoot data discussed here was acquired in 1995, in the Blackfoot area, Southern Alberta, Canada. In this area, the surface elevation is relatively flat, and the subsurface can be approximated as a layered structure with little lateral velocity variation. This results in relatively mild refraction statics correction, and the residual statics are also of smaller scale.

In the Blackfoot data, there are 189 shots and all 200 receivers are active for each shot, giving the source fold uniformly 200 and the receiver fold uniformly 189. Conventional processing with different conventional residual statics analysis methods has been done with this Blackfoot data, and excellent results have been obtained. In this section, only the residual statics analysis by the EOMAP method is discussed, and the application of the EOMAP statics method starts from the data after the preprocessing including amplitude recovery, refraction statics correction and spiking deconvolution.

5.2.1 Identify residual statics

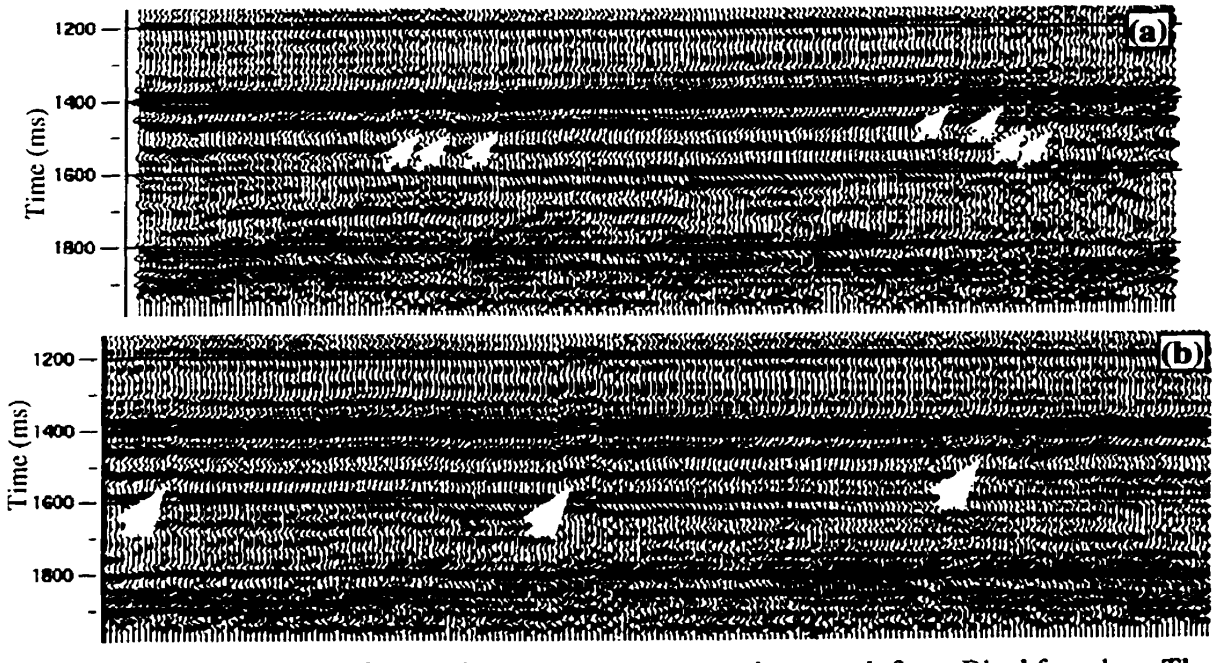

Figure 5-19: (a) common shot stack and (b) common receiver stack from Blackfoot data. The white arrows identify some static errors.

A common shot stack and a common receiver stack are obtained by using a preliminarily observed stacking velocity. Figure 5-19 (a) shows one time-window of the

common shot stack, which includes one of the strongest events at 1400ms. Figure 5-19 (b) shows the same time-window from the common receiver stack. Some easily recognizable static-shifts are indicated by small arrows.

Residual statics are also recognizable on shot gathers and receiver gathers. However, static effects are not obvious on CMP stacked sections because of the small magnitude of the statics and the high fold of the CDP coverage.

5.2.2 EOMAP static reference

A shot gather with recognizable static shifts is shown in Figure 5-20 (a), and as a comparison, the reference model shot gather created by EOMAP method is shown in Figure 5-20 (b). The static anomalies are attenuated during the forward and inverse EOMAP's. The model shot gather may have a narrower bandwidth than the original shot gather, but the traveltime consistency is enhanced.

Due to the simple subsurface structure in Blackfoot area, the statics reference model data is created without any velocity information. Based on this set of model data, residual statics have been estimated by the EOMAP method, and they are shown in Figure 5-21(a) and Figure 5-22 (a).

5.2.3 EOMAP static estimations

To demonstrate the accuracy of the statics estimations, a zoomed event on the common shot stack and the same event on the common receiver stack are shown respectively in Figure 5-21 (b) and Figure 5-22 (b). The high similarity between the traveltime deviations on the stacks and the corresponding estimated statics can be easily identified.

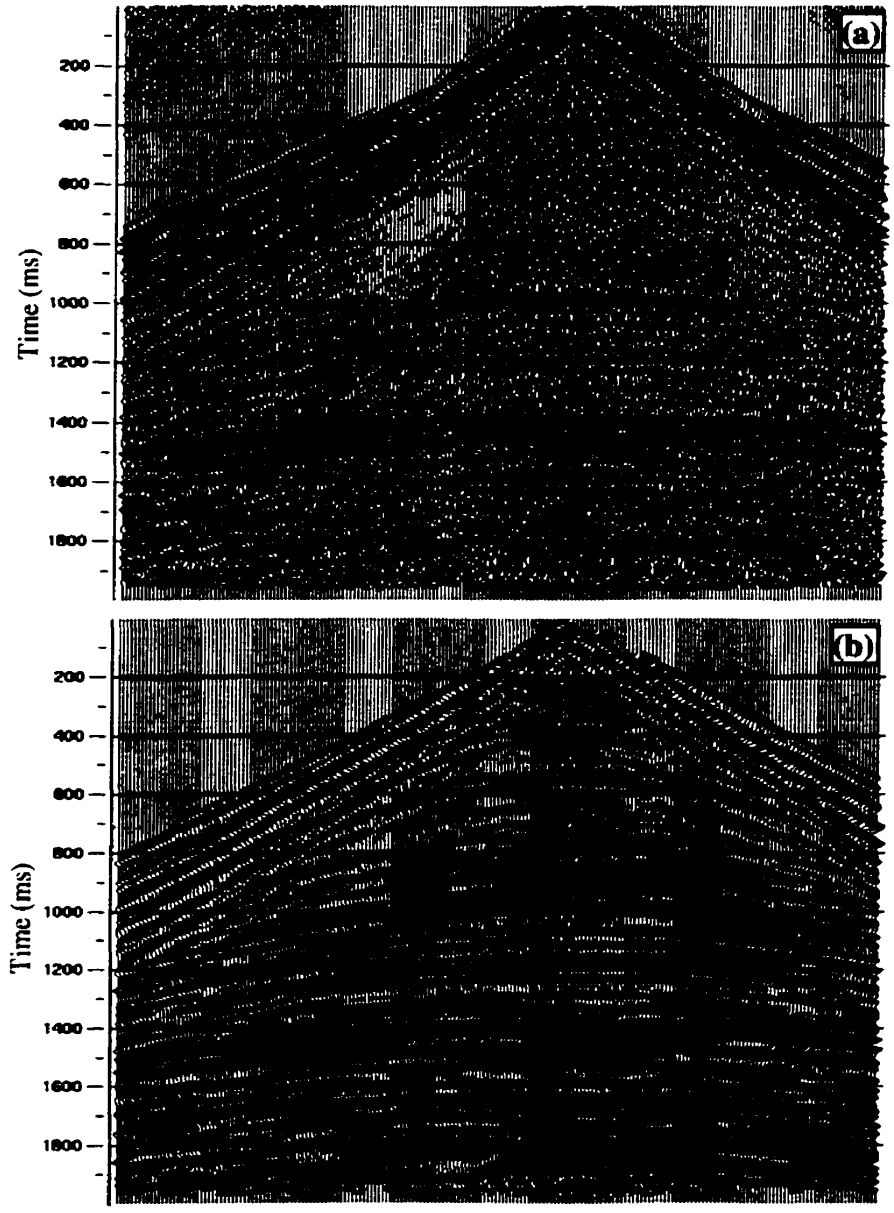

Figure 5-20: (a) a shot gather from Blackfoot data where statics problems are recognizable and (b) a model shot gather at the same location created by the EOMAP method. The traveltime deviations are attenuated by the forward and inverse equivalent offset mappings.

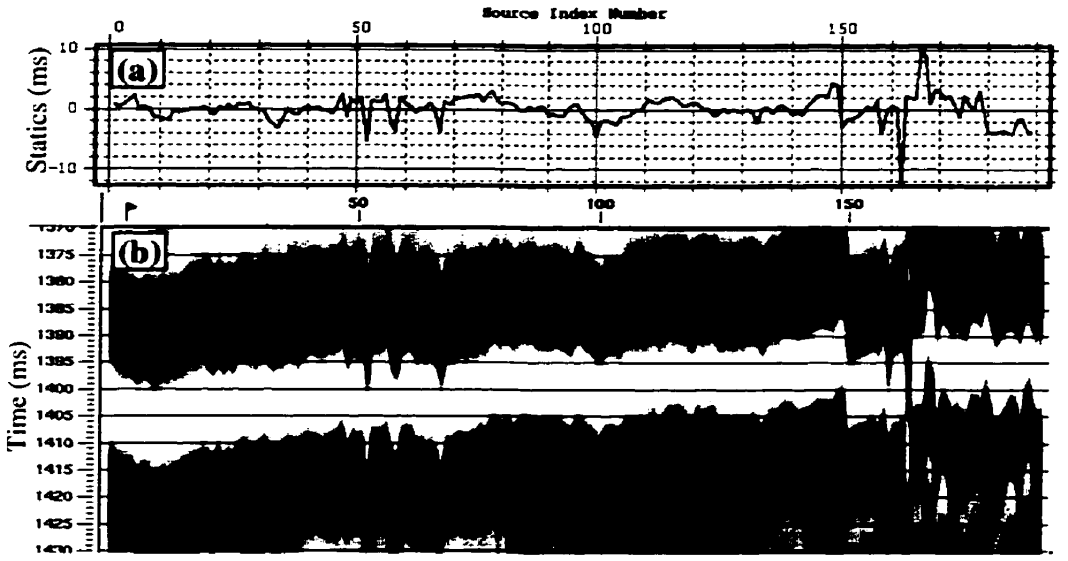

Figure 5-21: (a) EOMAP estimated source statics and (b) a zoomed event on the common shot stack.

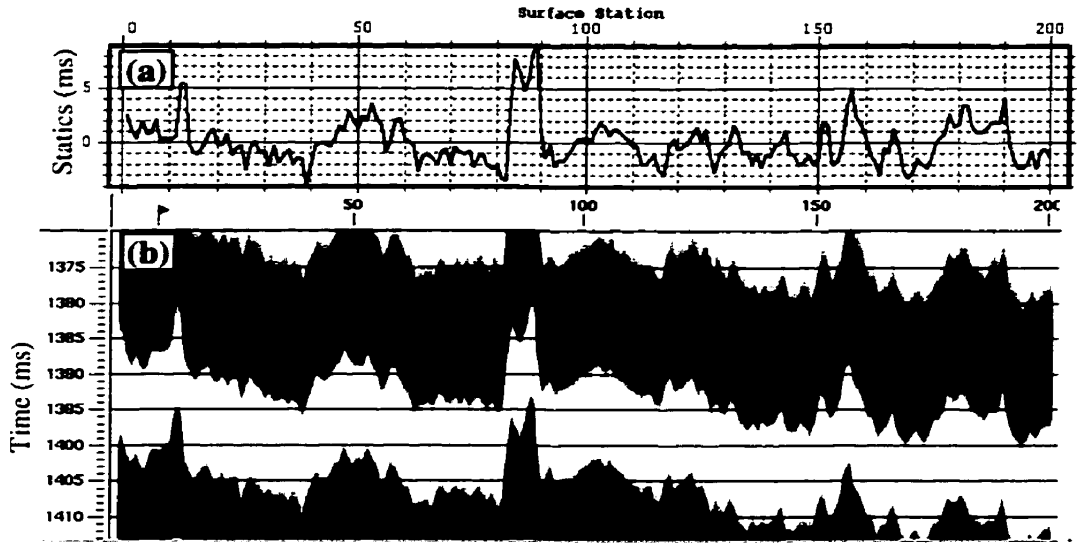

Figure 5-22: (a) EOMAP estimated receiver statics and (b) a zoomed event on the common receiver stack.

With the preliminary stacking velocity, a new pair of common shot stack and common receiver stack are obtained after the EOMAP static correction. As shown in Figure 5-23, static shifts on the two stacks are reduced.

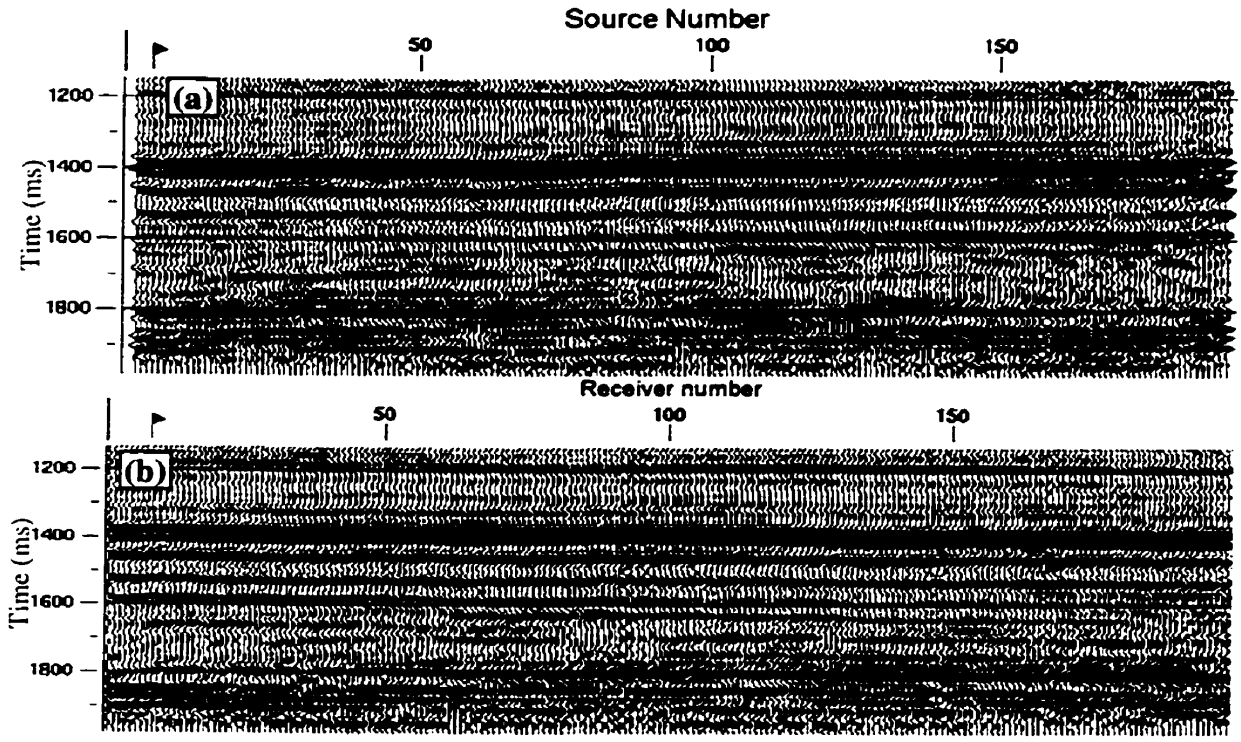

Figure 5-23: The common shot stack (a) and the common receiver stack (b) from Blackfoot data after residual statics corrected by the EOMAP estimations.

After applying the residual statics estimated by the EOMAP method, an updated stacking velocity field was estimated. Using the data before and after the EOMAP statics applied, and the two velocity fields, three different CMP stacked sections ware obtained. They are:

Section 1: from the data before the EOMAP residual statics applied, and with the stacking velocity observed before the EOMAP statics applied.

Section 2: from the data before the EOMAP residual statics applied, but using the revised stacking velocity field.

Section 3: from the data with the EOMAP statics applied and the revised stacking velocity.

Two different portions from each of the three sections have been selected to show the quality enhancements of the stacked sections in different ways. Shallower portions from the three sections are displayed together in Figure 5-24, and deeper portions from the three sections are displayed in Figure 5-25. In both figures, section 1 is at the left, section 2 is in the middle and section 3 is at the right.

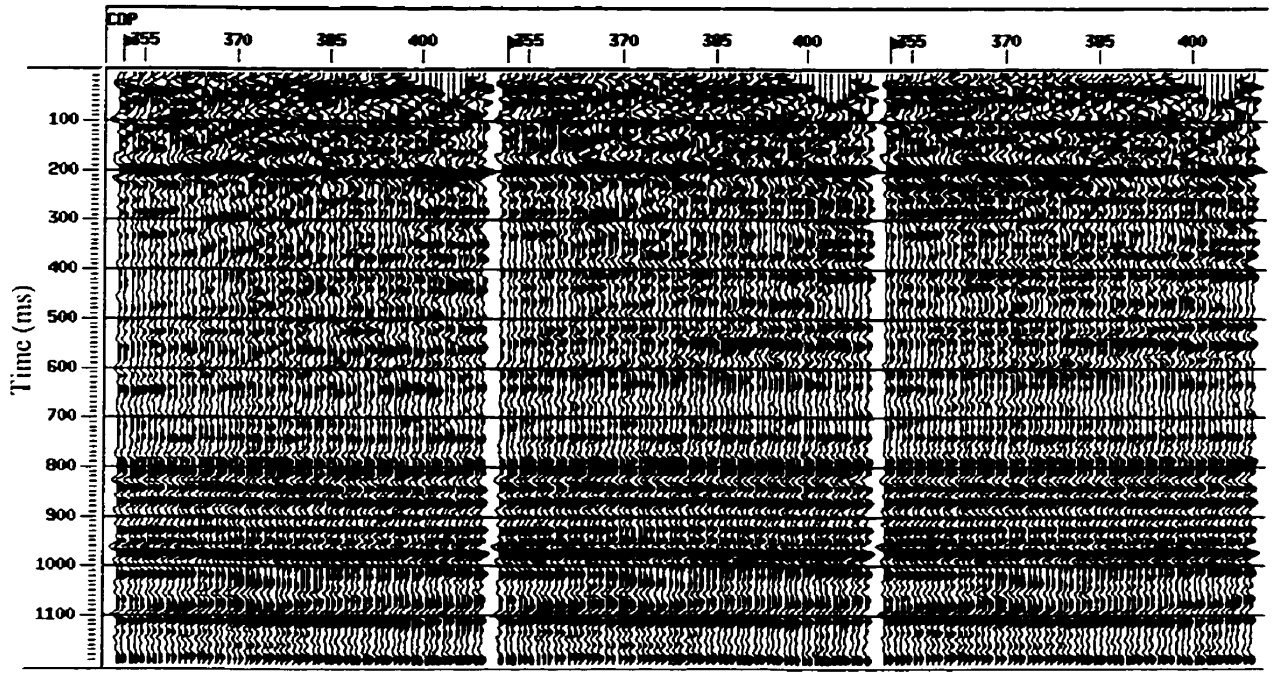

Figure 5-24: The shallower portion of the three stacked sections, where (a) is from section 1, (b) is from section 2 and (c) is from section 3 (detail in the text).

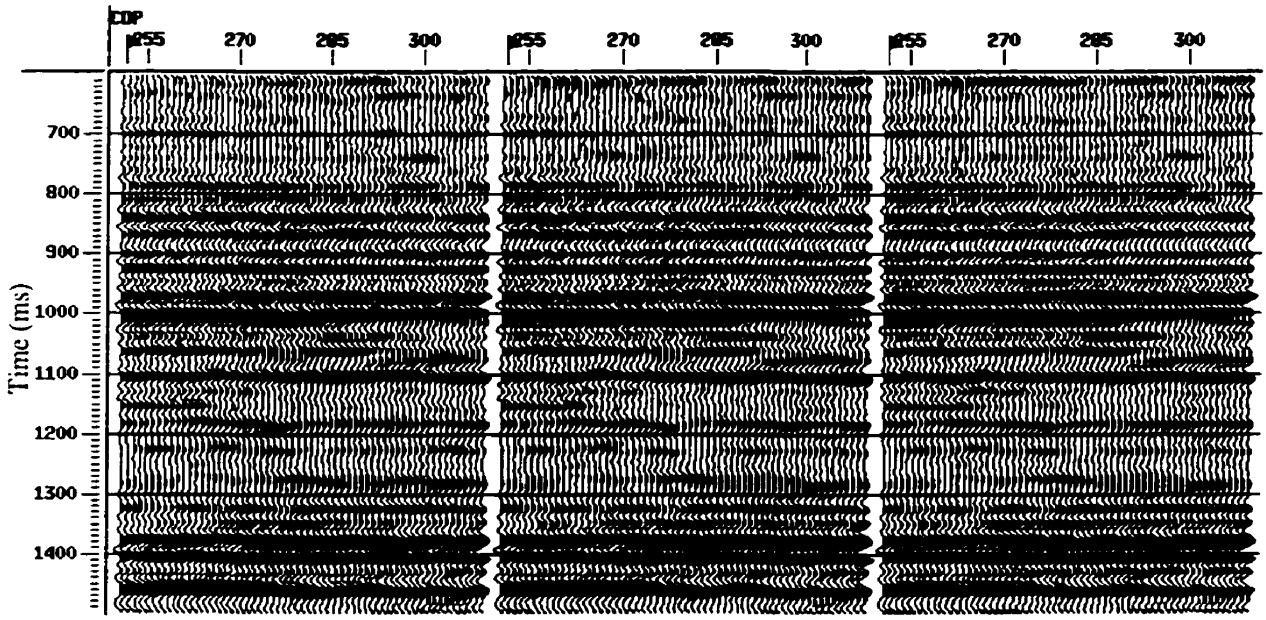

Figure 5-25: The deeper portion of the three stacked sections, where (a) is from section 1, (b) is from section 2 and (c) is from section 3 (detail in the text).

From the comparison among the three versions of the shallower portion, it can be seen that almost all the events are more or less enhanced from section 1 to section 2, and from section 2 to section 3. Some events that are consistent and continuous on section 3

can not even be recognized in section 1 (such as the events at time 250ms and 350 ms). This is how the residual statics correction helps improve the quality of shallow reflection events where the small scale traveltime deviations (residual statics as an example) can result in significant loss of signal in the stacking process. Two reasons for these are the higher sensitivity to the NMO velocity and the lower fold due to NMO stretch muting at earlier times.

Comparisons among the three deeper parts of the sections show the enhancements of the quality of those reflection events residing between stronger events. This resolution enhancement may benefit later migration imaging and final interpretation.

5.3 Marmousi model data

In this section, the Marmousi model data is used to test the EOMAP statics method. This is a challenge because the previous two datasets used in sections 5.1 and 5.2 do not have complex structure, and conventional methods of residual statics analysis can work very well. However, the EOMAP method is preferred for the Marmousi data because the traditional residual statics methods failed to obtain reasonable statics.

5.3.1 The model and the data

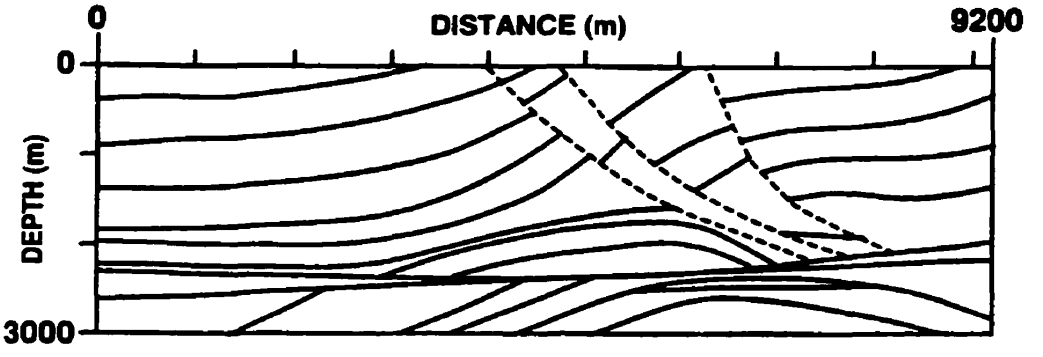

Figure 5-26: The structure elements of the Marmousi model. (after Versteeg, 1991)

The Marmousi model and seismic data were created at the Institut Français du Pétrole (IFP) in 1988. The motivation was to have a complex synthetic seismic data set for testing sophisticated velocity model determination methods (Versteeg 1991). The

Main structure elements of the Marmousi model is shown as in Figure 5-26, and the corresponding velocity model is shown in Figure 5-27.

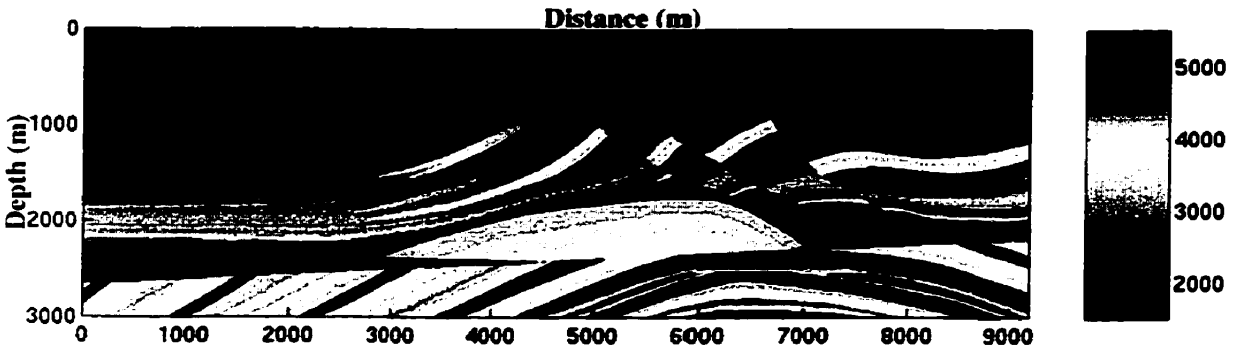

Figure 5-27: The velocity model of the Marmousi model. The color bar beside indicates the velocity value at each subsurface physical location.

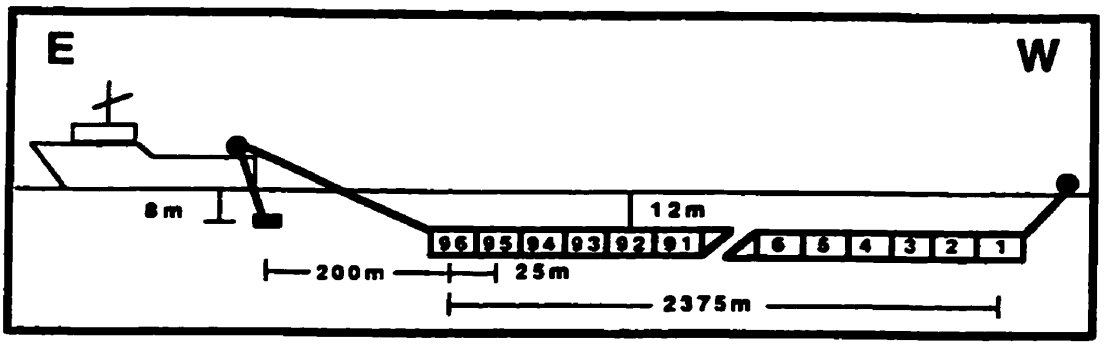

Figure 5-28: The streamer configuration of the generation of Marmousi seismic data. (after Versteeg, 1991)

The seismic data from this Marmousi model is generated numerically using a normal marine acquisition geometry. The acquisition is limited from west to east within about 9,000 meters as coordinated in Figure 5-26 and Figure 5-27. The first shot point started at 3,000 meters and the last ended at 8975 meters with a total of 240 shots and a shot interval equal to 25 meters. The streamer configuration is shown in Figure 5-28. The source depth is 8 meters, and the streamer depth is 12 meters. The streamer consists of 96 groups of hydrophones with the closest source receiver offset equal to 200 meters. And the streamer length is 2375 meters, with receiver group interval also equal to 25 meters.

As expected, from the subsurface structure shown in Figure 5-26 and Figure 5-27, the CDP gathers located above relatively simpler structure (within 3,000 meters from the west) should contain reflection events with their traveltime moveout trajectories close to

hyperbolic. However, the CDP gathers located in the middle of the line have non-hyperbolic reflection events. Figure 5-29 shows two CDP gathers located at 2,400 meters and 5,400 meters from the west respectively.

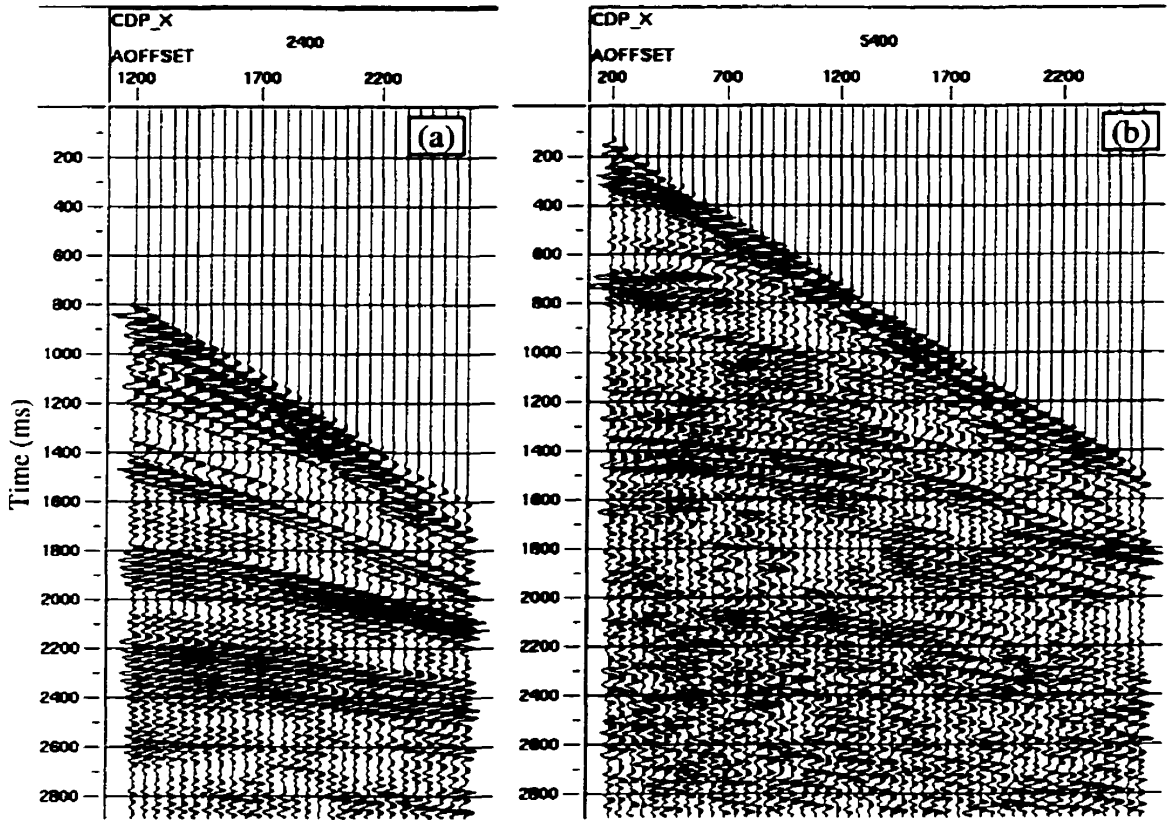

Figure 5-29: (a) A CDP gather at 2,400 meters where the traveltime moveout is close "to normal" and (b) a CDP gather located at 5,400 meters where the subsurface is complex and the reflection traveltime moveout deviates from hyperbolic trajectories.

5.3.2 Failure of conventional methods

The Marmousi seismic dataset does not contain any static problems. This original data was used to show how the conventional residual static methods fail to provide reliable statics solution. Two methods (the stack-power maximization method and the correlation autostatics method) have been applied to the Marmousi data with some preliminarily observed NMO velocities.

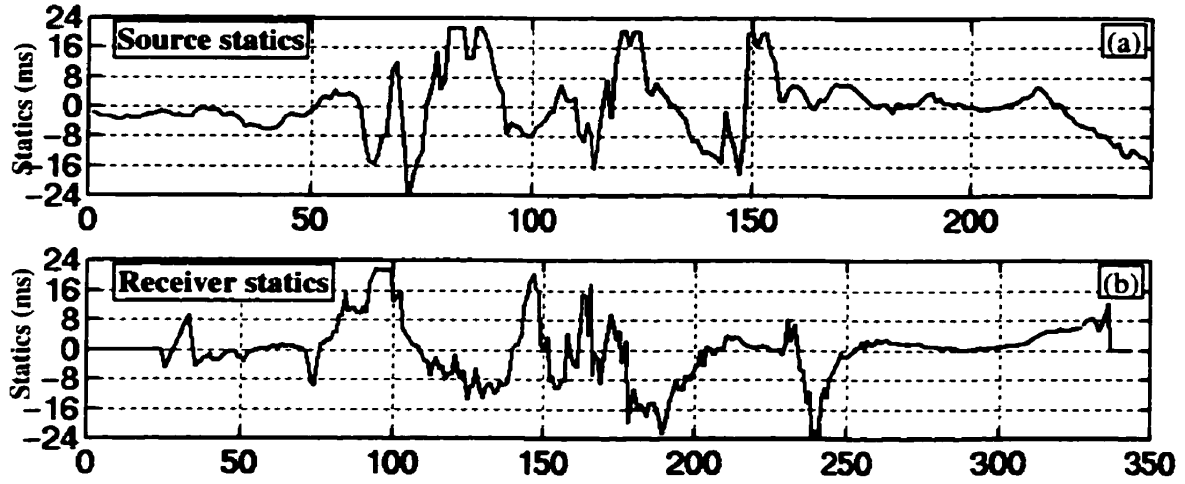

Figure 5-30: Source statics (a) and receiver statics (b) estimated by the correlation autostatics method from the Marmousi seismic data where no statics are present.

The reflection moveout trajectories on many of the CDP gathers can not be properly approximated by hyperbolas. Consequently, any NMO correction can not align the events at the same time levels. The results from some experiments with traditional methods provide statics as large as 36 ms, even when the NMO error terms are considered during the statics decomposition.

Figure 5-30 shows a set of statics estimated by the correlation autostatics method, with the maximum allowed static time shift set to 24 ms. The estimated statics at locations where the subsurface structure is not very complex were closer to the correct value of zero. However, the statics estimated at the locations where the subsurface structure is complex were very large, and their maximum values bounded by the maximum allow static time shift. The receiver statics were not estimated at the two ends of the line because the fold is too low and only far-offset traces are contained.

For comparison, the statics estimated by the EOMAP method from the static-free Marmousi data are shown in Figure 5-31. The estimation errors are mostly below 4 ms, which is the sample rate.

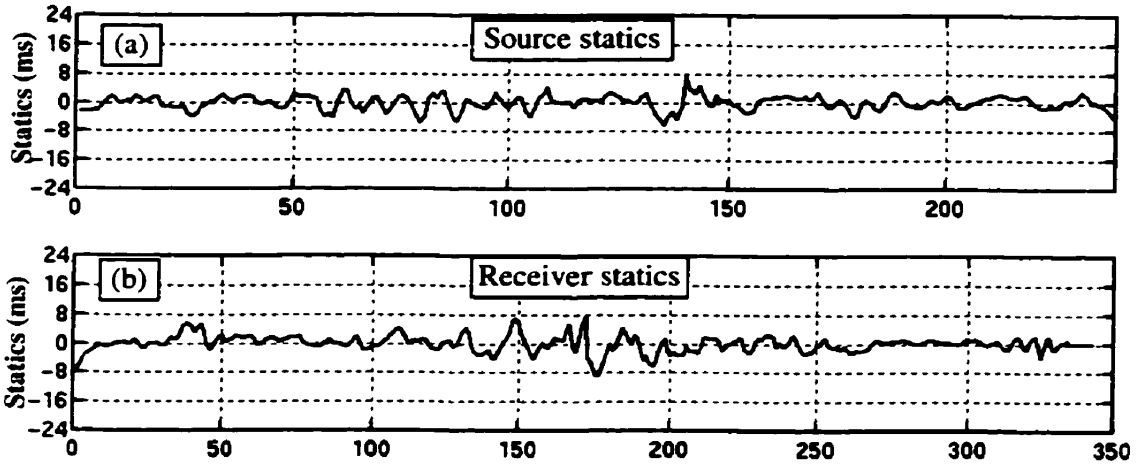

Figure 5-31: Source statics (a) and receiver statics (b) estimated by the EOMAP statics method from the Marmousi seismic data where no statics are present.

5.3.3 Synthetic static shifts

Two arrays of random numbers were independently created for the time-shifts at the shot and receiver locations. The time shifts for both shot and receiver range from –20 ms to 20 ms. The traces of the original Marmousi data are then time-shifted in the surface consistent manner. The maximum possible time-shifts applied on each trace is 40 ms, and then the maximum possible time-shifts between two traces can be as high as 80 ms. The following experiments with the EOMAP statics method used this Marmousi data contaminated with these surface consistent traveltime errors.

5.3.4 Migration velocity observation

Both the forward and inverse equivalent offset mappings (EOMAP) used a migration velocity that was estimated using the following steps:

1. Brute stacking velocity observed from the CMP supergathers containing 3 adjacent CMP gathers, and with 50-meter distance between the observation locations.
2. CSP gathers are formed at a series surface locations using the stacking velocity. The distance between those CSP locations are again 50 meters.
3. Analyzing the velocity semblance of the CSP gathers by conventional method, a velocity function can be observed at each CSP location.

This velocity can be used to form CSP gathers for final time migration. Because of the effects of statics, this velocity field may not be accurate enough for prestack migration, but it is proved accurate enough for the EOMAP statics method to create reference model data with reliable traveltime information.

5.3.5 EOM reference model data

The forward and inverse EOMAP's are applied to time-shifted Marmousi data and a set of reference data for residual statics analysis is formed. Figure 5-32 shows three CMP gathers at one location above the relatively simple structure. They are (a) a CMP gather from the original traveltime-error-free Marmousi data, (b) the same CMP gather but from the time-shifted Marmousi data and (c) the CMP gather from the reference model data created by the EOMAP method. Comparing the three gathers, it can be seen that the traveltime discontinuity caused by static time-shifts is attenuated by the EOMAP's, although they could not perfectly reconstruct the original error-free data.

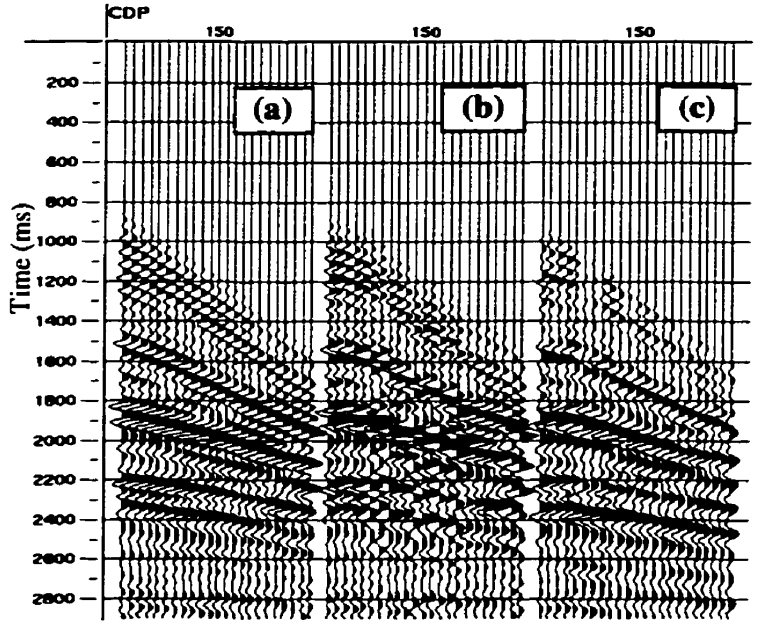

Figure 5-32: Three CMP gathers from the same location above the simple-structure area of the Marmousi model, where (a) is from the original traveltime-error-free data, (b) is from the data with traces time-shifted and (c) is from the reference model data created by the EOMAP method.

Figure 5-33 shows another three CMP gathers at one location above the complex structure in the Marmousi model. The model gather (c) shows better traveltime continuity than the time shifted gather (b), although some reflections in the gather (as circled) could not be recovered at all. This signal loss is partly because of the statics, but it is also because that the Marmousi model contains too strong lateral velocity variation for a prestack time migration algorithm. Fortunately, what is needed here is only the static reference model.

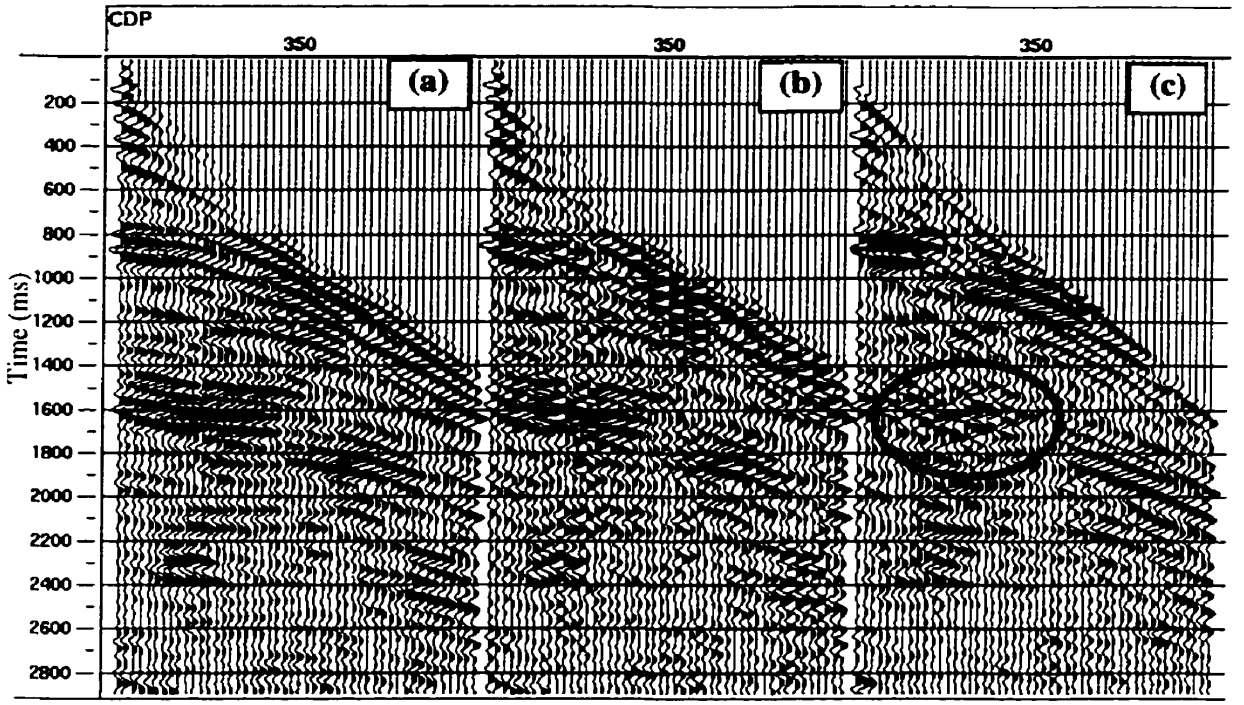

Figure 5-33: Three CDP gathers from the same location above the complex-structure area of the Marmousi model, where (a) is from the original traveltime-error-free data, (b) from the data with traces time-shifted and (c) from the reference model data created by EOMAP method.

Figure 5-34 and Figure 5-35 show two groups of shot gathers, with each group containing three gathers from the error-free Marmousi data, time-shifted Marmousi data, and the EOMAP reference model respectively.

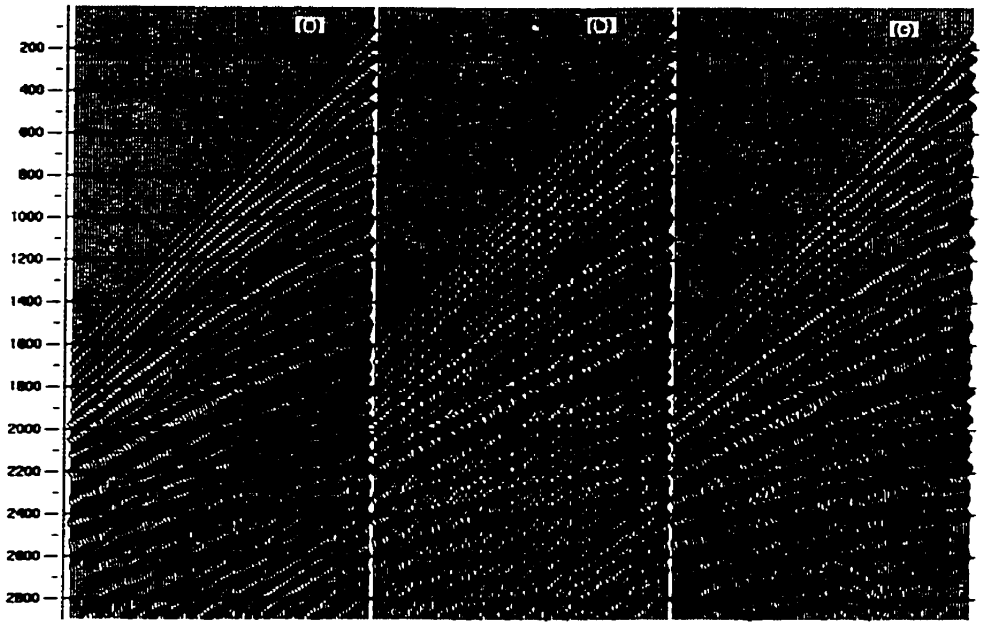

Figure 5-34: Three shot gathers from the same location above the simple-structure area of the Marmousi model, where (a) is from the traveltime-error-free data, (b) is from the data with traces time-shifted and (c) is from the reference model data created by the EOMAP method.

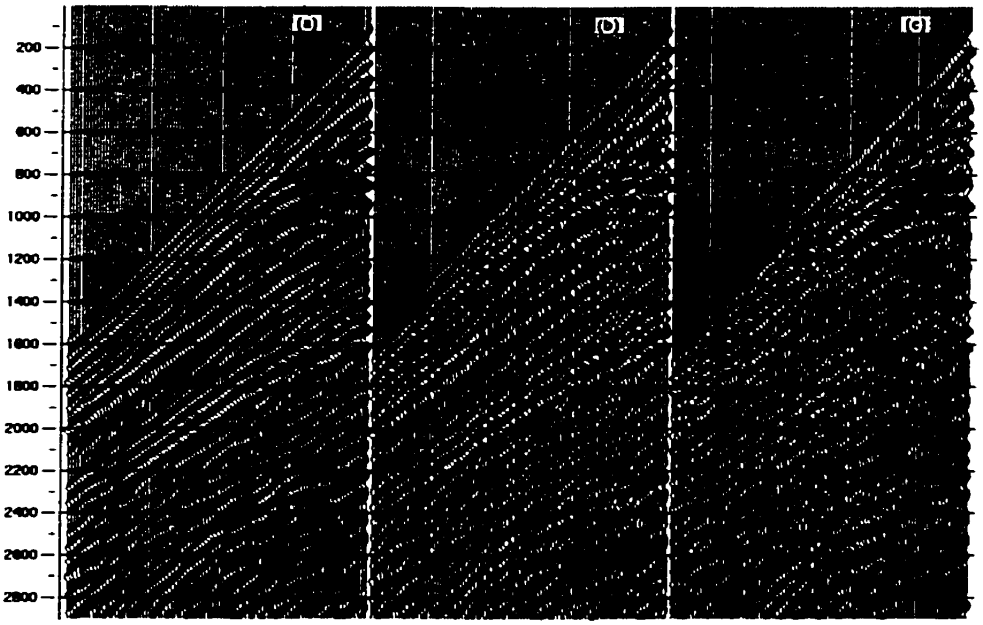

Figure 5-35: Three shot gathers from the same location above the complex-structure area of the Marmousi model, where (a) is from the traveltime-error-free data, (b) from the data with traces time-shifted, and (c) from the reference model data created by the EOMAP method.

5.3.6 Static estimation

Figure 5-36 shows the source and receiver statics added artificially to the Marmousi data and their corresponding estimations by the EOMAP statics method. In this figure, part (a) shows the added and the estimated source statics at all the source locations. The black colored line is the plot of the synthetic statics added, and the light grey line indicates the EOMAP estimations. Part (b) is the source statics estimation errors, i.e., the difference between the estimations and the synthetics. Similarly, (c) shows the added synthetic receiver statics with the black colored line and the EOMAP estimations of the receiver statics with the light grey line respectively, and (d) is the receiver statics estimation errors.

The following conclusions can be drawn from the displayed results in Figure 5-36:

- The short wavelength (about two shot or receiver intervals, which is 40 meters for this data) source and receiver statics are very well estimated by the EOMAP statics method. The estimation errors are of mid wavelength, which is about 10 to 20 shot intervals, i.e., 200 to 400 meters.
- The estimation errors are much smaller than the original static shifts added. The source statics estimation errors have an average less than 4 ms, and the receiver statics estimation errors have an average less than 8 ms.
- Source statics estimations have better accuracy than the receiver statics estimations. This is mainly because of the source fold (uniformly 96) is larger than the receiver fold.
- There is no recognizable very long wavelength (over 100 shot intervals, for example) trend in the static estimations, although the decomposition algorithm used (summation-trace cross-correlation) does not consider the geology (structure) terms.

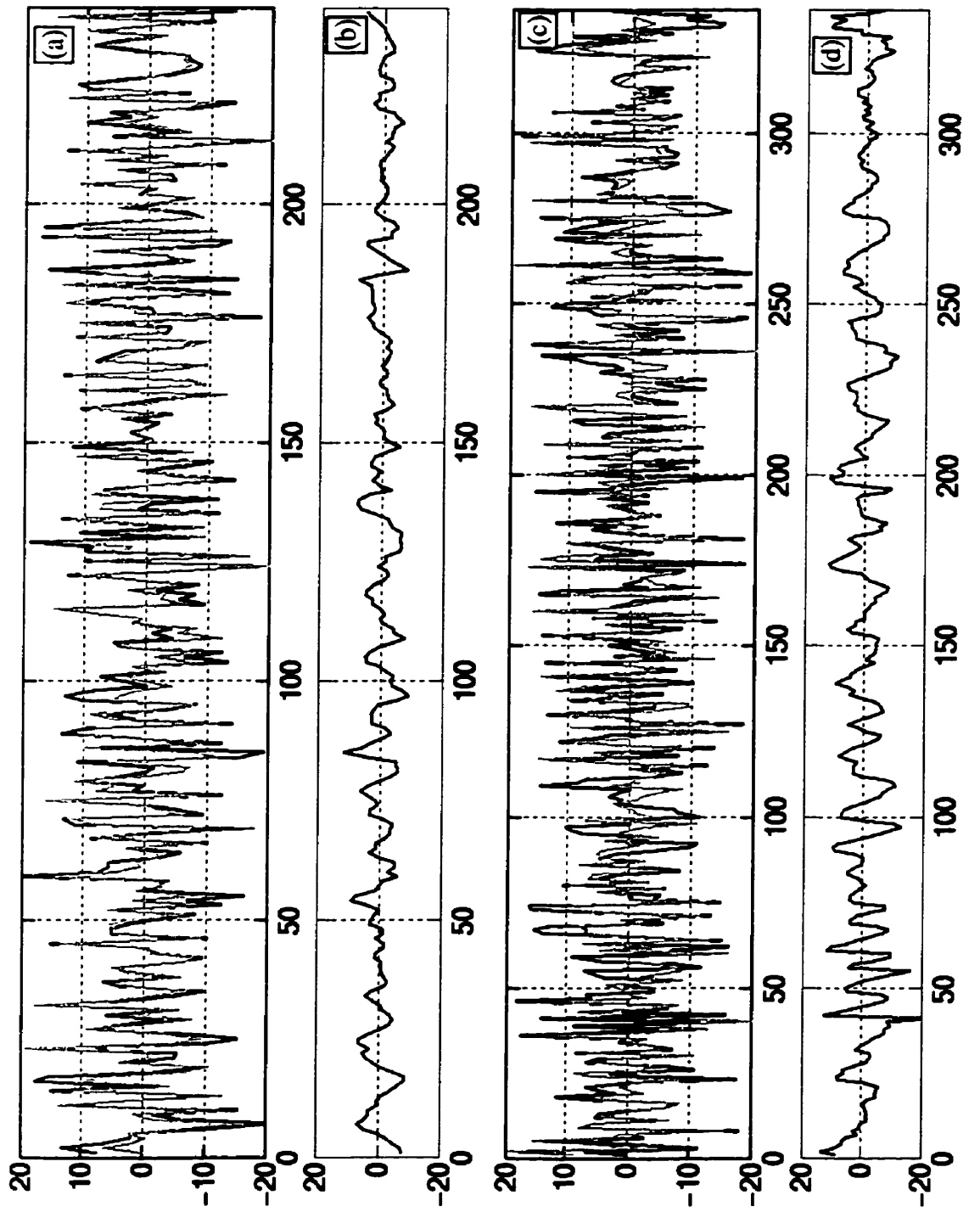

Figure 5-36: Statics estimated by the EOMAP method. Where (a) shows the added (dark color) and estimated (light color) source statics with their differences showing in (b), and (c) shows the added (dark color) and estimated (light color) receiver statics with (d) showing their differences.

Figure 5-37 (a) provides zoomed source statics in the range from source number 115 to 240 also with the black line standing for the synthetic and the light grey line standing for the EOMAP estimations. Figure 5-37 (b) shows the zoomed receiver statics ranging from receiver number 175 to 305.

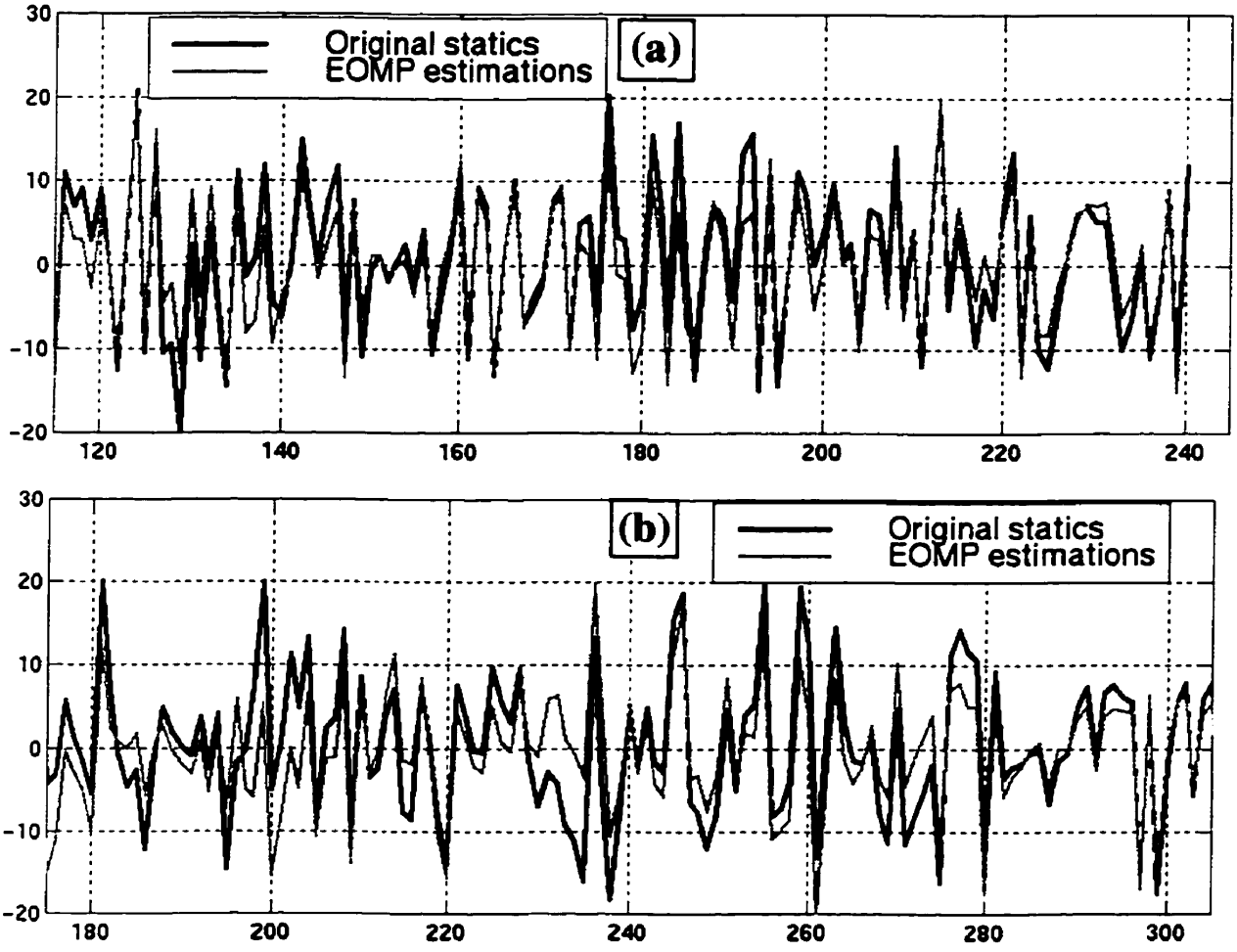

Figure 5-37: Zoomed details of the EOMAP estimations of the source statics (a) and the receiver statics (b).

In summary, these estimations are not perfect, but they show that the EOMAP statics method can estimate the residual statics residing in data from complex area, where the normal moveout assumption is no longer valid. Also, the results shown in the next section demonstrate that the data quality is very much improved by the static corrections by the EOMAP statics estimations.

5.3.7 Results after applying the EOMAP statics

After applying the statics estimated by the EOMAP method, the quality of the Marmousi data is reasonably improved. As in Figure 5-38, where the near-offset sections before and after the EOMAP static correction are shown, and the lateral consistency of the reflection events is enhanced. For example, some weak diffractions, which are very important for the final migration imaging, lost their recognizable continuity by the static time shifts. Many of them reappeared after the EOMAP statics are applied.

Figure 5-39 shows two stacked sections before and after applying the EOMAP statics. Both signal-to-noise ratio and the resolution are very much enhanced.

5.4 Practical consideration of applying the EOMAP statics method

In the practical application of the EOMAP statics method, the following issues should be considered.

5.4.1 Velocity dependence

The velocity dependence is always a concern for obtaining more accurate statics estimations without introducing too many artifacts to the seismic data, especially for data from areas with complex subsurface structure. The EOMAP method has its advantage of being able to estimate reliable statics without the requirement of accurate velocity information. This does not mean that the EOMAP processes are independent to velocity information. However, to reduce the dependence of the velocity information, the following suggestions may be considered:

- Using asymptotic EOMAP method, which is velocity independent.
- Using smaller migration aperture. Apertures that are too small may reduce the traveltime-error attenuation ability.
- Using later time window because of the weaker velocity dependence.

A set of reference traces were created for the Marmousi data using asymptotic EOMAP's. With later time windows, the statics estimations were almost the same as the one shown in Figure 5-36.

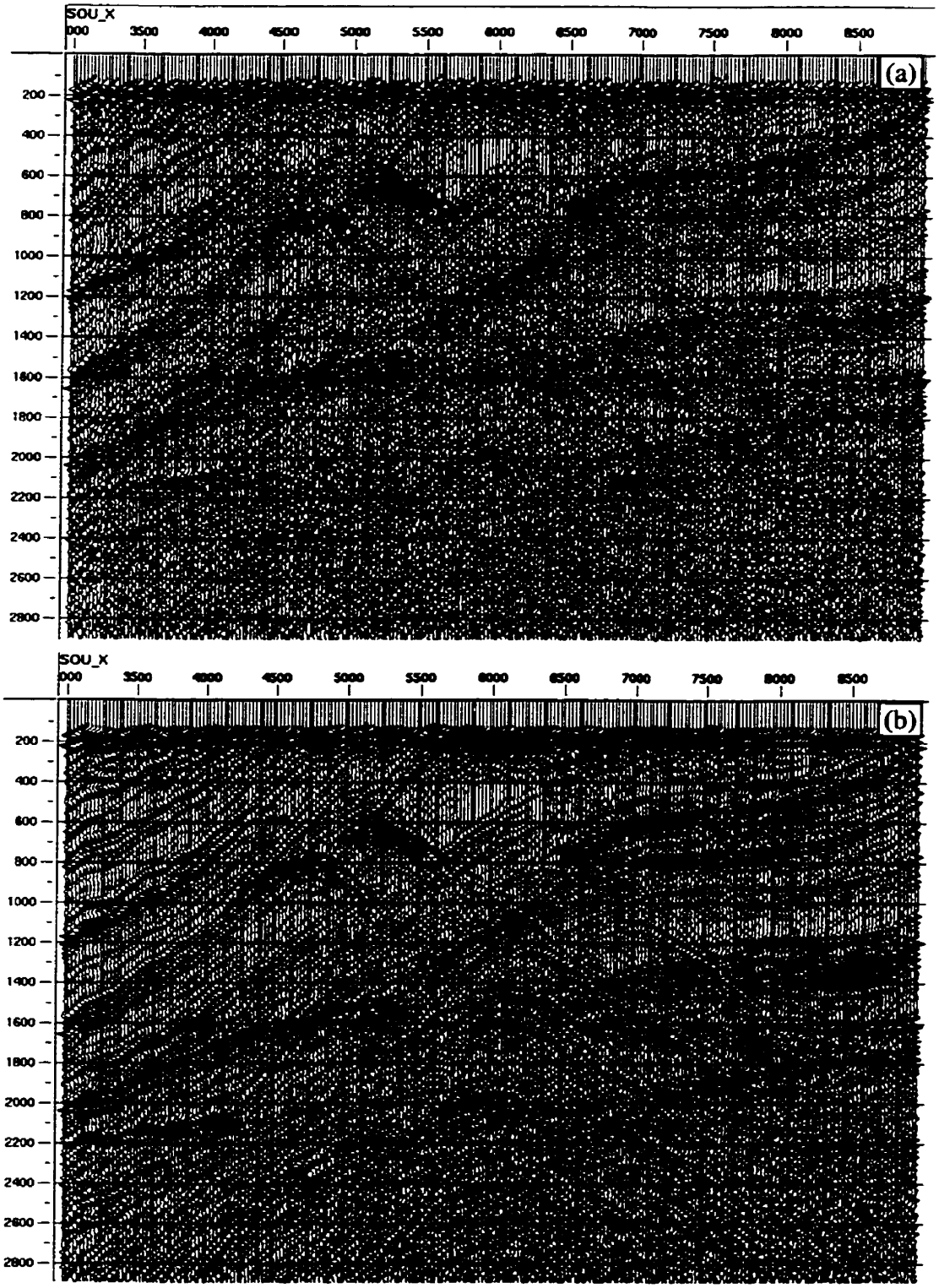

Figure 5-38: The near-offset sections before (a) and after (b) applying the residual statics estimated by the EOMAP statics method.

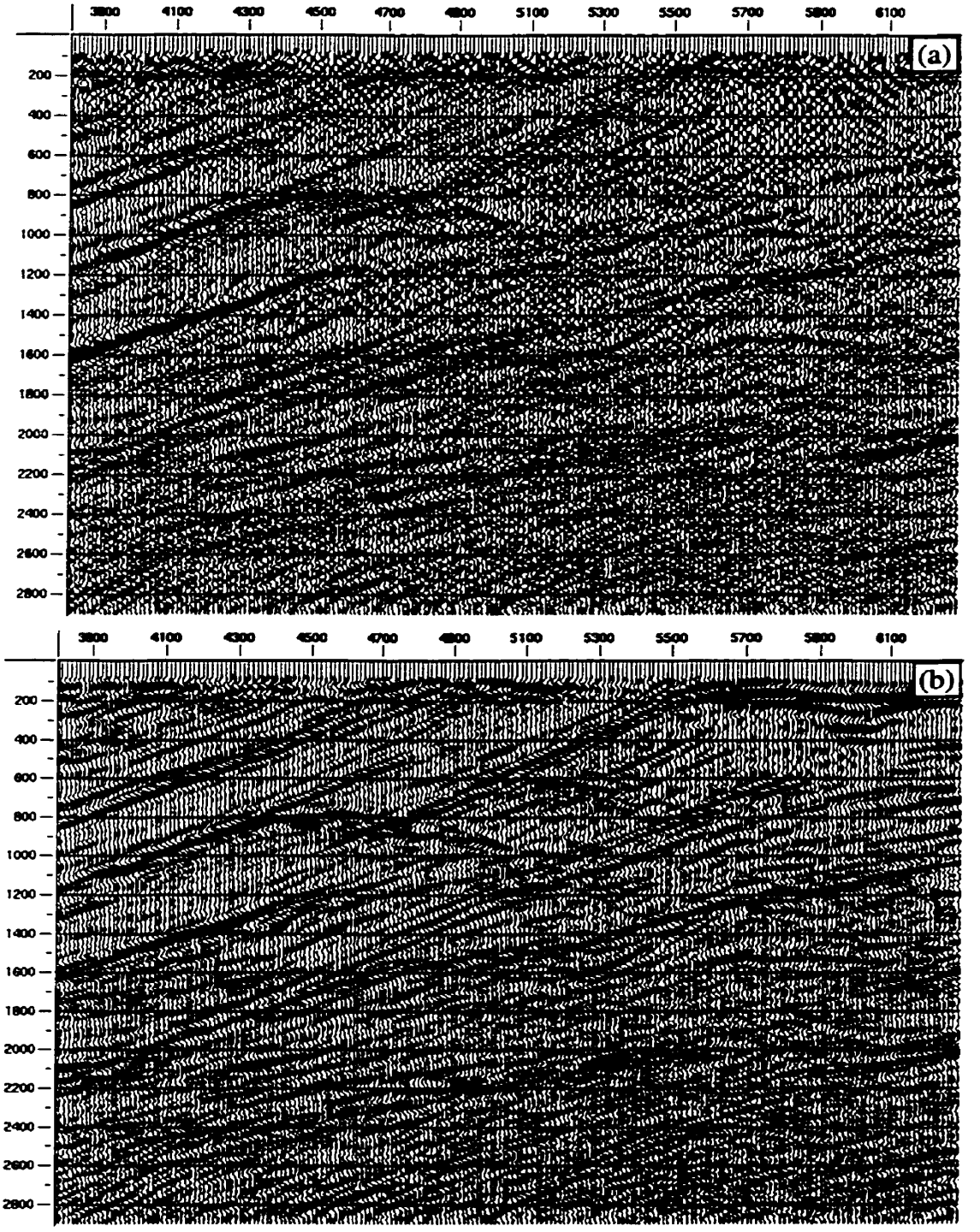

Figure 5-39: The stacked sections (portions) before (a) and after (b) applying the residual statics estimated by the EOMAP statics method. The same stacking velocity was used for the NMO correction of both datasets.

5.4.2 Efficiency: choosing EOM parameters

The efficiency is considered with EOMAP method when conventional methods can also provide reasonable static estimations. However, for data from a simple structured area, both forward and inverse equivalent offset mappings can be less time-consuming. This can be achieved by "relaxing" the parameters used in the two mappings. Because the computation cost of the EOMAP's mainly depends on the size of the volume of CSP gathers, changing the following parameters can reduce the cost:

- Using asymptotic EOMAP's, this at least saves one third of the computation.
- Increasing the CSP spacing (distance between CSP locations), which is usually the same as CDP spacing for the purpose of prestack migration. Double the spacing will half the computation cost.
- Increasing the equivalent offset bin size, which is usually also equal to the CDP spacing for the prestack migration. Double the bin size may reduce more than half the computation cost.
- Decreasing the maximum equivalent offset, which is usually determined by the maximum source-receiver offset and the migration aperture.
- Decreasing the migration aperture.
- Reducing the trace length or increasing the temporal sample rate.

All these suggestions should be considered with concerns of the quality of the reference model data. Sometimes a few model gathers can be created to evaluate the chosen parameters.

5.4.3 Frequency bandwidth – lowpass filter

The superposition of wavelets with time information contaminated by the statics is the essence of how the EOMAP method attenuates the traveltime errors. That the traveltime information on reference traces is reliable or not depends on how well the wavelets interfere constructively and destructively. The interference is determined by the time lags between the wavelets and the dominant frequencies of the wavelets. Consequently, a direct way to improve the quality of reference traces is to lowpass filter the input seismic traces.

During the experiments with the Marmousi data, lowpass filtering was an important process applied to input data of the EOMAP statics method.

5.4.4 Further processing of the model data

Reference model data can be further processed using some spatial filtering, such as f-x prediction filter. This may help make the traveltime continuity better.

5.4.5 Noise

The EOMAP statics method works for data with high signal-to-noise ratio. For data with noise, theoretically, it also works as long as a reasonably "stable" prestack time migration image can be obtained. Here "stable" means the traveltimes of some basic events are not very sensitive to the migration velocity.

Some experiments were performed with very noisy data where time migration could not improve the image. In this case, the EOMAP method could not provide reasonable static estimations.

Chapter 6
General conclusions and possible extensions

6.1 Conclusions

The EOMAP statics method can provide reliable residual static estimations:

- without NMO correction and without the normal moveout assumption,
- without accurate stacking velocity information, and can be totally velocity independent, and
- usually with only one iteration.

Specifically, for seismic data acquired from areas with simple subsurface structure (such as Blackfoot area), the EOMAP method can estimate residual statics with comparable accuracy to the results from conventional static methods. However, the EOMAP usually does not need any velocity information in these cases.

For data with very complex structure, such as Marmousi model data, conventional methods usually can not be applied because their hyperbolic normal moveout assumption is no longer valid. In these cases, the EOMAP method can still estimate residual statics with plausible accuracy. Some velocity information maybe needed but not essential.

All static estimations by EOMAP method shown in Chapter 5 are obtained by the first iteration.

The EOMAP statics method does not create long wavelength static errors. This is shown by the comparison with the static estimations from conventional methods in section 5.1. This is because that the EOMAP's, as a partial migration and its inverse, are less affected by the reflecting structure (long wavelength).

The EOMAP method is not only much faster but also less velocity sensitive comparing to the depth migration method presented by Tjan, et al (1994) and Larner, 1998. Practically, the EOMAP method can be efficient by choosing appropriate parameters.

The current implementation of the EOMAP method may have limited resolving ability of the details of the statics in areas with complex structure. Some experiments with the Marmousi data shows that the EOMAP method can detect a local time-shift of 4 ms, but could not resolve it. Trying the second iteration of the EOMAP method on the Marmousi data shows no improvement, and this also shows the resolving limitation. This limitation is partly due to the high-complexity of the Marmousi data, and may be also because that the current implementation still needs some improvements.

6.2 Possible extensions

The EOMAP statics method can not only work for 2D PP data, it can also be extended to analyzing residual statics for 3D or even converted wave data. This is possible, because the EOM concept has been successfully applied to different types of data as a prestack time migration algorithm.

The current implementation of the EOMAP method may have not been optimized. Some algorithm improvements related to both the equivalents offset mapping (migration part) and the surface consistent statics decomposition (statics part) are still possible. For example, the amplitude-scaling factor during both forward and inverse equivalent offset mappings can be more accurate.

Bibliography

Bancroft, J. C., 1996a, Natural antialiasing in equivalent offset prestack migration: 66th Annual Internat. Mtg., Soc. Expl. Geophys., Expanded Abstracts, 1465-1466.

Bancroft, J. C., 1996b An independent processing concept based on equivalent offsets: From statics to migration, CREWES Project Research Report, Vol.8, Ch. 24.

Bancroft, J. C., 1996c, The NMO stretch factor and dip limits in EOM, CREWES Project Research Report, Vol.8, Ch. 26.

Bancroft, J. C., 1996d, Fast 3-D Kirchhoff poststack time migration with velocity analysis, CREWES Project Research Report, Vol.8, Ch. 28.

Bancroft, J. C., 1997, Practical understanding of migration and dip moveout, SEG course notes.

Bancroft, J. C., 1998a, Dip limits on pre- and poststack Kirchhoff migrations, CREWES Project Research Report, Vol.9, Ch. 25.

Bancroft, J. C., 1998b Computational speed of EOM relative to standard Kirchhoff migration, CREWES Project Research Report, Vol.9, Ch. 43.

Bancroft, J. C., 1998c, Optimum CSP gathers with fixed equivalent offset, CREWES Project Research Report, Vol.9, Ch. 44.

Bancroft, J. C. and Geiger, H. D., 1994, Equivalent offsets and CRP gathers for prestack migration: 64th Ann. Internat. Mtg., Soc. Expl. Geophys., Expanded Abstracts, 672-675.

Bancroft, J. C., Geiger, H. D, 1995,Velocity sensitivity for equivalent offsets in CSP gathers, CREWES Project Research Report, Vol.7, Ch. 24.

Bancroft, J. C. and Geiger, H. D., 1996a, Energy concentration as a function of dip on Cheop's pyramid and CSP gathers, CREWES Project Research Report, Vol.8, Ch. 27.

Bancroft, J. C. and Geiger, H. D., 1996b, Velocity sensitivity for equivalent offset prestack migration: a contrast in robustness and fragility: CSEG National Convention, Expanded Abstracts, 149-150.

Bancroft, J. C. and Geiger, H. D., 1997, Anatomy of common scatterpoint (CSP) gathers formed during equivalent offset prestack migration (EOM), CREWES Project Research Report, Vol.9, Ch. 28.

Bancroft, J. C., Geiger, H. D., Foltinek, D. and Wang, S., 1995, Prestack migration by equivalent offsets and common scatter point (CSP) gathers: 57th Mtg. Eur. Assoc. Expl Geophys., Extended Abstracts, Session:P124.

Bancroft, J.C., Geiger, H. D. and Margrave, G. F., 1998, The equivalent offset method of prestack time migration: Geophysics, 63, 2042-2053.

Bancroft, J. C., Geiger, H. D., Wang, S. and Foltinek, D. S., 1995, Prestack migration by equivalent offsets and CSP gathers: An update, Vol.7, Ch. 23.

Bancroft, J.B. and Li, X., 1998, Efficient computation of the equivalent offset for EOM, 68th Annual Internat. Mtg., Soc. Expl. Geophys., Expanded Abstracts, ST 11.9.

Bancroft, J. C., Margrave, G. F. and Geiger, H. D., 1997, A kinematic comparisons of conventional processing, DMOPSI, and EOM, CREWES Project Research Report, Vol.9, Ch. 29.

Bancroft, J. C. and Wallace, R. A., 1997, Fast 3D Kirchhoff poststack migration with migration velocity analysis: 59th Mtg. Eur. Assoc. Expl Geophys., Extended Abstracts, Session:A046.

Bancroft, J. C., Xu, Y., 1998, Equivalent offset migration for vertical receiver arrays, CREWES Project Research Report, Vol.9, Ch. 11.

Carnahan, B., Luther, H. A., Wilkes, J. O., 1969, Applied numerical methods, John Wiley &Sons.

Chan, W-K. and Stewart, R. R., 1996, F-X statics: CREWES Project Research Report, Vol.7.

Chernis, L., 1998, Depth migration by a generalized equivalent offset mapping: 68th Ann. Internat. Mtg. Soc. Expl. Geophys., Expanded Abstracts, 1550-1553.

Chun, J. H. And Jacewitz, C., 1981, Fundamentals of frequency-domain migration: Geophysics, 46, 717-732.

Claerbout, J. F., 1985, Imaging the Earth's Interior, Blackwell Scientific Publications. Available over the internet at http://sepwww.stanford.edu/sep/prof/.

Deng, H. L., Wang, B. and Pann, K., 1996, Residual statics estimation by optimizing a complexity-reduced stacking-power function: EAGE 58th Conference and Technical Exhibition. Amsterdam, The Netherlands.

Disher, D. A., and Naquin, P. J., 1969, Statistical automatic statics analysis: Geophysics, 35, 574-585.

Dix, H. C., 1955, Seismic velocities from surface measurements: Geophysics, 20, 68-86.

Dobrin, M. B., 1960, Introduction to geophysical prospecting: McGraw Hill Book Co.

Foster, M. R. & Guinzy, N. J., 1967, the coefficient of coherence- its estimation and use in geophysical data processing: Geophysics, vol.32, pp602-616.

Forel, D. and Gardner, G. H. F., A three-dimensional perspective on two-dimensional dip moveout: Geophysics, 53, 604-610.

Fowler, P. J., 1987, A comparative overview of prestack time migration methods, 67th Ann. Internat. Mtg. Soc. Expl. Geophys., Expanded Abstracts, 1571-1574.

Fowler, P. J., 1988, A comparative overview of dip moveout methods, 68th Ann. Internat. Mtg. Soc. Expl. Geophys., Expanded Abstracts, ST 11.3.

Galdona, L. A., Bancroft, J. C., 1998, Energy Distribution on CSP gathers as they approach a scatter point, CREWES Project Research Report, Vol.9, Ch. 45.

Gardner, G. H. F., French, W. S. and Matzuk, T., 1974, Elements of migration and velocity analysis: Geophysics, 39, 811-825.

Gardner, G. H. F., Wang, S. Y., Pan, N. D. and Zhang. Z., 1986, Dip moveout and prestack imaging: 18th Ann. Offshore Technology Conference, OTC 5158.

Garotta, R., and Michon, D., 1968, Static corrections in reflection seismology: 13th EAEG meeting, Salzburg, Austria.

Geiger, H. D. and Bancroft, J. C., 1995a, Equivalent offset prestack migration for rugged topography, CREWES Project Research Report, Vol.7, Ch. 28.

Geiger, H. D. and Bancroft, J. C., 1995b, Prestack migration to an unmigrated zero offset section, CREWES Project Research Report, Vol.7, Ch. 29.

Geiger, H. D. and Bancroft, J. C., 1996a, Equivalent offset prestack migration for rugged topography: 66th Annual Internat. Mtg., Soc. Expl. Geophys., Expanded Abstracts, 447-450.

Geiger, H. D. and Bancroft, J. C., 1996b, Equivalent offset prestack migration - Application to rugged topography and formation of unmigrated zero-offset section: 58th Mtg. Eur. Assoc. Expl Geophys., Extended Abstracts, Session:P098.

Hagedoorn, J. G., 1959, The plus-minus method of interpreting seismic refraction sections: Geophys. Prosp., 7, 158-182.

Hampson, D. and Russell, B., 1984, First-break interpretation using generalized inversion: J. Can. Soc. Explor. Geophys,. 20, 40-54.

Hileman, J. A., Embree, P., and Pflueger, J. C., 1968, Automatic static correction: Geophysical Prospecting, 16, 326-358.

Hubral, P., 1977, Time migration - some ray theoretical aspects, Geophysical Prospecting, 25, 738-745.

Irvine, B. M. and Worley, J. K., 1969, The application and limitations of automatic residual static correction techniques: 39th SEG meeting, Calgary, Canada.

Kirtland Grech M. G. and Bancroft, J. C., 1998, Building complex velocity models using EOM - a case study, CREWES Project Research Report, Vol.9, Ch. 27.

Larner, K., 1998, CSEG Luncheon Presentation, Calgary, Canada.

Larner, K., Perez, G., Jenner, E., and Salinas, T., 1995, The quality of the surface-consistency assumption in residual-statics estimation: Extended Abstract, SEG Int. Mt.

Laski, J. D., 1970, Simultaneous estimation of parameters of reflection events (depth, dip, velocity) and relative static corrections: Geophysical Prospecting, 18, 269-276.

Li, X. and Bancroft, J. C., 1996a, Surface consistent statics correction associated with EOM procedure, CREWES Project Research Report, Vol.8, Ch. 17.

Li, X. and Bancroft, J. C., 1996b, An efficient and accurate algorithm for constructing common scatter point gathers, CREWES Project Research Report, Vol.8, Ch. 25.

Li, X. and Bancroft, J. C., 1997a, Integrated residual statics analysis with prestack time migration, 66th Annual Internat. Mtg., Soc. Expl. Geophys., Expanded Abstracts, 1452-1455.

Li, X. and Bancroft, J. C., 1997b, Residual statics analysis before NMO using prestack migration: 59th Mtg. Eur. Assoc. Expl Geophys., Extended Abstracts, Session:A032.

Li, X. and Bancroft, J. C., 1997c, Residual Statics using CSP gathers, CREWES Project Research Report, Vol.9, Ch. 23.

Li, X. and Bancroft, J. C., 1997d, A new algorithm for converted wave pre-stack migration 1997, CREWES Project Research Report, Vol.9, Ch. 26.

Li, X. and Bancroft, J. C., 1998, The natural relation between prestack time migration and residual statics analysis, CREWES Project Research Report, Vol.9, Ch. 38.

Li, X., Xu, Y. and Bancroft, J. C., 1997, Equivalent offset migration: the implementation and application update, CREWES Project Research Report, Vol.9, Ch. 27.

Margrave, G. F., 1999, personal communications.

Margrave, G. F. and Bancroft, J. C., 1996, The theoretical basis for prestack migration by equivalent offset: 66th Annual Internat. Mtg., Soc. Expl. Geophys., Expanded Abstracts, , 443-446.

Margrave, G. F., Bancroft, J. C. and Geiger, H. D, 1999, Fourier prestack migration by equivalent wavenumber: Geophysics, 64, 197-207.

Neidell, N. S., and Taner, M. T., 1971, Semblance and other coherency measures for multichannel data: Geophysics, 36, 482-497.

Palmer, D., 1981, The general reciprocal method of refraction seismic interpretation: geophysics, 46, 1508-1518.

Ronen, J., and Claerbout, J. F., 1985, Surface-consistent residual statics estimation by stack-power maximization: Geophysics, 50, 2759-2767.

Rothman, D. H., 1985, Nonlinear inversion, statistical mechanics, and residual statics estimation: Geophysics, 50, 2784-2796.

Saghy, G., and Zelei, A., 1975, Advanced method for self-adaptive estimation of residual static corrections: Geophysical Prospecting, 23, 259-274.

Taner, M. T., Cook, E. E. and Neidell, N. S., 1970, Limitations of the reflection seismic method: Lessons from computer simulation: geophysics, 35, 551-573.

Taner, M. T., Koehler, F., and Alhilali, A., 1974, Estimation and correction of near-surface time anomalies, Geophysics, 39, 441-463.

Tjan, T., Larner K., and Audebert, F. 1994, Prestack migration for residual statics estimation in complex media, Expanded Abstracts of SEG Annual meeting, 1513-1516.

Wang, S., Bancroft, J. C., Lawton, D. C. and Foltinek, D. S., 1995, Converted wave (P-S) prestack migration and migration velocity analysis, CREWES Project Research Report, Vol.7 Ch. 27.

Wang, S., Bancroft, J. C. and Lawton, D. C., 1996, Converted-wave (P-SV) prestack migration and migration velocity analysis: 66th Annual Internat. Mtg., Soc. Expl. Geophys., Expanded Abstracts, , 1575-1578.

Waters, K.H., 1987, Reflection Seismology—A tool for energy resource exploration: 3rd Ed. John Wiley & Sons, Inc.

Wiggins, R. A., Larner, K. L., and Wisecup, R. D., 1976, Residual statics analysis as a general linear inverse problem: Geophysics, 41, 922-938.

Yilmaz, O., 1987, Seismic data processing: SEG.

Appendix A

The Jacobi and Gauss-Seidel iterative algorithms for two-term surface consistent residual statics decomposition

The linear equation system (2-4-3) can be rewritten using simplified symbols as

$$T_{ij} = S_i + R_j, \tag{A-1}$$

where $i = 1, 2, \ldots, N_S$ and $j = 1, 2, \ldots, N_R$. For a trace with its source index i and receiver index j, T_{ij} is the time shift estimated from cross-correlation between this trace and its corresponding reference trace. Its source static S_i and receiver static R_j are assumed to be the main parts of the traveltime error because of the surface consistent assumption. Our problem is to find S_i for all the N_S source locations and R_j for all the N_R receiver locations from the known T_{ij}'s. There are totally not more than $N_S \times N_R$ equations and N_S+N_R unknowns.

It is proved in Chapter 2 that the system of linear equations (A-1) is usually over-determined and always under-constrained. The rank of the coefficient matrix is always less than N_S+N_R. This implies that this system does not have unique solutions. Even least-square technique can not be directly applied because of the singularity of the coefficient matrix.

There are some convenient additional constraints for this system in our residual statics problem. They are based on the assumption that the residual statics have zero mean, i.e.,

$$\sum_{i=1}^{N_S} S_i = 0 \text{ and } \sum_{j=1}^{N_R} R_j = 0. \tag{A-2}$$

Because of the source fold is usually higher than the receiver fold in seismic experiments, i.e., there are more equations containing S_i (denoted with $N(S_i)$) than those containing R_j (denoted with $N(R_j)$). Therefore, it is more statistically reasonable to assume the summation of all the receiver statics related to one source to be closer to zero

than the summation of all the source statics related to one receiver. This leads to the first trial of the source static solution of system as

$$S_i = \frac{1}{N(S_i)} \sum_{j \propto S_i} (T_{ij} - R_j) = \frac{1}{N(S_i)} \left[\sum_{j \propto S_i} T_{ij} - \sum_{j \propto S_i} R_j \right] \approx \frac{1}{N(S_i)} \sum_{j \propto S_i} T_{ij} = S_i^{(1)}, \quad \text{(A-3)}$$

Where $\sum_{j \propto S_i}$ means the summation over all the equations related to S_i. The condition used for the pseudo-equal sign "$\approx$" is

$$\sum_{j \propto S_i} R_j = 0, \quad \text{(A-4)}$$

which is an approximation of the R-part of (A-2).

With the first trial (denoted by the superscript (1)) solution of S_i, the value of R_j can be directly solved as

$$R_j^{(1)} = \frac{1}{N(R_j)} \sum_{i \propto R_j} \left(T_{ij} - S_i^{(1)} \right) \quad \text{(A-5)}$$

Because of the assumption (A-4), the first trial solution of the surface consistent statics, $S_i^{(1)}$ and $R_j^{(1)}$, may not be the satisfactory results. This naturally leads to the Gauss-Seidel iterative algorithm scheme. If the (n-1)-th iteration is done, the n-th iteration results can be expressed as

$$S_i^{(n)} = \frac{1}{N(S_i)} \sum_{j \propto S_i} \left(T_{ij} - R_j^{(n-1)} \right), \quad \text{(A-6a)}$$

$$R_j^{(n)} = \frac{1}{N(R_j)} \sum_{i \propto R_j} \left(T_{ij} - S_i^{(n)} \right). \quad \text{(A-6b)}$$

Note that the n-th iteration result of source statics, $S_i^{(n)}$, are immediately used for the n-th iteration result of receiver statics $R_i^{(n)}$. This property is different from the iterative scheme of Jacobi algorithm, in which both the source and receiver static estimations of each iteration are not used until the next iteration, i.e.,

$$S_i^{(n)} = \frac{1}{N(S_i)} \sum_{j \propto S_i} \left(T_{ij} - R_j^{(n-1)} \right), \tag{A-7a}$$

$$R_j^{(n)} = \frac{1}{N(R_j)} \sum_{i \propto R_j} \left(T_{ij} - S_i^{(n-1)} \right). \tag{A-7b}$$

The Gauss-Seidel algorithm usually converges faster than but may not be as stable as the Jacobi algorithm (Carnahan et al., 1969). A practical way to ensure the stability and the efficient convergence is to use a combination of these two methods. That is, instead of using equations (A-6b) or (A-7b), using

$$R_j^{(n)} = \frac{1}{N(R_j)} \sum_{i \propto R_j} \left[T_{ij} - pS_i^{(n-1)} - (1-p) S_i^{(n)} \right], \tag{A-8}$$

where $0 \le p \le 1$ represents the percentage of how much weight is applied to Gauss-Seidel estimations.

The following is a Matlab M-file for residual statics decomposition using Gauss-Seidel and Jacobi method. In the code, some mathematical condition is applied to ensure the convergence of the iterative scheme (Taner et al., 1974).

```
function [s_stat, r_stat, cdp_stat]=gauss_seidel(tij, sin, srf, ...
            mode, perc, niter, nsmooth, cdp, logfile);
%
%   GAUSS_SEIDEL
%
%         [s_stat, r_stat, cdp_stat]=gauss_seidel(tij, sin, srf, ...
%           mode, perc, niter, nsmooth, cdp, logfile);
%
%     Gauss-Seidel and Jacobi iterative method for surface consistent
%     residual statics estimation.
%
%   The input:
%     tij : the estimated time shifts on all the traces
%     sin : source index number of all the tarces
%     srf : receiver surface location number of all the traces
%     cdp : CDP number of all the traces.
%              If it is not available, it is OK.
%   niter : number of iterations for Gauss-Sedel
%    mode : three options - CDP, SIN and SRF
%              if = "CDP", the vector "cdp" must be given.
%                   The output "CDP_STAT" will have statics estimations
%              if = "SIN", start from calculate source statics first.
%                   no cdp term is involved.
```

```
%                   This is the default.
%               if = "SRF", start from calculate receiver statics first.
%                   no cdp term is involved.
%    perc : the percentage (0 - 100) of the previous iteration results
%           using in this iteration
% nsmooth : length of smooth for removal of long wavelength content
%
%   The output:
%     s_stat : source statics
%     r_stat : receiver statics
%   cdp_stat : cdp term of statics if available.
%
%   Author: Xinxiang Li
%           The CREWES Project
%           The Department of Geology and Geophysics
%           The University of Calgary
%   February, 1999.
%   Update : June, 1999
%

if (nargin < 3)
      error('INPUT at least 3 parameters!!');
end

ntr_total = length (tij);
if (ntr_total ~= length(sin))
   error('length of SIN not match NTR_TOTAL');
end
if (ntr_total ~= length(srf))
   error('length of SRF not match NTR_TOTAL');
end

if ((nargin < 4) | (length(mode) < 3))
   mode = 'SIN';
end
if (strcmp(mode, 'SRF')== 0)
   if (~strcmp(mode, 'CDP'))
   mode = 'SIN';
   end
end
mode = upper (mode(1:3));

if ((nargin < 8) & strcmp(mode,'CDP'))
   error('cdp numbers must be given!');
end

if (nargin < 5 )
      perc = 50;
end
if (perc < 0) | (perc > 100)
      perc = 50;
end

if (nargin < 6)
   niter = 3;
end
```

```
niter = max([1, niter]); niter = min ([niter , 50])

if (nargin < 7)
   nsmooth = max([ntr_total/200,20]);
end

if (nargin >= 8)& (mode == 'CDP')
   if (length(cdp)~=ntr_total)
      error('length of CDP not match NTR_TOTAL')
   end
end

if (nargin < 9)
   logfile = 'residual_statics_logs';
end

% Get the source fold and receiver fold
%     and the index numbers

s1 = min (sin); s2 = max (sin); r1 = min (srf); r2 = max (srf);
n_s = 1; n_r = 1;
ys = sort(sin); old_s = s1; yr = sort(srf); old_r = r1;
s_no(1) = s1; r_no(1) = r1;

if strcmp(mode, 'CDP')
   cdp1= min(cdp);
   n_cdp = 1;
   ycdp = sort(cdp); old_cdp = cdp1;
   cdp_no(1) = cdp1;
end
%
% number of SOURCEs, RECEIVERs, and CDPs if necessary
%
%  n_s : number of sources
%  s_no: index numbers of the sources
for itr = 1:ntr_total
    if (ys(itr) ~= old_s)
       n_s = n_s + 1;  old_s = ys(itr); s_no(n_s) = ys(itr);
    end
    if (yr(itr) ~= old_r)
       n_r = n_r + 1; old_r = yr(itr); r_no(n_r) = yr(itr);
    end
    if strcmp(mode, 'CDP')
       if (ycdp(itr) ~= old_cdp)
          n_cdp = n_cdp + 1; old_cdp = ycdp(itr);
          cdp_no(n_cdp) = ycdp(itr);
       end
    end
end

s_stat=zeros(n_s,1); r_stat=zeros(n_r,1);
s_jacobi = s_stat; r_jacobi = r_stat;
cdp_stat = []; cdp_jacobi = [];
if strcmp(mode, 'CDP')
   cdp_stat = zeros(n_cdp,1); cdp_jacobi = cdp_stat;
end
```

```
if (niter > 1)
   ddl = floor(50.0/(niter-1))/50;
end
fid_log = fopen(logfile,'w');
perc = perc*1.0/100.;

%%%%%%%%%%%%
if strcmp(mode, 'CDP')

for iter = 1: niter
    if (niter > 1)
    lamda = 2.0-(iter-1)*ddl;
    else
    lamda = 1.0;
    end

    fprintf (fid_log, '\n\n%s\n',['No. ' int2str(iter) ' iteration:']);

    % LOOP over CDP index
    for icdp = 1:n_cdp
        %
        % At the present CDP, find the trace index in the data set
        % for all traces in this CDP gather.
        %
        ind_tr = find (cdp == cdp_no(icdp));
        %
        % the length of this index is the fold of present CDP gather
        %
        % LOOP over traces in present gather
        for i = 1:length(ind_tr)
            %
            % for each trace in the CDP gather, find
            % (1) the Source Index Number, and
            %     then the sequence shot number
            % (2) the Surface receiver location, and
            %     then the sequqnce number
            %
            inds = find (s_no==sin(ind_tr(i)));
            indr = find (r_no==srf(ind_tr(i)));
            cdp_stat(icdp) = cdp_stat(icdp) + ...
                             tij(ind_tr(i))-s_stat(inds)-r_stat(indr);
        end
        cdp_stat(icdp)=cdp_stat(icdp)/max([3,(length(ind_tr)+lamda)]);
    end

      cdp_stat = wvremove(cdp_stat, nsmooth);

fprintf (fid_log,'%s\n','CDP statics');
fprintf(fid_log,'%8.2f%8.2f%8.2f%8.2f%8.2f%8.2f%8.2f%8.2f\n',cdp_stat);

    % LOOP over SIN index
    for is = 1:n_s
        ind_tr = find(sin  == s_no(is));
        for i = 1:length(ind_tr)
            indcdp = find (cdp_no==cdp(ind_tr(i)));
```

```
            indr = find (r_no==srf(ind_tr(i)));
            s_stat(is) = s_stat(is) + tij(ind_tr(i)) ...
            -(1.0-perc)* cdp_stat(indcdp)- perc*cdp_jacobi(indcdp) ...
            -(1.0-perc)* r_stat(indr) - perc*r_jacobi(indr);
        end
        s_stat(is)=s_stat(is)/max([3,length(ind_tr)+lamda]);
    end
      s_stat = wvremove(s_stat, nsmooth);

fprintf (fid_log,'\n\n%s\n','SOURCE statics');
fprintf(fid_log,'%8.2f%8.2f%8.2f%8.2f%8.2f%8.2f%8.2f%8.2f\n', s_stat);

    % LOOP over SRF index
    for ir = 1:n_r
        ind_tr = find(srf  == r_no(ir));
        for i = 1:length(ind_tr)
            indcdp = find (cdp_no==cdp(ind_tr(i)));
            inds = find (s_no==sin(ind_tr(i)));
            r_stat(ir) = r_stat(ir) + tij(ind_tr(i)) ...
            -(1.0-perc)* cdp_stat(indcdp)- perc*cdp_jacobi(indcdp) ...
            -(1.0-perc)* s_stat(inds)- perc*s_jacobi(inds);
        end
        r_stat(ir)=r_stat(ir)/max([length(ind_tr)+lamda, 3]);
    end

      r_stat = wvremove(r_stat, nsmooth);

fprintf (fid_log,'\n\n%s\n','RECEIVER statics');
fprintf(fid_log,'%8.2f%8.2f%8.2f%8.2f%8.2f%8.2f%8.2f%8.2f\n', r_stat);

    s_jacobi = s_stat; r_jacobi = r_stat; cdp_jacobi = cdp_stat;
end  % for iteration

end  % for if

%%%%%%%%%%%%%%%%%%%%%%%%%%%%%%
if strcmp(mode, 'SIN')
for iter = 1: niter
    if (niter > 1)
       lamda = 0.5-(iter-1)*ddl;
    else
       lamda = 0.01;
    end
    fprintf (fid_log, '\n\n%s\n',['No. ' int2str(iter) ' iteration:']);

    % LOOP over SIN index
    for is = 1:n_s
        ind_tr = find(sin  == s_no(is));
        for i = 1:length(ind_tr)
            indr = find (r_no==srf(ind_tr(i)));
            s_stat(is) = s_stat(is) + ...
                              tij(ind_tr(i))-r_stat(indr);
        end
        s_stat(is)=s_stat(is)/max([length(ind_tr)+lamda, 5]);
    end
fprintf (fid_log,'\n\n%s\n','SOURCE statics');
```

```
fprintf(fid_log,'%8.2f%8.2f%8.2f%8.2f%8.2f%8.2f%8.2f%8.2f\n', s_stat);

% removal of long wavelength content
      s_stat = wvremove(s_stat, nsmooth);

    % LOOP over SRF index
    for ir = 1:n_r
        ind_tr = find(srf  == r_no(ir));
        for i = 1:length(ind_tr)
            inds = find (s_no==sin(ind_tr(i)));
            r_stat(ir) = r_stat(ir) +  tij(ind_tr(i)) ...
                       -(1.0-perc)*s_stat(inds) - perc*s_jacobi(inds);
        end
        r_stat(ir)=r_stat(ir)/max([length(ind_tr)+lamda,5]);
    end
%
% removal of long wavelength content
      r_stat = wvremove(r_stat, nsmooth);

fprintf (fid_log,'\n\n%s\n','RECEIVER statics');
fprintf(fid_log,'%8.2f%8.2f%8.2f%8.2f%8.2f%8.2f%8.2f%8.2f\n', r_stat);

% some display information
      iter
      meanS=mean(s_stat)
      meanR=mean(r_stat)
      LSerrS=sqrt(sum((s_stat-s_jacobi).^2))
      LSerrR=sqrt(sum((r_stat-r_jacobi).^2))

    s_jacobi = s_stat; r_jacobi = r_stat;
end  % for iteration
end  % for if

%%%%%%%%%%%%%%%%%%
if strcmp(mode, 'SRF')
for iter = 1: niter
    if (niter > 1)
    lamda = 1.5-(iter-1)*dd1;
    else
    lamda =1.0;
    end

    fprintf (fid_log, '\n\n%s\n',['No. ' int2str(iter) ' iteration:']);

    % LOOP over SRF index
    for ir = 1:n_r
        ind_tr = find(srf  == r_no(ir));
        for i = 1:length(ind_tr)
            inds = find (s_no==sin(ind_tr(i)));
            r_stat(ir) = r_stat(ir) + ...
                              tij(ind_tr(i))-s_stat(inds);
        end
        r_stat(ir)=r_stat(ir)/max([length(ind_tr)+lamda, 5]);
    end

% removal of long wavelength content
```

```
      r_stat = wvremove(r_stat, nsmooth);

fprintf (fid_log,'\n\n%s\n','RECEIVER statics');
fprintf(fid_log,'%8.2f%8.2f%8.2f%8.2f%8.2f%8.2f%8.2f%8.2f\n', r_stat);

    % LOOP over SIN index
    for is = 1:n_s
        ind_tr = find(sin  == s_no(is));
        for i = 1:length(ind_tr)
            indr = find (r_no==srf(ind_tr(i)));
            s_stat(is) = s_stat(is) + tij(ind_tr(i)) ...
                       -(1.0-perc)*r_stat(indr)-perc*r_jacobi(indr);
        end
        s_stat(is)=s_stat(is)/max([length(ind_tr)+lamda, 5]);
    end

% removal of long wavelength content
      s_stat = wvremove(s_stat, nsmooth);

fprintf (fid_log,'\n\n%s\n','SOURCE statics');
fprintf(fid_log,'%8.2f%8.2f%8.2f%8.2f%8.2f%8.2f%8.2f%8.2f\n', s_stat);

    s_jacobi = s_stat; r_jacobi = r_stat;
end  % for iteration
end  % for if

fclose(fid_log);
```

Appendix B

The "CSP Statics" package in ProMAX

The EOMAP statics method has been implemented as a package in ProMAX 2D, which includes three modules as following.

The first one is for the forward EOMAP, which is the same as forming CSP gathers for migration purpose. The module is called "CSP Gathers".

The second is for the inverse EOMAP, and it is specific for the statics analysis purpose. It is called "CSP Statics Model".

The third one is called "CSP residual statics analysis", but it can be used as a general tool for residual statics analysis as long as the model data has the same number of traces and the same geometry with the original seismic data.

All three modules can still be optimized with the developments of either the new algorithms for equivalent offset migration methods or for the trace correlation and the surface consistent decomposition.